SINGLE-STEP INDUCTION OF RIGHT-SIDED COLON CANCER PHENOTYPE BY *BRAF*^{V600E} THROUGH ACQUIRED WNT ACTIVATION

by
Byunghak Kang

A dissertation submitted to The Johns Hopkins University in conformity with the requirements of the degree of Doctor of Philosophy

Baltimore, Maryland
June 2016

Abstract

BRAF mutant colorectal cancers (CRC) mostly arise via an alternate pathway distinguished from the classical adenoma-carcinoma sequence involving *APC* and *KRAS* mutations. *BRAF*-driven tumors have an increased incidence of promoter CpG island methylator phenotype (CIMP)-high, microsatellite instable (MSI) phenotype, lack of concurrent mutations of *APC*, mucinous histology, and location on the right side of the colon. Although these characteristics are constantly observed in *BRAF* mutant CRCs, how this *BRAF* mutation induces this type of tumor is not clear.

To understand this, we modeled the early carcinogenesis of colorectal cancer by inducing $BRAF^{V600E}$ and $KRAS^{G12D}$ individually in organoids prepared from mouse proximal colon and subsequently determined the genome-wide gene expression, DNA methylation, and genetic changes in combination with growth properties and induction of tumor formation.

The $BRAF^{V600E}$, but not $KRAS^{G12D}$, mutations induced various features of progressive transformation consisting of increased spheroid formation of the organoids with internal dysplastic polypoid growth. $BRAF^{V600E}$ organoids acquired an ability to grow without stem cell niche factors such as Wnt3a, R-Spondin and Noggin. These above phenotypic changes are phenocopies of *APC* mutations in organoids wherein the Wnt pathway is activated. Indeed, $BRAF^{V600E}$ drives sustained up-regulation of Wnt targets and stem cell genes and suppression of differentiation genes regardless of whether niche factors are added. Furthermore, in some of the transformed organoids, sequencing revealed

mutations in b-catenin. Finally, and most excitingly, induction of *BRAF*^{V600E}, but not *KRAS*^{G12D}, induced complete transformation forming xenograft tumors in immunodeficient mice. The tumors exhibit histological characteristics of mucinous adenocarcinoma, which is highly associated with the *BRAF*^{V600E} mutation in human CRCs. In addition, analyses of genome-wide methylation revealed increased DNA methylation in CpG island promoters of many genes including Wnt negative regulators such as *Sfrp1, Sfrp2, Wt1* and *Sox17* and CIMP genes including *p16* and *Igfbp7* in the *BRAF*^{V600E} mutant organoids.

In conclusion, mouse colon organoids expressing *BRAF*^{V600E} recapitulate features of the human right-sided CRC phenotype with adoption of a stem cell niche factor independency, activation of the Wnt pathway, induction of CpG island methylation in Wnt negative regulators and CIMP panel genes, and activating Wnt-pathway mutations.

Thesis advisor: Stephen B. Baylin, MD and Hariharan Easwaran, PhD

Thesis reader: Nicholas C. Zachos, PhD

Thesis Committee Members

Ben Ho Park, MD, PhD

Srinivasan Yegnasubramanian, MD, PhD

Nicholas C. Zachos, PhD

Preface

All the work presented in this dissertation is based on the experiments and analysis conducted in Baylin/Easwaran laboratory at the Sidney Kimmel Comprehensive Cancer Center of Johns Hopkins University School of Medicine or in collaboration with other core laboratories in Johns Hopkins University.

The project originally consisted of three parts: in vitro, ex vivo and in vivo modeling of colorectal cancer (CRC) by engineering mouse colon organoids with $BRAF^{V600E}$ or $KRAS^{G12D}$ mutations. This above ex vivo modeling is thus revealed to be an excellent system to study early events of tumorigenesis for CRC. I successfully induced mutations, $BRAF^{V600E}$ and $KRAS^{G12D}$ separately, in colon organoids and analyzed their phenotypes and molecular changes including gene expression and DNA methylation. Most of the work presented in this dissertation is based on the physiological and pathological phenotyping and molecular characterization of the mutant organoids.

Although most of the techniques used here pertain to growth of organoids , our phenotyping and molecular analyses of these were adopted from previously published articles and shared information from our collaborators, I modified their techniques to meet the objectives of this project. I hope the methods described here are also useful for other research projects in the future.

Acknowledgement

First and foremost, I would like to thank my co-mentors, Dr. Stephen Baylin and Dr. Harihran Easwaran, for their endless support and guidance during my thesis work. Their advice, support and guidance have been the most crucial components of this thesis project from its inception to completion. I cannot imagine how I would be able to finish this project without them. The regular discussions we had were very helpful and encouraging. I felt very fortunate to get trained under their mentorship.

I also would like to thank my thesis committee: Dr. Ben Ho Park, Dr. Srinivasan Yegnasubramanian and Dr. Nicholas C. Zachos for all their advice and help with the project. As a committee chair, Dr. Ben Ho Park gave me great advices keeping me on the right track. I really appreciate his advices on the thesis work and future career in general. I also appreciate Dr. Srinivasan Yegnasubramanian's help with methylation analysis and other great advices throughout the thesis work. It has been tremendous help for me to accomplish this thesis. I also need to thank Dr. Nicholas C. Zachos for his collaboration in establishment of organoid culture. Without his help and collaboration, I would not be able to learn and establish organoid culture for my thesis work.

I need to thank Dr. Julie In. I learned the organiod culture technique from Dr. Julie In. Without her help, it would be impossible for me to learn the technique in a very short time and establish organoid culture in our lab. I also want to thank Dr. Elana Fertig for her help with gene expression pattern analysis. It was a great opportunity to learn bioinformatics tools and statistical ideas behind it. I also need to thank Dr. Shinji Maegawa and Dr. Tao Yong for their

help with targeted methylation analysis. I really feel fortunate to have Dr. Julie, Dr. Elana Fertig, Dr. Shinji Maegawa and Dr. Tao Yong as collaborators and colleagues.

I also would like to thank members of Dr. Stephen Baylin and Dr. Hariharan Easwaran lab and tumor biology program. Especially, I would like to thank the faculty members in our group, Dr. Barry Nelkin, Dr. Cynthis Zahnow, Dr. Nita Ahuja, Dr. Douglas Ball, Dr. Robert Casero, Dr. James Herman and Dr. Malcolm Brock, for great advices and discussions. I am also very thankful to Kathy Bender, Tammy Means and JoAnn Murphy for their administrative helps and Ray-whay, Tina Largent and Lauren Murphy for their help with tissue culture, experiments and material procurement. In addition, I also want to thank Dr. Yi Cai, Dr. Wenbing Xie, Dr. Michelle Vaz, Dr. Kate Chiappinelli, Dr. Christina Destefano, Michael Topper, Dr. Benjamin Leadem, Dr. Heather O'Hagan, Dr. Hsing-Chen Tsai, Dr. Jianjun Luo, Dr. Lorraine Pelosof, Dr. Khadijah Mitchell, Dr. Weijie Poh, Dr. Yang Zhang and Dr. Andre Kydd for the helpful discussions and advices.

I also like to mention the Pathobiology graduate program for providing me the opportunity to pursue my PhD degree at Johns Hopkins. Especially, I would like to thank Mrs. Margaret Lee and Mr. Al Njoo for providing me and other Margaret Lee fellows funding for the first year. The fellowship provided us a great opportunity to start our scientific career in such a great scientific community, Johns Hopkins Univeristy. In addition, I want to thank former and present director, Dr. Noel Rose and Dr. Lee Martin, and program faculty members for providing me great advices throughout the PhD training and former and present

program administrative staffs, Wilhelmena Braswell, Nancy Nath, Stacey Morgan and Tracie McElroy for all the administrative helps during my PhD training. I also need to thank program colleagues and classmates for help during the course work and thesis work.

Finally, I would like to thank my family and friends for their limitless support and encouragement throughout my PhD training. Especially, I would like to thank my grandfathers from maternal and paternal sides. They had been always supportive and encouraging me to pursue my dreams. In addition, I also want to thank Stella Suyong Lee for being supportive and helpful during my entire PhD training.

Table of Contents

List of Tables

List of Figures

Chapter 1. Introduction

1.1 Cancer genetics and epigenetics

Cancer is a result of abnormal regulation of normal processes such as proliferation, cellular death, genome maintenance, angiogenesis, cellular metabolism and immune surveillance (Hanahan and Weinberg, 2011). The abnormal regulation of these processes gives the cancerous cells a selective advantage over normal cells in growth, survival and evasion from immune surveillance and allows for malignant progression. All of these abnormalities are direct or indirect results of genetic and epigenetic changes that cause loss of function for tumor suppressor genes(TSGs) and genome surveillance genes and activation of oncogenes(OCGs).

Genetic alterations are common causes of loss of function for TSGs and activation of oncogenes. Genetic alterations causing activation of oncogenes include gene amplification, activating missense point mutations, and translocation which causes formation of fusion proteins that induce inappropriate gene activation. In contrast, inactivating missense or nonsense point mutations and deletions of chromosome regions are common genetic alterations that cause loss of TSGs such as genome surveillance genes, cell cycle checkpoints and cell death related genes. In recent sequencing studies of 3284 tumors, a total 125 driver mutations were discovered based on mutation frequencies (Vogelstein et al., 2013). Genes with the driver mutations are

involved in 12 pathways that regulate three core cellular processes including cell fate, cell survival and genome maintenance (Vogelstein et al., 2013).

Another important way of losing TSGs function and activation of oncogenes is epigenetic alteration in the cancer genome. Although genetic alterations have traditionally been viewed as the main driver of cancer development, recently the paradigm has now been expanded to incorporate the disruption of epigenetic regulatory mechanisms (Baylin and Bestor, 2002; Baylin and Jones, 2011; Baylin and Ohm, 2006; You and Jones, 2012). Gene silencing of TSGs through promoter hypermethylation is a common form of epigenetic disruption in cancer (Baylin and Jones, 2011). For instance, genes controlling the cell cycle and DNA repair, such as RB, BRCA1/2, and PTEN, are known to have abnormal promoter region DNA methylation and associated abnormal gene silencing as well as undergoing mutations and deletions in cancer (Hatziapostolou and Iliopoulos, 2011). In addition, histone modification and nucleosome remodeling are other important epigenetic regulations that can be disrupted in cancer. Histone modifications at specific amino acid residues in gene regulatory regions can normally help control gene activation or repression. For instance, trimethylated H3 at lysine 4 is enriched in active gene promoters. In contrast, Trimethylated H3 at lysine 27 or trimethylation H3 at lysine 9 are enriched in inactive promoters (Arnold et al., 2016; Baylin and Jones, 2011; Hatziapostolou and Iliopoulos, 2011). These modifications are regulated by histone acetyltransferases, deacetylases methyltransferases and demethylases. Nucleosome remodeling is another key mechanism for regulation of gene

expression. As more and more mutations are discovered in the nucleosome remodeling proteins in cancers, the importance of their role in tumorigenesis is increasing(Bhattacharjee et al., 2016; Biegel et al., 2014; Geng et al., 2016; He et al., 2016; Huang et al., 2015; Kadoch and Crabtree, 2015; Levin et al., 2015; Malonia et al., 2014; Mayes et al., 2014; Nio et al., 2015; Oike et al., 2013; Pfister et al., 2015; Soshnikova et al., 2016; Wang et al., 2016; Wu et al., 2016a; Wu et al., 2016b; Wu et al., 2014; Xu et al., 2015; Zhang et al., 2016a; Zhang et al., 2016b; Zollner et al., 2015). However, the direct role in tumorigenesis is still unknown.

1.2 Specific genetics and epigenetics of colorectal cancer

It is estimated that 1.3 million persons in the world will be found to have colorectal cancer (CRC) in 2012. CRC is the third most common cancer in men and the second most in women (Arnold et al., 2016). It is also one of the most well studied cancers in terms of clinical, pathological and molecular characteristics. Although, in many instances, it is regarded as a single entity, CRCs are quite heterogeneous. There have been many efforts to separate CRCs into different types based on molecular or morphological features. For genetic changes, driver mutation status such as *KRAS, BRAF*, and *APC*, chromosomal instability and frequent mutations for repeat sequences (microsatellite instability) have been frequently used. For epigenetic changes, a phenotype wherein many genes undergo abnormal promote CpG island methylation known as the CpG island Methylator Phenotype (CIMP) has been appreciated since the studies of Minoru Toyota and colleagues (Toyota et al., 1999). These above genetic and

epigenetic features allow us to divide CRCs into the following 5 groups although the distinction is not always clear-cut due to the presence of some CRCs with mixed features, (Jass, 2007):

Group 1 (12%)- CIMP-high, *MLH1* methylation, Microsatellite instability (MSI)-high. Chromosomal instability (CIN)-negative and frequent *BRAF* mutations.

Group 2 (8%)- CIMP-high, partial *MLH1* methylation, Microsatellite stable or MSI-low, CIN-negative and BRAF mutations.

Group 3 (20%)- CIMP-low, *MGMT* methylation, MSS or MSI-low, CIN positive, and KRAS mutation.

Group 4 (57%)- CIMP-negative, MSS, CIN, *APC* and *KRAS* mutation.

Group 5 (3%)- CIMP-negative, MSI-H, CIN-negative and mutations in DNA mismatch repair genes (can occur as a genetic disorder in families termed the Lynch syndrome) and *APC* mutations.

Group 1 and 2 CRC tumors share the same precursor lesions, morphological features and anatomic location: serrated polyps, mucinous morphology, and occurrence on the right side of the colon. Group 5 tumors also occur predominantly on the right side but have adenoma as a precursor lesions and are rarely mucinous. Group 3 tumors have either serrated polyps or adenomas as precursor lesions and mostly occur on left side. Group 4 predominantly develop from adenoma on left side and are rarely mucinous (Figure 1.1).

As the most prevalent tumor type in colon, group 4 tumors were subjected to early sequencing efforts by Bert Vogelstein and colleagues and their studies documented sequential accumulation of mutations such as *APC, RAS, PI3K* and *TGF-β* in a paradigm commonly known as the Vogelgram (Jones et al., 2008). Group 1, 2 and 3 CRC, which are the main object of this thesis, were classified in later studies, and their origins in serrated precursor lesions were proposed (Bettington et al., 2013; Burnett-Hartman et al., 2013; Ensari et al., 2010; Inoue et al., 2015; Kambara et al., 2004; Kriegl et al., 2011; Li and Burgart, 2007; Makinen, 2007; Michalopoulos and Tzathas, 2013; Minoo et al., 2007; Mohammadi et al., 2013; Murakami et al., 2015; O'Brien et al., 2006; Sakai et al., 2016; Snover, 2011; Spring et al., 2006; Vakiani and Yantiss, 2009; Yang et al., 2004). Although recent studies with early serrated lesions discovered that *BRAF* mutation precedes accumulation of DNA methylation in group 1 and 2 (Hinoue et al., 2009), the exact sequential changes remain to be elucidated.

Among CRC subtypes, groups 1 and 5 have the best prognosis (Bettington et al., 2013; Ensari et al., 2010; Kriegl et al., 2011; Li and Burgart, 2007; Snover, 2011; Spring et al., 2006). In turn, this correlates with having a high MSI status and high number of infiltrating lymphocytes (Pai et al., 2012). It is suggested that MSI causes high mutation burden and the mutations themselves or neo-antigens from the mutated genes induce the immune reaction and cause infiltration of lymphocytes (Bettington et al., 2013; Ensari et al., 2010; Kriegl et al., 2011; Li and Burgart, 2007; Snover, 2011; Spring et al., 2006). It has also been recently shown that this mutational burden and lymphocyte infiltration scenario correlates with

better response to immune checkpoint blockade with Pembrolizumab (Anti-PD-1) (Le et al., 2015). In contrast, group2 tumors seem to have the worst prognosis. They tend to have less lymphocyte infiltration and poor differentiation and be more invasive (Bettington et al., 2013; Ensari et al., 2010; Kriegl et al., 2011; Li and Burgart, 2007; Snover, 2011; Spring et al., 2006).

1.3 Stem cell and Wnt in colorectal cancer

In humans the entire intestinal lining epithelium is replaced every 5 to 7 days (Basu et al., 2016). This rapid replacement is fueled by the proliferation of stem cells at the base of crypt and subsequent differentiation of progenies of these cells as they migrate upward toward the intestinal lumen where they undergo apoptosis. This cellular turnover enables normal homeostasis of the intestine (Basu et al., 2016). The normal process of proliferation and differentiation of intestinal stem cells is governed by a gradient of Wnt signaling (Basu et al., 2016) which is the strongest at the crypt base and gradually decreases toward the luminal side. The strong Wnt signaling supports stem cell maintenance and proliferation at the crypt base and the decreasing Wnt signaling along the crypt supports epithelial differentiation of stem cells (Basu et al., 2016).

Cancer stem cells in colorectal cancers are suggested to have a similar role as intestinal stem cells in giving rise to progenitors that populate the majority of the tumor cells. Two models have been proposed to describe the origin of cancer stem cells in CRCs: the top-down and the bottom up model (Basu et al., 2016). The top-down model suggests that differentiated epithelial cells re-acquire stem

cell-like properties through hyperactivation of Wnt signaling and form aberrant crypt foci. On the other hand, the bottom-up model proposes that stem cells at the crypt base acquire ability to migrate upward without normal differentiation through Wnt hyperactivation. Although the suggested origin of cancer is different, both models require Wnt activation in either differentiated cells or stem cells. The importance of Wnt signaling in CRC tumorigenesis was recently demonstrated by formation of tumors by loss of *APC* and regression of tumors by restoration of *APC* even with retention of other oncogenic mutations such as *KRAS* and *p53* (Basu et al., 2016; Dow et al., 2015; Guerrero-Preston et al., 2014; Jorissen et al., 2015; Matano et al., 2015; Pronobis et al., 2015; Strum, 2016; Zachos et al., 2016). Also, in model systems, Wnt suppression by expression of a Wnt antagonist protein HoxA5 in colon cancer cells also suppresses tumor growth and metastatic progression (Ordonez-Moran et al., 2015).

In CRCs, Wnt pathway activation can occur through genetic and epigenetic alterations in various components of the Wnt regulatory pathway (Basu et al., 2016; Dow et al., 2015; Guerrero-Preston et al., 2014; Jorissen et al., 2015; Matano et al., 2015; Pronobis et al., 2015; Strum, 2016; Zachos et al., 2016). Germline mutations of *APC* cause familial adenomatous polyposis and approximately 70-80% of sporadic CRCs also harbor *APC* mutations or deletions. APC is a major binding partner and regulator of the canonical Wnt signaling pathway. In the absence of Wnt ligand, APC forms a destruction complex with the scaffold protein Axin to promote subsequent phosphorylation of b-catenin by Casein kinase1(CK1) and Glycogen synthase kinase 3 beta(GSK3b) (Fearon, 2011).

The phosphorylation of b-catenin leads to its degradation by the ubiquitin proteasome pathway. In the presence of Wnt ligand, the destruction complex disintegrates when there is recruitment of Axin protein and GSK3b to a cognate Wnt receptor complex consisting of the Frizzled and lipoprotein receptor-related protein (Fearon, 2011). The disruption of this destruction complex will lead to accumulation of b-catenin in the cytoplasm and its localization to the nucleus where it activates Wnt target gene expression along with co-activators such as CBP/p300 (Figure 1.2). In the case of *APC* mutations or deletion, the b-catenin is accumulated regardless of the presence of Wnt ligand due to failure of proper formation of the destruction complex. Mutations in other components of Wnt pathway including Axin, b-catenin and TCF4 are also reported in CRCs. However, their functional role in tumorigenesis remains to be elucidated (Fearon, 2011).

An epigenetic change such as the abnormal promoter region DNA methylation, discussed earlier, can also play important role in activation of Wnt in CRCs. Occasionally, this occurs for *APC* (Arnold et al., 2004; Coyle et al., 2007; Erdem et al., 2014; Fu et al., 2009; Furlan et al., 2014; Haluskova et al., 2015; Hiltunen et al., 1997; Jin et al., 2001; Juhlin et al., 2010; Segditsas et al., 2008; Sievers et al., 2006; Wang et al., 2009; Zhang et al., 2007; Zhang et al., 2008). Also, extremely frequently in colon polyps and CRCs, such abnormal DNA methylation occurs in the promoter regions of the Wnt antagonists, *SFRP1, SFRP2, SFRP5, DKK2, WIF1* and *SOX17* in the transition from normal to colorectal cancers (Murakami et al., 2015; Silva et al., 2014). *SFRP2* and *SOX17* themselves are Wnt target genes which normally can work as a negative feedback

loop for the Wnt pathway (Silva et al., 2014) (Figure 1.2). The suppression of all of these genes through DNA methylation is proposed to disrupt the negative feedback loop and induce hyperactivation of the Wnt pathway. The increase in DNA methylation has been associated with Wnt activity in CRC (Silva et al., 2014).

1.4 Organoids as an *ex vivo* model of gastrointestinal pathology

Model systems have been the centerpiece of biomedical and biological research being used to recapitulate biological and pathological processes. Animal models are the most close recapitulation of human biology and pathology, but these can be limited by having a confounding variability and limited accessibility for imaging and molecular assays. Although 2D monolayer cultures have their advantages and have played a critical role in modern advancement of biomedical and biological research, they often lack proper cell to cell and cell to matrix interactions and hierarchal organization. More importantly, most 2D cultures are either cancer or transformed cell wherein the genome and epigenome have already undergone significant changes. Early 3D culture systems such as cell spheroid cultures also lack the hierarchal organization of stem cell and progenitor cells and thus are unable to have both ongoing self renewal and differentiation processes (Date and Sato, 2015). Thus, although the animal models, 2D cell culture and early 3D cell culture have been very important tools for discovery so far, they don't cover the gap between the cellular level and the organ level.

The recently developed methodology by Clevers and colleagues to use stem cell derived organoids as a model will potentially, and robustly fill the gap. The model, wherein mouse and human cells, best studied to date as below from intestine, closely recapitulates a renewing cell system wherein, crypt stem cells, differentiation of their progeny, and apoptosing cells filling a lumen-like structure are all represented(Sato et al., 2009; Visvader and Clevers, 2016). Organoids recapitulate the hierarchal organization, cell-cell interaction, and cell-matrix interaction and have the capacity for both self-renewal and differentiation. While a wide variety of organoids have been generated including brain, lung, liver and intestine, the intestinal organoid system is one of the most well established and most widely used system currently. Evans et al.(1994) firstly cultured primary adult intestinal crypt in collagen type I –coated tissue culture vessels (Date and Sato, 2015; Evans et al., 1994). However, the culture was good for 1-2 weeks. Later, long lasting culture of neonatal intestinal mucosa mixed with mesenchymal fibroblasts was developed as an air-liquid interface culture in 2009 by Ootani et al (Date and Sato, 2015; Ootani et al., 2009). More recently, a long lasting mini-gut organoid culture was developed for mouse ISCs (Intestinal stem cells), wherein the culture can be derived from a single intestinal stem cell without mesenchymal fibroblasts or other cells (Date and Sato, 2015). The mini-gut organoids culture is maintained in a mesenchymal-free environment comprising Matrigel and intestinal stem cell niche factors such as EGF, Wnt3a, Noggin and R-spondin. This mini-gut organoid recapitulates in vivo intestinal hierarchal organization and normal self-renewal and differentiation: single stem

cells initially form villus-like cystic structures and subsequently the cysts forms crypt-like budding structures. Intestinal stem cells and Paneth cells reside at the tip of the budding structure and differentiating cells migrate toward the central cystic structure recapitulating the normal process of self-renewal and differentiation of intestinal stem cells and epithelial cells.

1.5 Summary of dissertation

In this dissertation, I describe in Chapter 2, mutual exclusivity between *BRAF* mutation an *APC* mutations in CRCs based on my analysis of The Cancer Genome Atlas(TCGA) CRC database and previously published data(Cancer Genome Atlas, 2012; Jorissen et al., 2015). Unlike *KRAS* mutations, *BRAF* mutations have a tendency towards being mutually exclusive with *APC* mutations in CRCs. As discussed earlier, the latter are the main drivers of Wnt activation in CRC . In Chapter 3, I show how *BRAF* mutations, in contrast to *KRAS* mutations, induce stem cell niche factor independent growth and tumorigenic transformation in mouse proximal colon organoids without engineering a concurrent *APC* mutation. This *BRAF* mutation induced single-step transformation starkly contrasts with previous studies showing requirement of multiple genetic hits, including APC disruption, for *KRAS* mutation to drive tumorigenesis (Drost et al., 2015). Upon induction, both $BRAF^{V600E}$ mutation and $KRAS^{G12D}$ mutation promoted sphere formation which is the same phenotype as described in *APC* mutant organoids. Furthermore, only $BRAF^{V600E}$ mutant organoids gained independency in growth from having to add stem cell niche

factors such as EGF, Wnt3a, R-spondin and Noggin and tumorigenicity in Xenograft assays without any concurrent *APC* mutations. Molecular analysis revealed $BRAF^{V600E}$ mutant organoids autonomously activate Wnt signaling and stem cell signaling without external signaling from stem cell niche factors. Methylation analysis revealed the $BRAF^{V600E}$ organoids to have the CpG Island Methylator Phenotype (CIMP) with the genes affected by increased DNA methylation in promoter CpG islands including multiple Wnt negative regulator genes and genes that would normally cause senescence and blunt stem cell activity, and that would normally induce and maintain differentiation. These findings strongly suggest that the abnormal methylation plays an important role in the autonomous activation of Wnt and stem cell signaling pathways. Finally, b-catenin mutations were observed in two of the $BRAF^{V600E}$ mutant organoids indicating that $BRAF^{V600E}$ activation can lead to selection for genetic changes which foster Wnt-independency and cooperate with the epigenetic alterations.

Figure 1.1

A

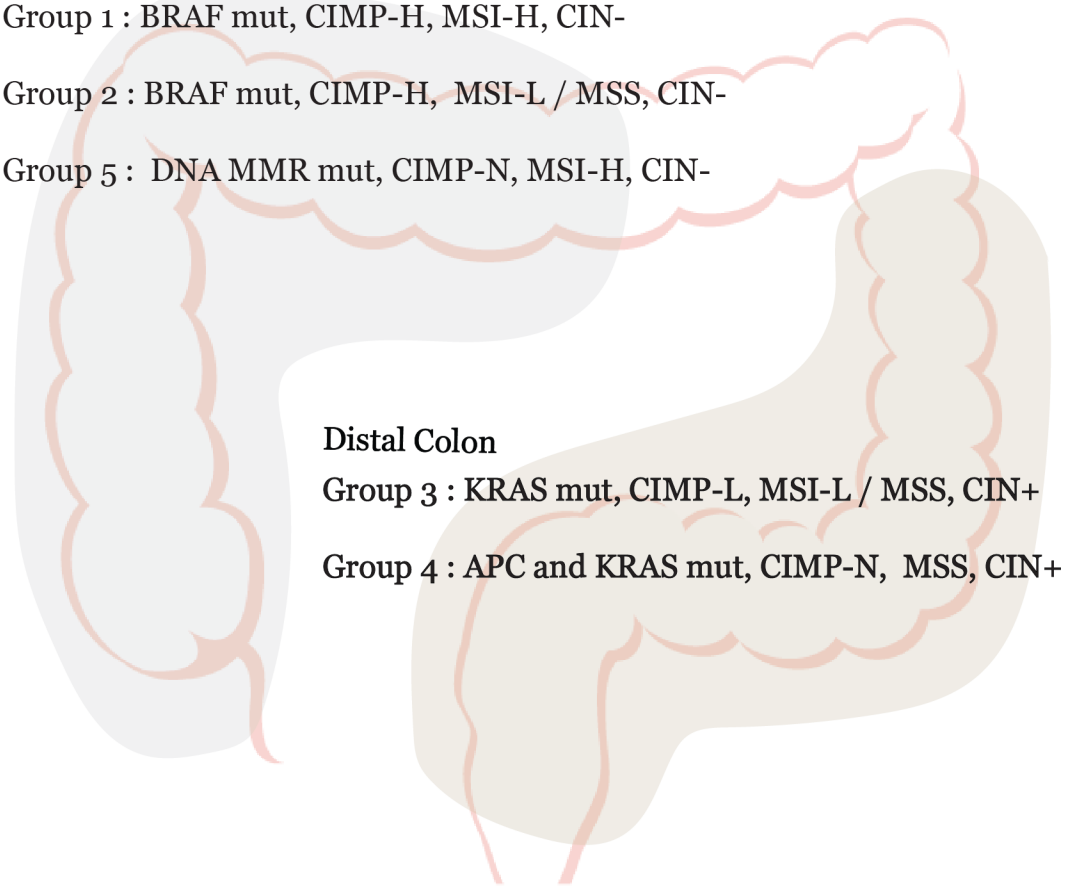
Proximal Colon
Group 1 : BRAF mut, CIMP-H, MSI-H, CIN-
Group 2 : BRAF mut, CIMP-H, MSI-L / MSS, CIN-
Group 5 : DNA MMR mut, CIMP-N, MSI-H, CIN-
Distal Colon
Group 3 : KRAS mut, CIMP-L, MSI-L / MSS, CIN+
Group 4 : APC and KRAS mut, CIMP-N, MSS, CIN+

Figure 1.1 Molecular subtypes of CRCs

(CIMP: CpG Island Methylator Phenotype, MSI: Microsatellite Instability, MSS: Microsatellite Stable, CIN: Chromosomal Instability)

Figure 1.2

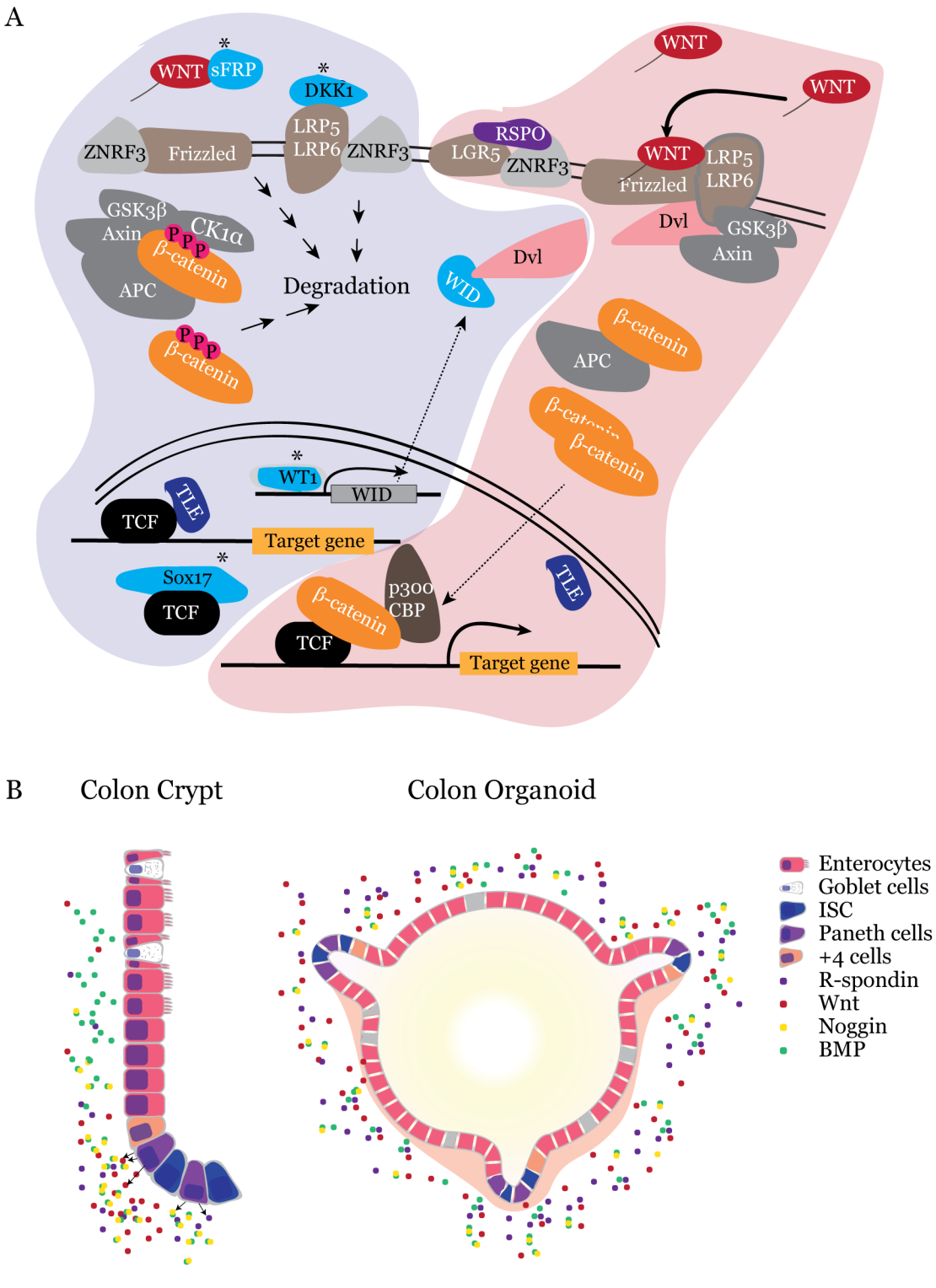
A
WNT
sFRP
DKK1
LRP5
LRP6
ZNRF3
Frizzled
RSPO
LGR5
GSK3β
Axin
CK1α
β-catenin
APC
Degradation
Dvl
WID
WT1
TCF
TLE
Target gene
Sox17
p300
CBP
B
Colon Crypt
Colon Organoid
Enterocytes
Goblet cells
ISC
Paneth cells
+4 cells
R-spondin
Wnt
Noggin
BMP

Figure 1.2 Summary of Wnt pathways and the cellular hierarchy and stem cell niche factors in colon crypts and colon organoids

(A) Red shade represents Wnt activation by Wnt ligands. As Wnt ligands bind to their receptor, Frizzled and LRP5/6, their cytosolic domains induce dissociation of β-catenin destruction complexes by sequestering their key components such as DVL, GSK3β, and AXIN. Therefore, β-catenins are protected from phosphorylation by GSK3β and subsequent degradation by uniquitin-proteasome pathway. Eventually, non-phosphorylated β-catenins are translocated to nucleus and activate its target gene expression in corporation with TCF. Purple shade represents a situation where Wnt ligand is not present or the Wnt pathway is negatively regulated by Wnt negative regulators. When Wnt ligands are not present, β-catenin destruction complex sequestrate β-catenins and subsequently induce their degradation through ubiquitin-protease pathway. The lack of β-catenin in the nucleus let TLE bind to TCF and suppress expression of Wnt target genes. There are several Wnt negative regulators. SFRP inhibits at the level of Wnt ligands through direct binding and sequestration of them. On the other hands, DKK binds to Wnt ligand receptor, LRP5/6 and Frizzled proteins and, therefore, inhibit their interaction with Wnt ligands. WT1 induces expression of WID, which is antagonist of Dvl. Sox17 is an antagonist of TCF though direct binding. (B) Colon crypt is consist of intestinal stem cells (ISC), Paneth cells, +4 cells, and differentiated enterocytes. The self-renewing ISCs reside at the bottom of the crypt and their progenies migrate upward along the crypt. The maintenance of this cellular hierarchy is highly regulated by the stem cell niche

factors such as Wnt3a, RSPO and Noggin and differentiation factors BMP. Colon organiod maintains the same cellular hierarchy. The ISC reside at the tip of budding structures that grow out from the central cystic structure. The differentiating enterocyte migrates toward the central cystic structure.

Chapter 2: Mutual exclusivity between *BRAF* and *APC* mutations in colorectal cancers

2.1 Introduction

APC mutations are regarded as the main driver genetic alterations in CRCs. In fact, these are one of the earliest events in many CRCs and one of the most prevalent mutations in these cancers (Jorissen et al., 2015). The majority of *APC* mutations are frameshift or nonsense mutations, which results in the loss of APC function, disruption of the destruction complex for beta catenin leading to accumulation of this protein and Wnt activation(Fearon, 2011). In the tumors with *APC* mutations, aberrant Wnt activation is observed early on at the low-grade adenoma stage and in the majority of the cells. Mouse models with *APC* mutations develop adenomas in the small and large intestine with hyperactivation of Wnt signaling (Fearon, 2011). Germline mutations of the *APC* gene also cause familial adenomatous polyposis (FAP) syndrome in humans which is characterized by increased incidence of polyp formation in the colon and increased predisposition to CRC development.

BRAF^{V600E} also has been considered as a driver mutation in a subtype of CRCs. The tumors with *BRAF*^{V600E} tend to have a sessile serrated polyp as a precursor lesion (Ensari et al., 2010; Kambara et al., 2004; Makinen, 2007; Minoo et al., 2007; Snover, 2011; Vakiani and Yantiss, 2009; Yang et al., 2004), mucinous adenocarcinoma as a histopathological type (Ensari et al., 2010;

Kambara et al., 2004; Makinen, 2007; Minoo et al., 2007; Snover, 2011; Vakiani and Yantiss, 2009; Yang et al., 2004) and have the CpG Island Methylator Phenotype(CIMP)-high and microsatellite instability as molecular features (Hinoue et al., 2009; Ogino et al., 2006). Despite having different histopathological and molecular features, *BRAF* mutant tumors also have increasing levels of Wnt activation as do the *APC* mutant tumors (Murakami et al., 2015). However, unlike for the more rapid increase of Wnt activation in *APC* mutant tumors, *BRAF* tumors undergo gradual increase of Wnt activity as they progress from low to high grade. The same gradual increase of Wnt activity is also observed in mouse intestinal tumors driven by *BRAF* mutation (Rad et al., 2013). In addition, the increase of Wnt activity is associated with increase of DNA methylation in promoter regions of Wnt negative regulators such as AXIN2, SFRP1, SFRP2, and SFRP4 but not with loss of APC expression. It is proposed that epigenetic silencing of these Wnt negative regulators could be the main driver of Wnt activation in the BRAF mutant tumors rather than *APC* mutations (Lee et al., 2008; Nosho et al., 2008; Suva et al., 2013; Toyota et al., 1999). There are only a few studies formally investigating these above relationships between *APC* and *BRAF* mutations although it is widely accepted that *KRAS* and *APC* mutations co-occur in vast majority of CRCs. In this chapter, I will discuss the relationships between *APC* and *BRAF* mutations and the unique molecular features of *BRAF* mutant tumors based on data from The Cancer Genome Atlas (TCGA) database and an Australian cohort database.

2.2 Results

2.2.1 *APC* and *BRAF* mutations have a tendency to be mutually exclusive in an Australian CRC cohort

A recent study of an Australian CRC patient cohort included the mutation status of 746 colorectal tumors (Jorissen et al., 2015). Using the data, we examined the relationships between major driver mutations including *BRAF*, *KRAS* and *APC* in the above CRCs. Among 746 tumors, 67 have *BRAF* mutations and only 14 of the 67 tumors have *APC* mutations at the same time. The Fisher's exact test revealed a strong tendency toward mutual exclusivity with Odds Ratio (OR) of 0.09782335 and p-value less than 2.2e-16 (Figure 2.1A) (Gao et al., 2013). Among the same cohort, 262 tumors harbor *KRAS* mutations and 211 out of 262 tumors have concurrent *APC* mutations. Fisher's test showed a tendency toward co-occurrence with OR of 2.556757 and p-value of 1.096e-07 (Gao et al., 2013).

2.2.2. *APC* and *BRAF* mutations also have a tendency to be mutually exclusive in the TCGA CRC cohort

Mutational status of *APC*, *KRAS* and *BRAF*, CIMP status, microsatellite instability(MSI) status, hyerpmutator phenotype, anatomic location and histopathological type of CRCs in the TCGA cohort were retrieved from the TCGA data(Table 2.1) (Cancer Genome Atlas, 2012). As previously reported (Guinney et al., 2015; Hinoue et al., 2009; Hughes et al., 2012; Jass, 2007; Lee et al., 2008; Li

and Lai, 2009; Makinen, 2007; Morkel et al., 2015; Nosho et al., 2008; O'Brien et al., 2006; Ogino et al., 2006; Treanor and Quirke, 2007; Vakiani and Yantiss, 2009; Weisenberger et al., 2006; Yamamoto et al., 2012), *BRAF* mutant tumors are associated with CIMP-H and MSI-H and *KRAS* tumors with CIMP-L and MSS (Figure 2.2) consistent with data from other cohorts.

Among 224 tumors, 21 have *BRAF* mutations and only 8 of the 21 tumors have *APC* mutations at the same time. The Fisher's exact test revealed some tendency toward mutual exclusivity with OR of 0.1388884 and p-value less than 4.25e-05 (Figure 2.3A) (Gao et al., 2013). Among the same cohort, 94 tumors harbor *KRAS* mutations and 80 out of 94 tumors have concurrent *APC* mutations. Fisher's test showed a tendency toward co-occurrence with OR of 2.181095 and p-value of 2.3e-02 (Gao et al., 2013).

In addition, *BRAF* mutant tumors in this cohort tend to have less homozygous *APC* loss (2 out of 8 tumors), which accounts for more than half of the *APC* mutations in *KRAS* mutant tumors (40 out of 77 tumors) and tumors without mutations in *BRAF* and *KRAS* (51 out of 85 tumors) (Table 2.1 and Figure 2.4). Pearson Chi square test revealed that *BRAF* mutant tumors positively associate with wild type *APC* and negatively associate with homozygous *APC* loss.

2.3 Discussion

As discussed in chapter one, among CRC, there are different disease entities rather than one(Guinney et al., 2015; Hughes et al., 2012; Jass, 2007; Lee

et al., 2008; Li and Lai, 2009; Makinen, 2007; Morkel et al., 2015; Nosho et al., 2008; O'Brien et al., 2006; Ogino et al., 2006; Treanor and Quirke, 2007; Vakiani and Yantiss, 2009; Weisenberger et al., 2006; Yamamoto et al., 2012). Among those groups, Group 1 and 2 have a tendency to have mutations in *BRAF* not in *APC* (Figure 1.1). It has been proposed that in these latter tumors epigenetic modulation of the Wnt pathway replaces the role of *APC* mutations. However, the exact process has not been modeled and yet proven. Even the relationships between *BRAF* mutations and *APC* mutations has not been well studied. In this chapter, the association studies with the Australian and TCGA CRC cohorts revealed a negative correlation between *BRAF* and *APC*. Although there is difference in the strength of tendency and significance, both cohorts suggest a mutual exclusivity implicating *BRAF* mutations may not require concurrent *APC* mutations to initiate and drive progression of CRCs in contrast to CRCs with *KRAS* mutations, which appear to require Wnt-activation by *APC* mutations for progression. How *BRAF* mutations drive tumorigenesis without a preceding requirement for Wnt-activation by *APC* mutations will be discussed in detail in Chapter 3 with new evidence discovered through modeling of the *BRAF* mutant CRCs in organoid culture.

2.4 Material and Methods

2.4.1 Analysis of TCGA CRCs

Mutation, CIMP phenotype, MSI status, MLH1 methylation, hypermutator phenotype, anatomic location, histopathologic type and patient's gender were acquired from supplementary data from a previously published article (Cancer Genome Atlas, 2012). The associations were evaluated by Fisher's exact test or Chi square test.

2.4.2 Analysis of Australian CRCs

The mutational information of CRC in the Australian cohort was acquired from a previously reported article (Jorissen et al., 2015). The associations were evaluated by Fisher's exact test or Chi square test.

Table 2.1

Patient	APC1	APC2	BRAF	KRAS	CIMP	MLH1	MSI	HM	Location	Type	Gender
TCGA-AG-A002	R1432X	E1518X	F247L		Cluster3	-	MSS	HM	rectum	ADC	M
TCGA-AA-A00D	R546X	R1432X	V600E		CIMP-H	-	MSS	nHM	Rt colon	ADC	M
TCGA-AA-3715	A1089V		V600E	G12D	CIMP-H	Me	MSI-H	HM	Rt colon	ADC	M
TCGA-AA-3947	E829fs		V600E		CIMP-H	Me	MSI-H	HM	Rt colon	Muc	F
TCGA-AA-A00J	R536X		V600E		CIMP-H	Me	MSI-H	HM	Rt colon	Muc	M
TCGA-AA-A01D	deletion		V600E		CIMP-L	-	MSS	nHM	Lf colon	Muc	F
TCGA-AA-3684	E966X		V600E		CIMP-L	-	MSS	nHM	Rt colon	Muc	F
TCGA-AG-3578	deletion		V600E		Cluster3	-	MSS	nHM	rectum	Muc	F
TCGA-AA-3664			V600E		CIMP-H	-	MSS	nHM	Rt colon	ADC	F
TCGA-AA-3833			V600E		CIMP-H	Me	MSI-H	HM	Rt colon	ADC	F
TCGA-AA-A01P			V600E		CIMP-H	Me	MSI-H	HM	Rt colon	ADC	F
TCGA-AA-A022			V600E		CIMP-H	Me	MSI-H	HM	Rt colon	ADC	F
TCGA-AA-3525			V600E		CIMP-H	Me	MSI-H	HM	Rt colon	ADC	M
TCGA-A6-2676			V600E		CIMP-H	Me	MSI-H	HM	Rt colon	Muc	F
TCGA-AA-3516			V600E		CIMP-H	Me	MSI-H	HM	Rt colon	Muc	F
TCGA-AA-3821			V600E		CIMP-H	Me	MSI-H	HM	Rt colon	Muc	F
TCGA-AA-3949			V600E		CIMP-H	Me	MSI-H	HM	Rt colon	Muc	F
TCGA-AA-3543			V600E		CIMP-H	Me	MSI-H	HM	Rt colon	Muc	M
TCGA-A6-2672			V600E		CIMP-H	Me	MSI-H	HM	Tr colon	ADC	F
TCGA-AA-3877			V600E		CIMP-H	Me	MSI-H	HM	Tr colon	Muc	F
TCGA-AA-3966			V600E		CIMP-L	Me	MSI-H	HM	Rt colon	Muc	F
TCGA-AA-A00A	E1560fs	V291fs		G12D	CIMP-H	-	MSI-H	HM	Rt colon	ADC	M
TCGA-AG-A02X	E1291X	deletion		Q61L	CIMP-H	-	MSS	nHM	rectum	ADC	M
TCGA-AA-A03F	R787X	R1432X		G12D	CIMP-H	-	MSS	nHM	Rt colon	Muc	F
TCGA-AA-3837	Q1276X	E190fs		G12V	CIMP-H	-	MSS	nHM	Rt colon	Muc	M
TCGA-AA-3994	R787X	T1469fs		G12D	CIMP-H	-	MSS	nHM	Tr colon	Muc	M
TCGA-AA-A01R	R858X	R1432X		G13D	CIMP-L	-	MSI-H	HM	Rt colon	Muc	M
TCGA-AA-3680	S1145fs	E1555fs		G13D	CIMP-L	-	MSI-L	nHM	Rt colon	ADC	F
TCGA-AA-3930	R1432X	S945fs		G12D	CIMP-L	-	MSI-L	nHM	Rt colon	ADC	M
TCGA-AA-3555	R499X	R1450X		A146T	CIMP-L	-	MSS	HM	Rt colon	Muc	F
TCGA-AA-3848	R216X	deletion		G12D	CIMP-L	-	MSS	nHM	Lf colon	ADC	F
TCGA-AA-3558	R554X	Q1378X		G12V	CIMP-L	-	MSS	nHM	Lf colon	ADC	M
TCGA-AG-3599	C507X	R1432X		G12D	CIMP-L	-	MSS	nHM	rectum	NA	M
TCGA-AA-3681	R906X	R1432X		A146T	CIMP-L	-	MSS	nHM	Rt colon	ADC	F
TCGA-AA-3695	R223X	deletion		G12D	CIMP-L	-	MSS	nHM	Rt colon	ADC	F
TCGA-AA-3818	S1393fs	S960fs		G12D	CIMP-L	-	MSS	nHM	Rt colon	ADC	F
TCGA-AA-3522	C1392X	deletion		G12C	CIMP-L	-	MSS	nHM	Rt colon	ADC	M
TCGA-AA-3864	R330X	R1432X		G12D	Cluster3	-	MSI-H	HM	Rt colon	ADC	M
TCGA-AA-3977	R1096X	E1291X		K117N	Cluster3	-	MSS	HM	Lf colon	ADC	M
TCGA-AA-A01K	R858X	Q1411X		G12V	Cluster3	-	MSS	nHM	Lf colon	ADC	F
TCGA-AA-3521	L1471X	deletion		Q61L	Cluster3	-	MSS	nHM	Lf colon	ADC	M
TCGA-AG-3909	V812fs	1275fs		A146T	Cluster3	-	MSS	nHM	rectum	ADC	F
TCGA-AG-3999	E200X	deletion		G12S	Cluster3	-	MSS	nHM	rectum	ADC	F
TCGA-AG-3726	Q649X	S1264X		G12V	Cluster3	-	MSS	nHM	rectum	ADC	F
TCGA-AG-A00C	E1191X	E1379X		G12V	Cluster3	-	MSS	nHM	rectum	ADC	F
TCGA-AG-3611	G549X	deletion		A146V	Cluster3	-	MSS	nHM	rectum	ADC	M
TCGA-AG-4005	S1180X	Q1310X		G12V	Cluster3	-	MSS	nHM	rectum	ADC	M
TCGA-AG-3586	S752X	Y938C		G12V	Cluster3	-	MSS	nHM	rectum	NA	F
TCGA-AA-3851	R1432X	deletion		G12D	Cluster3	-	MSS	nHM	Rt colon	ADC	M
TCGA-AA-3939	Q524X	R1432X		G12D	Cluster3	-	MSS	nHM	Rt colon	ADC	M
TCGA-AA-3986	deletion	deletion		A146T	Cluster3	-	MSS	nHM	Tr colon	ADC	M
TCGA-AA-A00N	S1263X	E1390X		G13D	Cluster4	-	MSI-L	HM	Rt colon	Muc	M
TCGA-AA-A02W	R858X/E1356X	deletion		G12C	Cluster4	-	MSI-L	nHM	Lf colon	ADC	F
TCGA-AG-3892	R1096X	N1143K		E98X	Cluster4	-	MSS	HM	rectum	ADC	F
TCGA-AA-3975	R481X	E1288X		K68N	Cluster4	-	MSS	nHM	Lf colon	ADC	M
TCGA-AG-A032	R284X	E1304X		G12C	Cluster4	-	MSS	nHM	rectum	ADC	M
TCGA-AG-3887	Q1242X	1291fs		G12D	Cluster4	-	MSS	nHM	rectum	Muc	M

Table 2.1 (Continued)

Patient	APC1	APC2	BRAF	KRAS	CIMP	MLH1	MSI	HM	Location	Type	Gender
TCGA-AA-3530	Q1451X	deletion		G12V	Cluster4	-	MSS	nHM	Rt colon	ADC	M
TCGA-AG-A02N	R232X	R1432X		A146T	NA	NA	MSI-H	HM	rectum	ADC	M
TCGA-AG-A01W	R858X	deletion		G13D	NA	NA	MSS	nHM	rectum	ADC	F
TCGA-AG-A020	R1432X	Q1244fs		G12V	NA	NA	MSS	nHM	rectum	Muc	F
TCGA-AA-A029	Y935fs			G12V	CIMP-H	-	MSI-L	nHM	Rt colon	ADC	M
TCGA-AA-A02O	T1283fs			G12D	CIMP-H	-	MSS	nHM	Tr colon	ADC	M
TCGA-AA-3870	R858X			G12D	CIMP-H	Me	MSS	nHM	Rt colon	ADC	F
TCGA-AA-3854	S1380fs			G12V	CIMP-L	-	MSI-L	nHM	Lf colon	Muc	F
TCGA-A6-2683	deletion			G12V	CIMP-L	-	MSI-L	nHM	Rt colon	ADC	M
TCGA-AA-3852	S1403fs			G12A	CIMP-L	-	MSI-L	nHM	Tr colon	Muc	M
TCGA-AA-A00Q	deletion			G12D	CIMP-L	-	MSS	nHM	Lf colon	ADC	F
TCGA-AA-3979	Q739X			A146T	CIMP-L	-	MSS	nHM	Lf colon	ADC	M
TCGA-AA-A01I	Y917X			G12V	CIMP-L	-	MSS	nHM	Lf colon	ADC	M
TCGA-AA-3556	Y917X			G12R	CIMP-L	-	MSS	nHM	Lf colon	NA	M
TCGA-AF-2691	S1328X			G12D	CIMP-L	-	MSS	nHM	rectum	ADC	F
TCGA-AG-3605	Q1360X			G13D	CIMP-L	-	MSS	nHM	rectum	ADC	F
TCGA-AG-3878	S578X			G12D	CIMP-L	-	MSS	nHM	rectum	ADC	M
TCGA-AG-3902	G1270X			G13D	CIMP-L	-	MSS	nHM	rectum	ADC	M
TCGA-AA-A01Z	P1453fs			G12D	CIMP-L	-	MSS	nHM	Rt colon	ADC	M
TCGA-AA-3673	K975X			G12D	CIMP-L	-	MSS	nHM	Tr colon	ADC	F
TCGA-AA-A00K	Q1349X			G12V	Cluster3	-	MSI-L	nHM	Lf colon	ADC	M
TCGA-AA-A01F	R827H			G12V	Cluster3	-	MSS	nHM	Lf colon	ADC	M
TCGA-AG-3896	R858X			G12C	Cluster3	-	MSS	nHM	rectum	ADC	F
TCGA-AG-3602	S1328X			G12D	Cluster3	-	MSS	nHM	rectum	ADC	F
TCGA-AG-A015	E1268X			G12D	Cluster3	-	MSS	nHM	rectum	ADC	F
TCGA-AG-3727	E1277X			G13D	Cluster3	-	MSS	nHM	rectum	ADC	F
TCGA-AG-A025	Q1360fs			Q22K	Cluster3	-	MSS	nHM	rectum	ADC	F
TCGA-AG-3580	E1239X			G12D	Cluster3	-	MSS	nHM	rectum	ADC	M
TCGA-AG-4008	deletion			G12L	Cluster3	-	MSS	nHM	rectum	ADC	M
TCGA-AG-3581	R546X			G13D	Cluster3	-	MSS	nHM	rectum	ADC	M
TCGA-AG-3901	M1413fs			A146T	Cluster3	-	MSS	nHM	rectum	Muc	F
TCGA-AG-3594	1219fs			G12V	Cluster3	-	MSS	nHM	rectum	Muc	M
TCGA-AA-3548	R787X			G12D	Cluster3	-	MSS	nHM	Rt colon	ADC	F
TCGA-AA-3814	E1390X			G12S	Cluster3	-	MSS	nHM	Rt colon	ADC	F
TCGA-AA-3561	R858X			G12D	Cluster3	-	MSS	nHM	Rt colon	ADC	M
TCGA-AG-3583	Q173X			G12D	Cluster4	-	MSI-L	nHM	rectum	Muc	M
TCGA-AA-3696	S1385fs			G12C	Cluster4	-	MSS	nHM	Lf colon	ADC	F
TCGA-AA-3532	Q636X			G12D	Cluster4	-	MSS	nHM	Lf colon	ADC	M
TCGA-AG-A014	E1191X			G12S	Cluster4	-	MSS	nHM	rectum	ADC	M
TCGA-AG-A008	K1067X			G12V	Cluster4	-	MSS	nHM	rectum	Muc	F
TCGA-AF-2692	S695X			G12V	Cluster4	-	MSS	nHM	rectum	NA	F
TCGA-AG-3575				G12V	CIMP-H	-	MSS	nHM	rectum	ADC	M
TCGA-AA-3845				Q61K	CIMP-H	Me	MSI-H	HM	Rt colon	NA	F
TCGA-AA-3672				Q61K	CIMP-H	Me	MSI-H	HM	Tr colon	ADC	F
TCGA-AA-A01G				K117N	CIMP-L	-	MSI-L	nHM	Rt colon	Muc	M
TCGA-AA-A03J				G12C	CIMP-L	-	MSS	nHM	Lf colon	ADC	F
TCGA-AA-3842				G13D	CIMP-L	-	MSS	nHM	Lf colon	ADC	M
TCGA-AF-2689				G13D	CIMP-L	-	MSS	nHM	rectum	ADC	F
TCGA-AA-A02Y				G12V	CIMP-L	-	MSS	nHM	Rt colon	ADC	M
TCGA-AA-3520				G12V	Cluster3	-	MSI-L	nHM	Rt colon	ADC	F
TCGA-AA-3560				G12D	Cluster3	-	MSS	nHM	Lf colon	ADC	F
TCGA-AA-A01X				G12V	Cluster3	-	MSS	nHM	Lf colon	ADC	F
TCGA-AG-A00H				A146T	Cluster4	-	MSS	nHM	rectum	ADC	M
TCGA-AA-3710	A209V	I1236N			CIMP-H	Me	MSI-H	HM	Rt colon	ADC	F
TCGA-AA-A01Q	R546X	I2497V			CIMP-L	-	MSI-H	HM	Rt colon	ADC	F
TCGA-AG-4007	Q1285X	E1361X			CIMP-L	-	MSI-L	nHM	rectum	ADC	M
TCGA-AG-3598	R216X	R232X			CIMP-L	-	MSS	nHM	rectum	ADC	M

Table 2.1 (Continued)

Patient	APC1	APC2	BRAF	KRAS	CIMP	MLH1	MSI	HM	Location	Type	Gender
TCGA-AG-A011	K652X	Q1388X			CIMP-L	-	MSS	nHM	rectum	ADC	M
TCGA-AG-3881	Q1349X	deletion			CIMP-L	-	MSS	nHM	rectum	NA	F
TCGA-AA-A01V	R1432X	S1401N			CIMP-L	-	MSS	nHM	Rt colon	ADC	M
TCGA-AA-A00U	R858X	R1432X			CIMP-L	-	MSS	nHM	Rt colon	ADC	M
TCGA-AA-3982	R284X	R1432X			Cluster3	-	MSI-L	nHM	Lf colon	ADC	M
TCGA-AA-3866	Q1017X	deletion			Cluster3	-	MSI-L	nHM	Rt colon	ADC	F
TCGA-AA-A02H	H289fs	deletion			Cluster3	-	MSS	nHM	Lf colon	ADC	F
TCGA-AA-3976	Q883X	M1395fs			Cluster3	-	MSS	nHM	Lf colon	ADC	M
TCGA-A6-2670	E1353X	deletion			Cluster3	-	MSS	nHM	Lf colon	ADC	M
TCGA-AA-3562	R481X	deletion			Cluster3	-	MSS	nHM	Lf colon	ADC	M
TCGA-AA-3858	V1334fs	deletion			Cluster3	-	MSS	nHM	Lf colon	ADC	M
TCGA-AA-3544	Q960X	S1328X			Cluster3	-	MSS	nHM	Lf colon	ADC	M
TCGA-AG-A01L	S836fs	deletion			Cluster3	-	MSS	nHM	rectum	ADC	M
TCGA-AG-3890	T916fs	deletion			Cluster3	-	MSS	nHM	rectum	ADC	M
TCGA-AG-3898	R787X/Q1023E	deletion			Cluster3	-	MSS	nHM	rectum	ADC	M
TCGA-AG-A026	C1252X	deletion			Cluster3	-	MSS	nHM	rectum	ADC	M
TCGA-AA-3519	R216X	E1288X			Cluster3	-	MSS	nHM	rectum	ADC	M
TCGA-AA-3552	R1432X	deletion			Cluster3	-	MSS	nHM	Rt colon	ADC	M
TCGA-AA-A010	R1432X	A513V			Cluster4	-	MSI-L	HM	Tr colon	ADC	F
TCGA-AA-3553	S1297X	deletion			Cluster4	-	MSI-L	nHM	Lf colon	ADC	F
TCGA-AA-A00O	Q1349X	deletion			Cluster4	-	MSI-L	nHM	Lf colon	ADC	F
TCGA-AA-3531	R232X	Q1134X			Cluster4	-	MSI-L	nHM	Lf colon	ADC	F
TCGA-AA-3667	R546X	S1382X			Cluster4	-	MSI-L	nHM	Lf colon	ADC	F
TCGA-AA-3973	R265X	Q1360X			Cluster4	-	MSI-L	nHM	Lf colon	ADC	M
TCGA-AA-3688	E923X	deletion			Cluster4	-	MSI-L	nHM	Lf colon	ADC	M
TCGA-AA-3692	R787X	E1356X			Cluster4	-	MSI-L	nHM	Lf colon	Muc	F
TCGA-AG-3601	Q246X/S1297X	deletion			Cluster4	-	MSI-L	nHM	rectum	ADC	M
TCGA-AA-3984	R1096X	F2766C			Cluster4	-	MSS	HM	Lf colon	ADC	F
TCGA-AA-A02F	L478fs	G1312fs			Cluster4	-	MSS	nHM	Lf colon	ADC	F
TCGA-AA-3538	K921X	deletion			Cluster4	-	MSS	nHM	Lf colon	ADC	F
TCGA-AA-3678	1293fs	deletion			Cluster4	-	MSS	nHM	Lf colon	ADC	F
TCGA-AA-3812	S1403fs	V539A			Cluster4	-	MSS	nHM	Lf colon	ADC	F
TCGA-AA-3860	L235X	Q1320X			Cluster4	-	MSS	nHM	Lf colon	ADC	F
TCGA-AA-A02J	R223X	T1380fs			Cluster4	-	MSS	nHM	Lf colon	ADC	F
TCGA-AA-3542	E1356X	deletion			Cluster4	-	MSS	nHM	Lf colon	ADC	M
TCGA-AA-3872	T1420fs	deletion			Cluster4	-	MSS	nHM	Lf colon	ADC	M
TCGA-AA-3679	R216X	1289fs			Cluster4	-	MSS	nHM	Lf colon	ADC	M
TCGA-AA-3685	Q960X	K1352X			Cluster4	-	MSS	nHM	Lf colon	ADC	M
TCGA-AG-3612	Q1388X	deletion			Cluster4	-	MSS	nHM	rectum	ADC	F
TCGA-AG-3882	V579fs	deletion			Cluster4	-	MSS	nHM	rectum	ADC	F
TCGA-AG-4015	Y1358X	deletion			Cluster4	-	MSS	nHM	rectum	ADC	F
TCGA-AG-3609	Q1349X	Y1165X			Cluster4	-	MSS	nHM	rectum	ADC	F
TCGA-AG-A02G	R223X	deletion			Cluster4	-	MSS	nHM	rectum	ADC	M
TCGA-AG-3587	R1096X	E1288X			Cluster4	-	MSS	nHM	rectum	ADC	M
TCGA-AA-A01S	Q394X	R546X			Cluster4	Me	MSI-L	nHM	Lf colon	ADC	F
TCGA-AG-A01Y	Q1276X	deletion			NA	NA	MSS	nHM	rectum	ADC	F
TCGA-AG-A036	R284X	Q1388X			NA	NA	MSS	nHM	rectum	ADC	M
TCGA-AA-3972	E829fs				CIMP-L	-	MSI-L	nHM	Lf colon	ADC	M
TCGA-AA-3855	F1336fs				CIMP-L	-	MSI-L	nHM	Lf colon	ADC	M
TCGA-AG-3584	R1432X				CIMP-L	-	MSS	nHM	rectum	ADC	M
TCGA-AA-3527	Q1210X				CIMP-L	-	MSS	nHM	Rt colon	ADC	F
TCGA-AA-3549	C1392S				CIMP-L	-	MSS	nHM	Rt colon	ADC	M
TCGA-AA-3989	R216X				CIMP-L	-	MSS	nHM	Tr colon	ADC	M
TCGA-AA-A00R	R876X				CIMP-L	Me	MSI-H	HM	Rt colon	ADC	F
TCGA-AA-A024	R387X				Cluster3	-	MSI-L	nHM	Lf colon	Muc	M
TCGA-AA-3846	Q1360X				Cluster3	-	MSS	nHM	Lf colon	ADC	F
TCGA-AA-A01T	R1096X				Cluster3	-	MSS	nHM	Lf colon	ADC	F

Table 2.1 (Continued)

Patient	APC1	APC2	BRAF	KRAS	CIMP	MLH1	MSI	HM	Location	Type	Gender
TCGA-AA-A00F	deletion				Cluster3	-	MSS	nHM	Lf colon	ADC	M
TCGA-AA-A00W	R858X				Cluster3	-	MSS	nHM	Lf colon	ADC	M
TCGA-AY-4071	R1417fs				Cluster3	-	MSS	nHM	NA	NA	F
TCGA-AG-3593	E1335X				Cluster3	-	MSS	nHM	rectum	ADC	F
TCGA-AG-3894	R216X				Cluster3	-	MSS	nHM	rectum	ADC	M
TCGA-AG-3883	R265X				Cluster3	-	MSS	nHM	rectum	ADC	M
TCGA-A6-2677	Q462X				Cluster3	-	MSS	nHM	Rt colon	ADC	F
TCGA-AA-A00L	R1096X				Cluster3	-	MSS	nHM	Tr colon	ADC	M
TCGA-AA-3554	A2028T				Cluster4	-	MSI-H	HM	Rt colon	ADC	F
TCGA-AA-3529	V291fs				Cluster4	-	MSI-L	nHM	Lf colon	ADC	F
TCGA-AG-4001	R858X				Cluster4	-	MSI-L	nHM	rectum	ADC	F
TCGA-A6-3807	R223X				Cluster4	-	MSS	nHM	Lf colon	ADC	F
TCGA-AA-3693	E1277fs				Cluster4	-	MSS	nHM	Lf colon	ADC	F
TCGA-AA-A017	Q1226X				Cluster4	-	MSS	nHM	Lf colon	ADC	F
TCGA-AA-3524	Q215ss				Cluster4	-	MSS	nHM	Lf colon	ADC	M
TCGA-AA-3856	R858X				Cluster4	-	MSS	nHM	Lf colon	ADC	M
TCGA-AA-3952	R223X				Cluster4	-	MSS	nHM	Lf colon	ADC	M
TCGA-AA-3955	M1383fs				Cluster4	-	MSS	nHM	Lf colon	ADC	M
TCGA-AA-A00Z	R216X				Cluster4	-	MSS	nHM	Lf colon	ADC	M
TCGA-A6-2674	R536X				Cluster4	-	MSS	nHM	Lf colon	Muc	M
TCGA-AF-3913	P1301fs				Cluster4	-	MSS	nHM	rectum	ADC	M
TCGA-AG-3893	S1338X				Cluster4	-	MSS	nHM	rectum	ADC	M
TCGA-AF-3400	Q1276X				Cluster4	-	MSS	nHM	rectum	Muc	M
TCGA-AA-3666	F1336fs				Cluster4	-	MSS	nHM	Rt colon	ADC	M
TCGA-AG-3600					CIMP-H	-	MSS	nHM	rectum	ADC	M
TCGA-AA-3518					CIMP-H	Me	MSI-H	HM	Rt colon	ADC	F
TCGA-AA-A00E					CIMP-H	Me	MSI-H	HM	Rt colon	ADC	M
TCGA-AA-A004					CIMP-L	-	MSI-L	nHM	Lf colon	ADC	M
TCGA-AA-3831					CIMP-L	-	MSS	nHM	Lf colon	ADC	M
TCGA-AG-3608					CIMP-L	-	NA	nHM	rectum	ADC	F
TCGA-AA-3819					Cluster3	-	MSI-L	nHM	Lf colon	ADC	F
TCGA-AA-3526					Cluster3	-	MSI-L	nHM	Lf colon	ADC	M
TCGA-AG-3574					Cluster3	-	MSS	nHM	rectum	ADC	F
TCGA-AG-A016					Cluster3	-	MSS	nHM	rectum	ADC	M
TCGA-AA-3514					Cluster3	-	MSS	nHM	Rt colon	ADC	F
TCGA-AA-3534					Cluster3	-	MSS	nHM	Rt colon	ADC	F
TCGA-AA-3875					Cluster3	-	MSS	nHM	Rt colon	ADC	F
TCGA-AY-4070					Cluster3	-	MSS	nHM	Rt colon	ADC	F
TCGA-AA-3956					Cluster3	-	MSS	nHM	Rt colon	ADC	M
TCGA-A6-2678					Cluster3	-	MSS	nHM	Tr colon	ADC	F
TCGA-AA-3517					Cluster4	-	MSI-L	nHM	Lf colon	ADC	M
TCGA-AA-3971					Cluster4	-	MSS	nHM	Lf colon	ADC	M
TCGA-AG-3582					Cluster4	-	MSS	nHM	rectum	ADC	M
TCGA-AA-3869					Cluster4	-	MSS	nHM	Rt colon	ADC	M
TCGA-AA-3941	H1472fs	NA		G12D	CIMP-H	-	MSI-L	nHM	Rt colon	ADC	F
TCGA-A6-3808	R787X	NA		G12D	Cluster3	-	MSI-L	nHM	Rt colon	Muc	M
TCGA-AA-3844		NA		G12V	Cluster3	-	MSS	nHM	Lf colon	ADC	F
TCGA-AG-A00Y		NA		G12D	Cluster3	-	MSS	nHM	rectum	ADC	M
TCGA-AA-3980	R232X	NA			Cluster3	-	MSS	nHM	Lf colon	ADC	F
TCGA-A6-3810	I1286fs	NA			Cluster4	-	MSS	nHM	Lf colon	ADC	M
TCGA-AA-3850		NA			CIMP-L	-	MSS	nHM	Tr colon	ADC	M
TCGA-AA-3867		NA			Cluster4	-	MSS	nHM	Lf colon	ADC	M
TCGA-AA-3811		NA			Cluster4	Me	MSI-H	HM	Rt colon	ADC	F

Table 2.1 Summary of TCGA CRC data for *APC*, *BRAF* and *KRAS* mutations, CpG Island Methylator Phenotype, Microsatellite Instability, anatomic location and histopathology type

Blue color represents APC mutation status. Darkest blue means deletion, lighter blue for frame shift, non-sense or point mutation. Orange and brown stand for *BRAF* and *KRAS* mutations respectively. (Me : methylation, HM: hypermutator, nHM: non-hypermutator, Rt: right, Lf: left, ADC: adenocarcinoma, Muc: mucinous adenocarcinoma, M: male, F: female)

Figure 2.1

A : Australian cohort of 746 cases

	APC Mutant	Wild type *APC*
BRAF mutant	14	53
Wild type *BRAF*	496	183

* Fisher's exact test
p< 2.2e-16, Odd Ratio=0.09782335
*Strong tendency toward mutual exclusivity

B : Australian cohort of 746 cases

	APC Mutant	Wild type *APC*
KRAS mutant	211	51
Wild type *KRAS*	299	185

* Fisher's exact test
p=1.096e-07, Odd Ratio=2.556757
*Tendency toward co-occurence

C

Odd Ratio	**Interpretation**
0 - 0.1	Strong tendency toward mutual exclusivity
0.1 - 0.5	Some tendency towards mutual exclusivity
0.5 - 2	No association
2 - 10	Tendency toward co-occurrence
>10	Strong tendency toward mutual exclusivity

Figure 2.1 *BRAF* and *APC* mutations in 746 CRCs in the Australian cohort have a strong tendency toward mutual exclusivity

(A) Fisher's exact test for an exclusivity / co-occurrence between *BRAF* and *APC*. p-value is lower than 2.2e-16 and odds ratio is 0.09782335. Based on cBioPortal's odds ratio interpretation, there is a strong tendency toward mutual exclusivity between *BRAF* and *APC* mutations in this cohort. (B) Fisher's exact test for an exclusivity / co-occurrence between *KRAS* and *APC*. p-value is 1.096e-07 and odds ratio is 2.556757. Based on cBioPortal's odds ratio interpretation, there is a tendency toward co-occurence between *KRAS* and *APC* mutations in this cohort. (C) Interpretation criteria for odds ratio in cBioPortal (Gao et al., 2013).

Figure 2.2

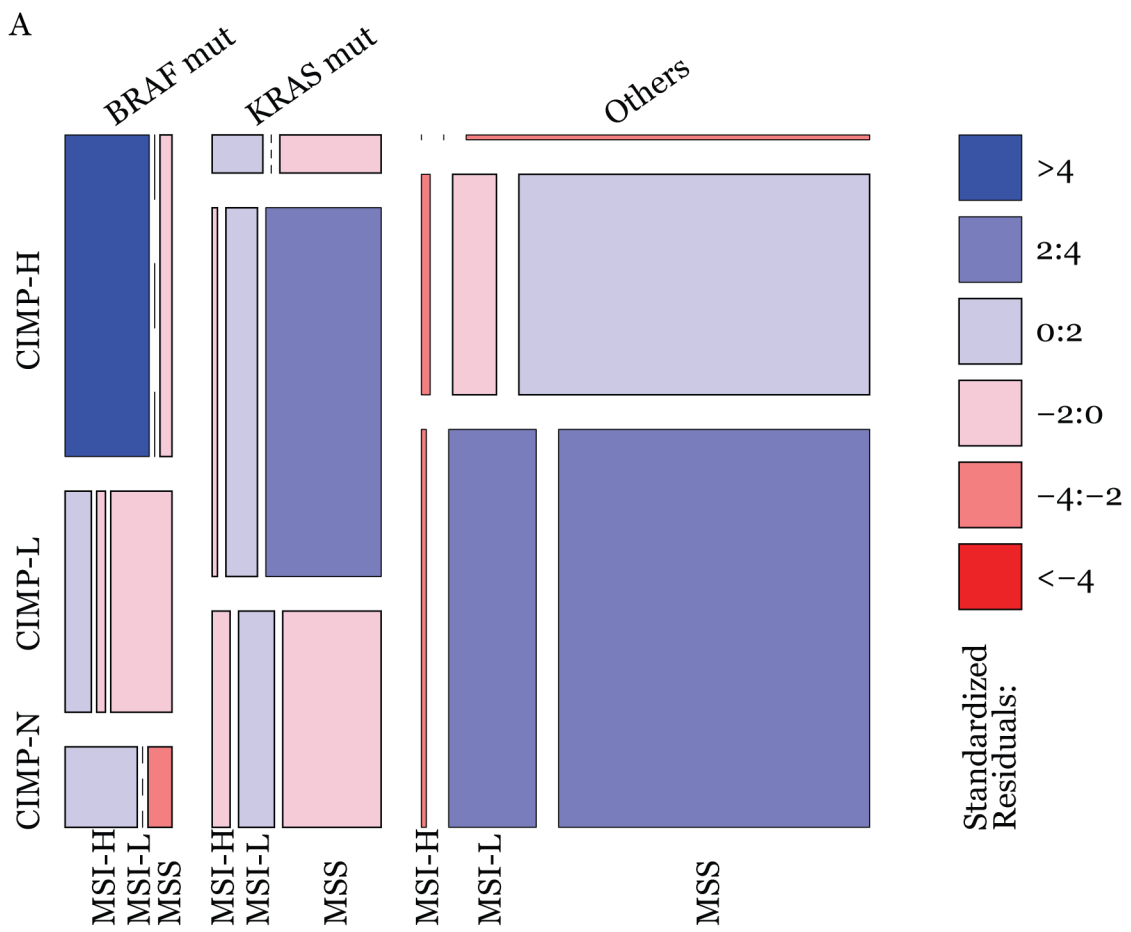
A
BRAF mut
KRAS mut
Others
CIMP-H
CIMP-L
CIMP-N
MSI-H
MSI-L
MSS
MSI-H
MSI-L
MSS
MSI-H
MSI-L
MSS
>4
2:4
0:2
−2:0
−4:−2
<−4
Standardized Residuals:

Figure 2.2 Molecular features of 224 CRC in the TCGA cohort correlate with previous reports on these cancers

(A) Mosaic plot and Pearson Chi square for molecular features such as *BRAF* mutation, CpG Island Methylator Phenotype(CIMP) status and Microsatellite Instability(MSI). As previously reported *BRAF* mutant tumors have a strong association with CIMP-H and MSI-H phenotype and *KRAS* mutant tumors are associated with CIMP-L and MSS phenotype indicating the cohort represents a good spectrum for CRC samples collected.

Figure 2.3

A : TCGA cohort of 224 cases

	APC Mutant	Wild type *APC*
BRAF mutant	8	13
Wild type *BRAF*	166	37

* Fisher's exact test
p= 4.25e-05, Odd Ratio=0.1388884
*Some tendency toward mutual exclusivity

B : TCGA cohort of 224 cases

	APC Mutant	Wild type *APC*
KRAS mutant	80	14
Wild type *KRAS*	94	36

* Fisher's exact test
p=2.3e-02, Odd Ratio=2.181095
*Tendency toward co-occurence

C

Odd Ratio	**Interpretation**
0 - 0.1	Strong tendency toward mutual exclusivity
0.1 - 0.5	Some tendency towards mutual exclusivity
0.5 - 2	No association
2 - 10	Tendency toward co-occurrence
>10	Strong tendency toward mutual exclusivity

Figure 2.3 *BRAF* and *APC* mutations in 224 TCGA CRCs cohorts have some tendency toward mutual exclusivity

(A) Fisher's exact test for an exclusivity / co-occurrence between *BRAF* and *APC* mutations. p-value is 4.25e-05 and odds ratio is 0.1388884. Based on cBioPortal's odds ratio interpretation, there is some tendency toward mutual exclusivity between *BRAF* and *APC* mutations in this cohort. (B) Fisher's exact test for an exclusivity / co-occurrence between *KRAS* and *APC* mutations. p-value is 2.393e-02 and odds ratio is 2.181095. Based on cBioPortal's odds ratio interpretation, there is a tendency toward co-occurence between *KRAS* and *APC* mutations in this cohort. (C) Interpretation criteria for odds ratio in cBioPortal (Gao et al., 2013).

Figure 2.4

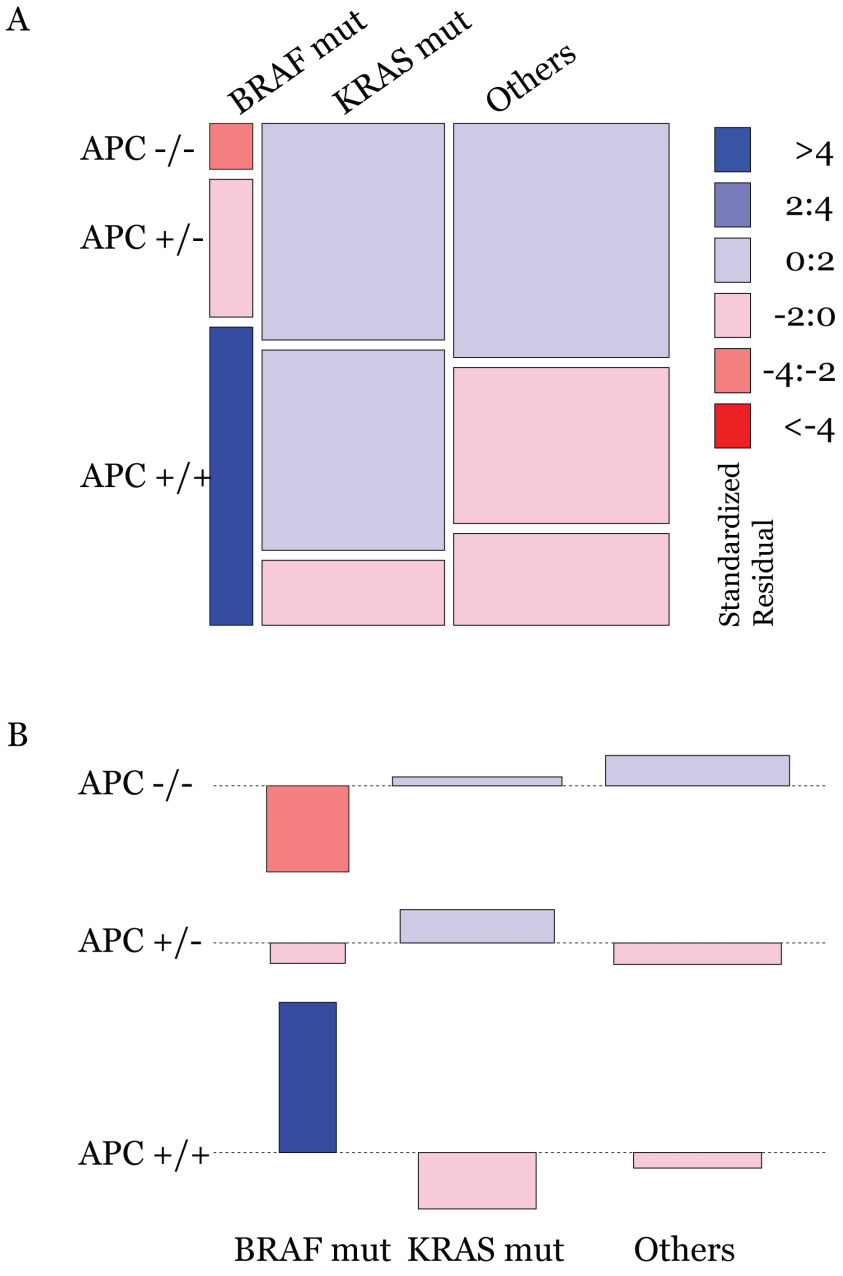
A
BRAF mut
KRAS mut
Others
APC -/-
APC +/-
APC +/+
>4
2:4
0:2
-2:0
-4:-2
<-4
Standardized Residual
B
APC -/-
APC +/-
APC +/+
BRAF mut
KRAS mut
Others

Figure 2.4 *BRAF* mutant CRC in the TCGA cohort are positively associated with wild type *APC* and negatively with homozygous *APC* loss.

(A) Mosaic plot and Pearson Chi square test result. *BRAF* mutant tumors are positively associated with wild type *APC* and negatively with homozygous *APC* loss. In contrast, *KRAS* mutant tumor and tumors without mutations in *KRAS* and *BRAF* are positively associated with homozygous *APC* loss. (B) Bar graph for Standardized Pearson residual.

Chapter 3: Single-step induction of right-side colon cancer phenotype by *BRAF*^{V600E} through acquired Wnt activation

3.1. Introduction

A major question in cancer biology is how distinct cancer phenotypes evolve within the same organ system. In this regard, sporadic colorectal adenocarcinomas (CRC) differ in their phenotypes between right and left sided tumors (Ensari et al., 2010; Jass, 2007; Jorissen et al., 2015; Li and Lai, 2009; Pai et al., 2012). While both types of tumors evolve as progression from benign adenomas to carcinomas, their molecular and pathological features are distinct from one another. It is much more common that left-sided CRCs have chromosomal instability (CIN), much less mutational burden, particularly with regards to not manifesting mismatch repair deficiencies (microsatellite stable, MSS) and less DNA methylation in promoter CpG island classified as non-CpG island methylator phenotype (CIMP-N) (Ensari et al., 2010; Jass, 2007; Jorissen et al., 2015; Pai et al., 2012; Weisenberger et al., 2006). Pathologically, the left-sided CRCs arise from conventional adenomas such as tubular or villous adenomas (Li and Burgart, 2007). On the contrary, right-sided CRCs have a tendency to have no CIN phenotype, higher mutational burden with regard to mismatch repair deficiencies (microsatellite instable, MSI) due to epigenetic silencing of *MLH1* gene and much more prevalent CpG island DNA methylation classified as CIMP-H/L(Fearon, 2011; Jass, 2007; Li and Lai, 2009; Toyota et al.,

1999; Weisenberger et al., 2006). In terms of pathological features, the right-sided tumors originate from serrated polyps such as sessile serrated adenoma (SSA) or traditional serrated adenoma (TSA) and tend to develop mucinous adenocarcinomas (Li and Burgart, 2007). Different genetic mutational landscapes exist for the above tumors (Rad et al., 2013; Sugai et al., 2006; Yamamoto et al., 2012). The left sided tumors mostly have inactivating mutations or deletions of *APC*, leading to overactivity for Wnt signaling and have frequent activating *KRAS* mutations, 18q loss and inactivating p53 mutations (Fearon, 2011). In contrast, the right-sided tumors frequently have activating *BRAF* mutations, mostly *BRAF*^{V600E} mutation and less frequent inactivating mutations or deletions of *APC* as discussed in Chapter 2 (Fearon, 2011; Toyota et al., 1999; Weisenberger et al., 2006; Yamamoto et al., 2012).

It is well accepted that early Wnt activation by *APC* mutations, plus the co-ocurring early KRAS mutations provide the prime driving events for evolution of left-sided CRCs (Murakami et al., 2015). Importantly, recent mouse models suggest that the *KRAS* mutations provide their role virtually always in the context of co-occuring inactivating mutations of *APC, p53* and *SMAD4* (Drost et al., 2015; Matano et al., 2015). Mouse models for *BRAF* mutations, in contrast, suggest that these alone lead to small intestinal (Carragher et al., 2010) and colon carcinomas (Rad et al., 2013), but the mechanisms are much less clear than for the above events for the left-sided lesions. Precisely how the Wnt pathway is involved, and how CIMP arises is not known and the latter abnormality could be a key event

since among the genes that are abnormally silenced in the association with CIMP are those that have a normal role in suppressing Wnt signaling such as SFRP1 and SFRP2 (Baylin and Ohm, 2006; Hinoue et al., 2009; Suzuki et al., 2004).

The recent development of three dimensional (3D) intestinal organoids culture has made it possible to recapitulate the *in vivo* intestinal epithelial structure *in vitro*. These organoids consist of villus-like cystic structure and crypt-like structures budding outward (Date and Sato, 2015). Similar to the cellular hierarchy *in vivo*, the intestinal stem cells and Paneth cells locate at the bottom of the crypt-like budding structures, whereas differentiating epithelial cells migrate to the central cystic structure (Date and Sato, 2015; Sato et al., 2011). In addition, the organoids recapitulate a normal process of continual cell turnover: stem cells in the budding structure continue to divide and the progenitors differentiate while migrating to the central cyst structure and undergo apoptosis as they reach terminal differentiation. Therefore, the organoids can be maintained indefinitely without artificial immortalization process (Date and Sato, 2015; Sato et al., 2011).

To enhance understanding of the functional implications of *BRAF* and *KRAS* mutations in the evolution of the distinct molecular and pathological phenotypes of CRC including epigenomic landscape, we developed a 3D organoid culture model harboring inducible *BRAF*^{V600E} or *KRAS*^{G12D} mutations and closely investigated early changes in cellular behavior and molecular profiles including DNA methylation and gene expression.

3.2 Results

3.2.1 Generation of proximal colon organoids with inducible mutations of *BRAF^{V600E}* or *KRAS^{G12D}*

To investigate the functional implication of *KRAS^{G12D}* and *BRAF^{V600E}* in colon tumorigenesis, Cre-inducible *BRAF^{V600E}*, *KRAS^{G12D}* and wild type colon organoid lines were established from mice heterozygous for *BRAF^{V600E}* (termed *BRAF$^{+/LSL}$*) or heterozygous for *KRAS^{G12D}* (termed *KRAS$^{+/LSL}$*) or wild type for both proteins (WT) respectively (Figure 3.1, A and B). Both BRAF$^{+/LSL}$ and *KRAS$^{+/LSL}$* organoids carry the corresponding targeted insertion of a mutant exon preceded by loxp flanked STOP cassette with polyadenylation sequence. Thus, the alleles do not express the mutant genes until Cre-mediated recombination of the loxp sites is instituted (Dankort et al., 2007; Jackson et al., 2001). In addition, both mouse strains were bred to carry Cre-inducible tdTomato which is used as surrogate marker for Cre-mediated recombination (Figure 3.1, C and D). The organoids were isolated from proximal 2.5 cm of mouse colon (Figure 3.1E).

Cre-mediated activation of the oncogenes (BRAF^{CA}, KRAS^{CA}) was achieved by lentiviral delivery of constitutively expressed Cre with a hygromycin selection marker (Figure 3.1F), while infection with lentivirus encoding only the selection marker served as a control (EV) (Figure 3.1F). Before Cre-mediated induction, the *BRAF$^{+/LSL}$* and *KRAS$^{+/LSL}$* organoids, identically to wild type (WT) organoids express only wild type BRAF and KRAS proteins, and are thus identical to the

wild type organoids. After expression of Cre, the BRAF^{CA} and KRAS^{CA} organoids express one copy of the wild-type protein and one copy of the respective mutant protein, along with tdTomato, while the WT organoids express only tdTomato (Figure 3.1D).

3.2.2 *BRAF*^{V600E} and to a lesser extent, *KRAS*^{G12D} induce spheroid formation and inward polypoid growth

Immediately after Cre expression and hygromycin-selection, both the BRAF^{CA} and KRAS^{CA} organoids grow as cystic spheroid with a smooth periphery and clear lumen (Figure 3.2, C and D). The WT and EV control organoids (BRAF^{EV}) have the typical structures previously defined with stem cell containing, intestinal crypt-like structures as buds on the outer surface of the central cystic structures, more mature intestinal cells in the central cystic structure, and a lumen-like structure with many dying mature cells modeling the course of generation and cell death that rapidly occurs in the intestine (Figure 3.2, A and B) (Date and Sato, 2015; Onuma et al., 2013). Within 11 weeks, a high frequency of spheroid structures is observed for each expressed mutation (88.5% for BRAF^{CA} and 84.7% for KRAS^{CA}) (Figure 3.2E).

Despite that induction of both *KRAS* and *BRAF* mutations produced the above spheroidal growth of the organoids, important characteristics of the latter emerged which suggested more evolution towards having neoplastic properties. While WT and BRAF^{EV} organoids in culture and in H&E staining show the typical

crypt-like buddings growing outwards (Figure 3.3, A and B) (Date and Sato, 2015), these structures grow inwards for the *BRAF* mutant organoids (BRAF^{CA}) indicating polypoid growth with dysplastic changes (Figure 3.3, C and D). Similar polypoid growth has been reported in *APC* knock out mutant organoids (Li et al., 2014). The cells in the BRAF^{CA} organoids also show other dysplastic changes such as high nuclear to cytoplasm ratio and atypical columnar changes (Figure 3.3C). The KRAS^{CA} organoids much less frequently show the polypoid growth into the lumen (Figure 3.3E), and for the most part grow as cystic structures with a clear lumen (Figure 3.3F). The above spheroidal structures are characteristic of CRC organoids with introduced *APC* mutations, which drive, in primary CRC and in the organoids, oncogenic Wnt autonomous signaling (Drost et al., 2015; Matano et al., 2015; Onuma et al., 2013).

3.2.3 *BRAF*^{V600E} promotes acquisition of stem cell niche factor growth independency and maintenance of stemness in the organoids

Pursuant to the above data, we investigated stem cell niche factor dependency of the organoids by culturing them for three weeks in five different media conditions including fully factor ENSW media, partially deficient media such as NSW, NS and N and fully deficient Base media (Figure 3.4A). The full support media for normal organoids contains, in addition to the Wnt activators (R-Spondin1 and Wnt3a), other stem cell niche growth factors such as Noggin and EGF (Figure 3.4B). By 5 months of growth, only BRAF^{CA} organoids acquired

the property to grow in base media, which completely lacks of all four niche factors used to support stemness and growth of WT organoids including any of Wnt activators (Figure 3.4C) (Date and Sato, 2015; Sato et al., 2011; Sato et al., 2009). Among all of our organoid cultures, the KRAS^{CA} and WT organoids derived at 2 months post Cre-induction are independent of EGF but require Wnt3a, R-spondin1 and Noggin (Figure 3.4C) to sustain their growth for three weeks. However, BRAF^{CA} organoids at 2 months is independent of Wnt3a in addition to EGF although R-spondin1 and Noggin are required (Figure 3.4C). As above, at 5 months, KRAS^{CA} (KRAS^{CA}1 and KRAS^{CA}2) and wild type organoids (WT, BRAF^{EV}1, BRAF ^{EV}2 and BRAF ^{EV}3) still require R-spondin1 and Noggin to sustain their growth and stemness (Figure 3.4C). The independent organoids from three BRAF^{CA} replicates were continuously cultured in base, factor free media and three separate BRAF$^{CA\text{-}IND}$ replicates are established from the culture. The polypoid growth observed previously in BRAF^{CA} organoids (Figure 3.3, C and D) is now even more prominent in the BRAF$^{CA\text{-}IND}$ organoids, indicating a progressive accumulation and selection of dysplastic cells in Base medium (Figure 3.5A). The multi-layered polypoid growth in the BRAF$^{CA\text{-}IND}$ fills up the lumen, which otherwise in WT or EV organoids consists of many dead cells (Figgure 3.5, A and B).

We next find that the above niche-factor independency, and autonomous Wnt signaling of BRAF$^{CA\text{-}IND}$ organoids is due to cell intrinsic mechanisms and not secretion of Wnt3a from Paneth cell or Paneth-like cells in the BRAF$^{CA\text{-}IND}$

organoids. Thus, when equal proportions of BRAF$^{CA\text{-}IND}$ organoids were co-cultured for one week in Base media and ENSW media with BRAF^{EV} or KRAS^{CA} organoids (Figure 3.6A), only the recombined *BRAF*^{V600E} allele originating from BRAF$^{CA\text{-}IND}$ was detected in both ENSW and Base media culture (Figure 3.6B). In contrast, BRAF^{EV} or KRAS^{CA} existed only in the full ENSW medium but not in Base media as indicated by the presence of recombined and non-recombined *BRAF*^{V600E} alleles or the recombined *KRAS*^{G12D} allele in the respective co-cultures in ENSW media not in Base media (Figure 3.6B). Moreover, tdTomato+ BRAF$^{CA\text{-}IND}$ and tdTomato- BRAF^{EV} organoids were observed in ENSW media but in Base medium only tdTomato-positive BRAF$^{CA\text{-}IND}$ organoids survived (Figure 3.6A).

To further pursue the conclusions that BRAF^{CA} organoids have acquired autonomous Wnt-activation rendering them independent of Wnt in the medium, we used porcupine inhibitor IWP2 to further clarify the scenario. Palmitoylation of Wnt ligand by Porcupine (Porcn) is a critical step for Wnt secretion and subsequently action of Wnt ligands on their receptors (Chen et al., 2009). The IWP2 will prevent secretion of Wnts from any type of cells and their subsequent paracrine or autocrine action (Figure 3.7, A and B). In this experiment, the organoids are treated with IWP2 in NS media, which is deficient of external Wnt3a (Figure 3.7B). The IWP2 completely inhibit growth of WT and BRAF^{EV} at low dose of 2.5mM (Figure 3.7B). KRAS^{CA} replicates are slightly resistant to IWP2 but their growth is inhibited more than 50% at higher dose of 10mM (Figure 3.7B). Two BRAF^{CA} replicates also have partial resistance as KRAS^{CA} but

the other one replicate is completely resistant to IWP2 (Figure 3.7B). Moreover, all BRAF$^{CA\text{-}IND}$ replicates are completely resistant to IWP2 indicating that they are enriched for organoids that are completely autonomous and independent of external Wnt signaling.

3.2.4 A single step transformation by *BRAF^{V600E}* induces right-sided CRC phenotype forming invasive mucinous adenocarcinomas

All the above results indicate that *the BRAF^{CA} organoids* have abnormal and aggressive growth properties and independency to environmental signalings hinting that these cells are transformed by *BRAF^{V600E}* alone. To test if this indeed is the case, we performed xenograft assay in NOD *scid* gamma immunodeficient mice (NSG). All wild type organoids, WT and BRAF^{EV}1-3, and the KRAS^{CA}1-2 organoids didn't form any tumors in the NSG mice. In contrast, BRAF^{CA}1, BRAF^{CA}3, BRAF$^{CA\text{-}IND}$1-3 formed tumors in all injection sites although the size of tumor and growth rate were variable within and between the samples (Figure 3.8A). Grossly, the tumors were gelatinous with copious amount of mucin (Figure 3.8B). Histologically, the tumors display features of mucinous carcinomas with dysplastic changes. The tumors consist of mucin filled cysts lined by dysplastic epithelial cells displaying piled up cells, high nuclear to cytoplasm ratio, bizarre looking mitotic figures and multinucleated cells (Figure 3.8B). A fair number of goblet cells spread between the epithelial cells. Signet rings, a pathognomonic feature of mucinous carcinoma, also are observed in the tumors (Figure 3.8B).

These morphological features are also observed in human mucinous colon adenocarcinomas as shown here in Figure 3.8, A and B.

In addition, two injection sites of BRAF$^{CA\text{-}IND}$1 and 3, formed tumor which invaded into the peritoneum. One of these xenografts also resulted in a tumor infiltrating the kidney capsule (Figure 3.9A). Both tumors in subcutaneous and kidney capsule shared the same features of dysplasia and mucinous characteristics (Figure 3.9C). The integrity of muscle layer between the tumors inside and outside was disrupted with tumor cells seeded between the muscle fibers (Figure 3.9 C). The ability of tumor cells to survive in blood stream and metastasize to distal regions is also verified by formation of xenograft tumor after tail vein injection of single cells of BRAF$^{CA\text{-}IND}$1 (Figure 3.9B). Thus, the cells from BRAF mutant organoids were able to survive in the blood stream, extravasate from the vessel and grow as a tumor outside of the blood stream (Figure 3.9B). The xenograft tumor formation indicates that BRAF^{CA} organoids are capable to make an invasive mucinous adenocarcinoma, which is frequently found in human right-sided *BRAF* mutant CRC (Bettington et al., 2013; Nosho et al., 2008; Pai et al., 2012; Song et al., 2005; Tanaka et al., 2006). Notably in the TCGA CRC database (Figure 3.10, A and B) BRAF mutations are strongly associated with mucinous adenocarcinoma in Fisher's exact test with *p* value of 1.676e-06 (Figure 3.10A)

3.2.5 *BRAF^{V600E}* organoids promotes sustained up-regulation of intestinal stem cell and proliferation genes and intestinal Wnt targets during deprivation of all stem cell niche factors.

To investigate how the BRAF^{CA} organoids were able to survive without stem cell niche factors, gene expression profiling was performed in WT, BRAF^{EV}, BRAF^{CA}, BRAF$^{CA\text{-}IND}$ and KRAS^{CA} organoids grown in two different media conditions, ENSW and Base media for 48hr (Figure 3.11A). In ENSW media condition, the BRAF^{CA} and BRAF$^{CA\text{-}IND}$ organoids show a very similar gene expression pattern as WT, BRAF^{EV} and KRAS^{CA} organoids. This is probably due to prevailing activation of Wnt and others pathways by stem cell niche factors in ENSW media (Sato et al., 2009). In contrast, the BRAF^{CA} and BRAF$^{CA\text{-}IND}$ organoids show very distinct gene expression pattern from WT, BRAF^{EV} and KRAS^{CA} organoids in Base media. Firstly, with the gene expression pattern from those organoids in Base media, Gene Set Enrichment Analysis(GSEA) with Hallmark gene sets (Figure 3.11B) indicates that BRAF^{CA}, BRAF$^{CA\text{-}IND}$ and KRAS^{CA} are enriched with proliferation pathways such as E2F targets, G2M checkpoint, mitotic spindle and DNA repair and cancer related pathways including Myc targets (Figure 3.11C) and Mtorc1 signaling (Table 3.1). More interestingly, only BRAF^{CA} and BRAF$^{CA\text{-}IND}$,organoids but not KRAS^{CA} organoids, are enriched for Wnt / β-catenin signaling (Table 3.1 and Figure 3.11C). To further delineate the expression patterns, the CoGAPS (Coordinated Gene Activity In Pattern Sets) algorithm was applied to the dataset to find patterns of

gene expression changes in the organiods with different genotypes (Figure 3.12, A and B) (Fertig et al., 2010; Fertig et al., 2013; Fertig et al., 2012; Fertig et al., 2014; Speier and Ochs, 2012; Stansfield et al., 2016). Four different patterns of gene expression were found (Figure 3.12C). Pattern 1 contains genes up-regulated in ENSW media and down-regulated in Base media in WT / BRAF^{EV}. However, the up-regulation of the gene remain in BRAF$^{CA\text{-}IND}$ and BRAF^{CA}1 even under deprivation of all niche factors (Figure 3.12C) and these genes are those up-regulated in intestinal stem cells and proliferating cells (TA cells) (Merlos-Suarez et al., 2011) and intestinal Wnt target genes (de Lau et al., 2011). Two important stem-cell marker genes, CD44 and SOX9 (Du et al., 2008; Feng et al., 2013), are among these genes and we verified their high levels by quantitative PCR (Figure 3.14, A and B). Although their expression is not sustained in KRAS^{CA} and the other two BRAF^{CA} replicates in Base media as in WT / BRAF^{EV}, the extent of down-regulation is less than in WT / BRAF^{EV} (Figure 3.12C). The pattern 2 has the opposite direction containing gene down-regulated in ENSW and up-regulated in BASE in WT / BRAF^{EV} (Figure 3.12C) but which remain low in BRAF$^{CA\text{-}IND}$ and BRAF^{CA}1 during deprivation of all factors (Figure 3.12C). These genes are those normally up-regulated in differentiated epithelial cells (Merlos-Suarez et al., 2011) (Figure 3.13B). Pattern 3 and 4 contain genes with high expression in WT / BRAF^{EV} (Figure 3.12C). Pattern 4 genes have high expression in BRAF$^{CA\text{-}IND}$ and low expression in WT / BRAF^{EV} (Figure 3.12C).

3.2.6 *BRAF^{V600E}* organoids exhibit sustained up-regulation of intestinal stem cell population

In addition to the gene expression pattern outlined in the preceding section, increased stemness in BRAF$^{CA\text{-}IND}$ was also confirmed by flow cytometry assay for CD44, which is a stem-cell marker (Du et al., 2008; Kuhnert et al., 2004). In organoids grown in ENSW, the CD44 positivity was highest in BRAF$^{CA\text{-}IND}$, followed by BRAF^{CA}, KRAS^{CA} and WT (Figure 3.15 A and C). On average, about 39% of cells in BRAF$^{CA\text{-}IND}$, 25% of cells in BRAF^{CA}, 22% of cells in KRAS^{CA} and 1.6% of cells in WT were CD44 positive (Figure 3.15 A and C). Upon deprivation of stem cell niche factors, the number of CD44+ stem cells in BRAF^{CA} and KRAS^{CA} was further decreased to 12% and 4% on average, respectively (Figure 3.15 B and C) and in WT, to below 1% (Figure 3.15 B and C). In contrast, CD44+ stem cell population in BRAF$^{CA\text{-}IND}$ was increased in all three replicates upon deprivation of the niche factors (Figure 3.15 B and C) to an average of around 60% in BRAF$^{CA\text{-}IND}$ in Base media (Figure 3.15 B and C). Thus, the data above show that in contrast to the dynamic regulation of stemness and differentiation genes in WT, KRAS^{CA} and BRAF^{CA} organoids in response to the deprivation of niche factors, expression of these genes is stably maintained in BRAF$^{CA\text{-}IND}$ in a pattern reflecting pro-stemness and anti-differentiation.

3.2.7 *BRAF^{V600E}* exhibit similar methylation profile as human right-sided CRC including presence of CIMP and increased methylation of

genes for stemness, differentiation maintenance and regulation of the Wnt pathway

Right sided human CRCs with *BRAF*^{V600E} mutations frequently have an important epigenetic characteristic termed the gene promoter, CpG island DNA hypermethylation phenotype or CIMP positive (Bettington et al., 2013; Burnett-Hartman et al., 2013; Hinoue et al., 2012; Hinoue et al., 2009; Hughes et al., 2012; Hughes et al., 2013; Jass, 2007; Kambara et al., 2004; Kriegl et al., 2011; Lee et al., 2008; Nosho et al., 2008; O'Brien et al., 2006; Ogino et al., 2006; Pai et al., 2012; Phipps et al., 2015; Silva et al., 2014; Song et al., 2005; Sugai et al., 2006; Tanaka et al., 2006; Toyota et al., 1999; Weisenberger et al., 2006; Yamamoto et al., 2012; Yang et al., 2004). In contrast, the-left sided tumors with frequent *KRAS*$^{G12D/V}$ mutations are associated with CIMP- and CIMP-intermediate groups (Bettington et al., 2013; Burnett-Hartman et al., 2013; Hinoue et al., 2012; Hinoue et al., 2009; Hughes et al., 2012; Hughes et al., 2013; Jass, 2007; Kambara et al., 2004; Kriegl et al., 2011; Lee et al., 2008; Nosho et al., 2008; O'Brien et al., 2006; Ogino et al., 2006; Pai et al., 2012; Phipps et al., 2015; Silva et al., 2014; Song et al., 2005; Sugai et al., 2006; Tanaka et al., 2006; Toyota et al., 1999; Weisenberger et al., 2006; Yamamoto et al., 2012; Yang et al., 2004). Why the right-sided *BRAF*^{V600E} tumors have CIMP and whether this epigenetic abnormality is a “driver versus passenger” event for evolution of these cancers has not been clarified. Thus we tested for methylation differences among the WT, KRAS^{CA}, BRAF^{EV}, BRAF^{CA} and BRAF$^{CA\text{-}IND}$ organoids. One replicate of

each was subjected to a genome-wide methylation analysis at 5 months after induction of mutations using MBD-seq (Figure 3.16A) (Guerrero-Preston et al., 2014). The result indicates that CIMP is a feature of our *BRAF* mutant organoid model and many of the involved genes are those that may play an essential driver role in cells escaping from senescence, stem cell features, lack of differentiation and especially Wnt autonomous signaling. Thus, as compared to WT and empty vector control BRAF^{EV} organoids, there is increased DNA methylation of normally unmethylated promoter CpG islands of ~ 225 genes at 5 months in BRAF^{CA} organoids with even more, ~ 500 in BRAF$^{CA\text{-}IND}$ organoids while only 20-50 such genes exist in KRAS^{CA} organoids (Figure 3.17A). KEGG gene ontology analysis of these genes differentially methylated in BRAF$^{CA\text{-}IND}$ revealed Wnt signaling as the second most significant pathway enriched following melanogenesis which is also driven by a Wnt signature (Figure 3.17B). Thus the sustained stem cell features and autonomous Wnt activation accompanying induction of *BRAF*^{V600E} might well be due to epigenetic modulation of Wnt pathway. The methylation patterns for individual Wnt genes are shown in Figure 3.18A with hypermethylation seen for important Wnt negative regulators, including *Sfrp1 and 2, Hic1, Wt1, Sox7, Sox17, Frzb* and *Cdh2* in BRAF$^{CA\text{-}IND}$ organoids and partially in BRAF^{CA} but not in WT and KRAS^{CA} organoids (Figure 3.18A). All of these genes are methylated in CIMP CRC (Hinoue et al., 2012; Hinoue et al., 2009; Toyota et al., 1999; Weisenberger et al., 2006; Yamamoto et al., 2012). In addition, there is increased DNA methylation in other CIMP genes

such as *Socs1, Gata3, Galnt4, Fzd10, Cdkn2a* and *Igfbp7* (Figure 3.18B). Of these, epigenetic suppression of *Cdkn2a* (Carragher et al., 2010) and *Igfbp7* (Wajapeyee et al., 2010) were previously reported to play a critical role in escape from oncogene induced senescence. The methylation of these two genes in BRAF$^{CA\text{-}IND}$ correlates well with the previous reports and explains why BRAF$^{CA\text{-}IND}$ organoids may not show any signs of senescence. Lastly, very important genes which normally are expressed to control intestine differentiation, including *Bmp4* and *Bmpr1b* are abnormally methylated as well in BRAF$^{CA\text{-}IND}$ organoids and partially in BRAF^{CA} organoids (Figure 3.18C). As discussed in section 3.2.5 and 3.2.6, stem cell gene expression signature and high stem cell population characterize BRAF$^{CA\text{-}IND}$ organoids and also, partially in BRAF^{CA} organiods and each of the above silenced genes may play important roles in these phenotypic features. For example, without Noggin added to the media, BMP4 should have induced differentiation through inhibition of Wnt signaling (Foulke-Abel et al., 2016; He et al., 2004; Mahe et al., 2015; Saxena et al., 2016; Zachos et al., 2016).

3.3 Discussion

This work shows that, unlike *KRAS*^{G12D}, *BRAF*^{V600E} mutation drives stem cell niche factor independent growth and tumorigenic transformation in colon organoids. These properties are acquired through accumulation of DNA methylation in Wnt negative regulators, CIMP genes including cell cycle check point genes, genes that induce differentiation, and genetic mutations in Wnt

activators such as b-catenin. Importantly, transformation of organoids by *BRAF*^{V600E} recapitulates human *BRAF* mutant tumors in terms of molecular changes and morphological features. Thus the data in this thesis shows that in the serrated pathway to colon cancers, *BRAF*^{V600E} mutation alone induces and selects for a combination of key epigenetic and genetic alterations that lead to acquisition of Wnt pathway activation and stemness (Figure 3.19).

The major observation here that *BRAF*^{V600E} causes a gradual acquisition of Wnt independency presents novel molecular insights into the alternate or sessile-serrated pathway to CRC. The serrated pathway has been invoked to explain non-*APC* mutant CRCs which do not fit with the classical pathway model known as Vogelgram (Jorissen et al., 2015). While *BRAF* mutation is highly associated with cancers in the sessile-serrated pathway, *APC* mutations are much less frequent. The observation that in one step *BRAF*^{V600E} is able to cause Wnt independency and transformation without other mutations to start with may explain why *BRAF* mutant CRCs have a tendency not to have concurrent *APC* mutation even though Wnt activation is a known characteristic of these tumors (Morkel et al., 2015; Murakami et al., 2015). The molecular changes we observe in the BRAF$^{CA\text{-}IND}$ organoids, especially altered epigenetic and genetic changes involved in Wnt activation, appears to provide a basis for how *BRAF*^{V600E} results in CRC in the absence of starting Wnt activating mutations. In this context, the data here supports the study by Rad and colleagues which showed that activation of *BRAF*^{V600E} in mouse intestine caused adenomas and carcinomas, about a third of

which can be attributed to mutations in Wnt pathway genes, including β-catenin (Rad et al., 2013). In contrast, the classical CRC pathway generally begins with Wnt activation by mutations in *APC*, followed by activation of *KRAS*. Previous studies have shown that *APC* knock out or knock down can make organoids independent to Wnt3a and R-spondin and induce them to form tumors in conjunction with other mutations such as activating *KRAS* mutation, inactivating *p53* and *SMAD4* mutations (Li et al., 2014; Matano et al., 2015). Further, a small group of serrated CRCs have *KRAS* mutations, and do not activate the Wnt pathway, but are dependent on inactivation of p16^{Ink4a}/Rb pathway (Bennecke et al., 2010). Thus our studies in conjunction with the other studies discussed above shows that although activating mutations in *KRAS* and *BRAF* are key driver mutations of CRCs, *BRAF* activating mutation in the colon epithelial stem cell niche causes distinct epigenetic and genetic changes, the key result of which is Wnt activation, helping to explain the sessile-serrated route to CRC.

The observation that *BRAF*^{V600E}, but not *KRAS*^{G12D}, causes stem cell niche factor independent growth and transformation is intriguing given that both mediate their effect through activating the RAS-RAF-MEK signaling pathway. Most importantly, genome-wide DNA methylation analyses shows DNA methylation of normally unmethylated promoter CpG islands for ~ 225 genes at 5 months in BRAF^{CA} organoids with even more, ~500 in BRAF$^{CA\text{-}IND}$ organoids, while only 20-50 such genes in KRAS^{CA} organoids are affected as compared to WT organoids. Thus, this epigenetic change appears to not only evolve after

induction of *BRAF*^{V600E} but to be further selected in BRAF$^{CA\text{-}IND}$ cells. Furthermore, the involved genes are highly represented in the CIMP+ marker genes for human right-sided CRC as found in TCGA analyses. The genes methylated in BRAF$^{CA\text{-}IND}$ organoids, include negative regulators of Wnt such as *Sfrp1*, *Sfrp2, Hic1, Wt1, Sox7, Sox17, Frzb* and *Cdh2*, while *KRAS*^{G12D} organoids do not show methylation at these genes. The differential effect of *BRAF*^{V600E} and *KRAS*^{G12D} on inducing the epigenetic alteration is not only relevant to the tumorigenesis process, but also extremely important in terms of the mechanisms involved in methylation of the promoter CpG islands. Previous studies have causally implicated both *KRAS* (Serra et al., 2014) and *BRAF* (Fang et al., 2014) in mediating the CIMP phenotype through two different proteins, ZNF304 and MAFG, respectively. However, these experiments have been performed in cancer cell lines, which already have high level of DNA methylation. Further, our studies here and the inferred relation between CIMP and *BRAF* or *KRAS* mutations in CRCs from TCGA data and other clinical studies (Hinoue et al., 2012; Hinoue et al., 2009; Hughes et al., 2012; Hughes et al., 2013; Jass, 2007; Kambara et al., 2004; Lee et al., 2008; Nosho et al., 2008; Sugai et al., 2006; Tanaka et al., 2006; Toyota et al., 1999; Weisenberger et al., 2006; Yang et al., 2004) (Figure 3.18B) suggest a dominant role for *BRAF* in inducing the CIMP phenotype. The exact mechanism underlying the gradual accumulation of methylation in BRAF^{CA} and BRAF$^{CA\text{-}IND}$, but not KRAS^{CA} organoids, need to continue to be investigated. Our organoid model developed here will be invaluable to study the mechanisms

mediating the differential effect of mutant *BRAF* and *KRAS* on modulating the epigenome in a natural and non-transformed cellular context rather than transformed cancer cells.

Our present study has major implications in understanding and treating human right-sided CIMP positive CRCs. The stem cell niche factor independent *BRAF* organoids recapitulate many features of right-sided CIMP positive *BRAF* mutant CRCs. Non-*APC* mutant / *BRAF* mutant tumors tend to be mucinous adenocarcinoma in human (Bettington et al., 2013; Nosho et al., 2008; Pai et al., 2012; Song et al., 2005; Tanaka et al., 2006) (Figure 3.10 A and B). Subcutaneous xenografting of BRAF^{CA} and BRAF$^{CA\text{-}IND}$ organoids resulted in mucinous adenocarcinoma highlighted by signet ring and formation of mucin filled glandular cysts. This category of right-sided human CRCs, which also display MSI (microsatellite instable), have recently been shown to have increased T cell infiltration and better prognosis to immunotherapy (Le et al., 2015). However, MSS tumors with *BRAF* mutations have the worst prognosis (Jorissen et al., 2015). There have been controversies over whether the increased T cell infiltration is due to higher number of neoantigen generated from the high mutational burden in *BRAF* mutant MSI tumors or overall cellular stress due to increased mutation in the MSI tumors. Our organoid model, with appropriate manipulations to inactivate *Mlh1* to create the MSI phenotype, can be used to address the interaction between the immune system and the tumor cells in an immunocompetent syngeneic xenograft or orthotopic transplantation model.

Finally, the ability for *BRAF*^{V600E} to cause transformed phenotype in the absence of a microenvironment deserves special mention. The original inducible construct for our model was first engineered for internal expression throughout the mouse intestine and we induced the mutation in this setting as well. In contrast to the results in our organoid model, with induced transformation in 2-5 months, we observed only hyperplastic growth in the colon epithelium up to about 6 months after *BRAF*^{V600E} induction in LGR5+ stem cells or CDX2+ colonocytes. The mice develop severe skin lesions and other tumors beyond this point so they could not be monitored further. In the *BRAF* mutation mouse model, it takes a prolonged period of greater than a year to form colon adenomas (Rad et al., 2013). Thus the native colonic setting of the crypts and the microenvironment appears, at least initially to be anti-tumorigenic, and this fact accentuates our findings for the intrinsic pathway signaling and tumorigenesis of *BRAF*^{V600E} in the *ex vivo* organoid setting. Key questions thus will be how the microenvironment prevents tumorigenesis. It is already known that stroma can have suppressive role in tumorigenesis that can be mediated through Hedgehog signaling pathway (Shin et al., 2011; Vaegler et al., 2012) and other pathways. The accentuated tumorigenesis we see in our organoid culture could be due to the absence of stromal interaction. The effect of interaction between epithelial cells and stroma can be investigated with the organoid model in conjunction with an organoid / stroma co-culture model (Figure 3.20).

3.4 Material and Methods

3.4.1 Mouse breeding and animal experimentation

All animal experiments were implemented in accordance with an animal protocol approved by the Johns Hopkins University Animal Care and Use Committee (Protocol# MO10M388). All the mice were housed in Helicobacter negative and SPF (Specific Pathogen Free) environment.

Homozygous tdTomato reporter (B6;129S6-Gt(ROSA)26Sor$^{tm9(CAG-tdTomato)Hze}$/J) mouse was bred with heterozygous inducible *BRAF* mouse (B6.129P2(Cg)-Braf^{tm1Mmcm}/J) or heterozygous inducible *KRAS* mouse (B6.129S4-Kras^{tm4Tyj}/J) to generate mice that are heterozygous *BRAF* with heterozygous tdTomato reporter, heterozygous *KRAS* with heterozygous TomatoRed reporter and wild type with heterozygous TomatoRed.

3.4.2 Isolation of crypt cells from colon

Male mice from each genotype between the age of 35 days and 40 days were euthanized by carbon dioxide and subjected to a necropsy. The first 2 cm of proximal colon is collected from the mice. The collected colons were washed 5 times with sterile Complete Chelating Solution (CCS: 5.6mM Na^2HPO^4, 8mM KH^2PO^4, 96.2mM NaCl, 1.6mM KCl, 43.4mM Sucrose, 54.9mM D-Sorbitol and 0.5mM DL-dithioteritol and incubated in sterile CCS with cocktail of antibiotics: Primocin (Invivogen ant-pm-1) and Normocin (Invivogen ant-nr-1) for 30 minutes in 4°C. The clean proximal colons were incubated in CCS with 2mM

EDTA for 20 minutes at 37°C to release crypt from the tissue. After incubation, the crypts on the proximal colon were gently scraped with cell scraper to collect crypts. The crypts were collected with CCS with EDTA in 15ml tubes and the tubes were centrifuged at 300g for 10 minutes. Subsequently, the crypt pellets were washed with CCS with cocktail of antibiotics for 4 times by repeated resuspension and centrifugation. After the serial washing, the crypts were resuspended in growth factor reduced phenol red free Matrigel® (Corning® #356231) and plated on regular cell culture plates.

3.4.3 Organoids culture

The plated organoids were cultured with ENSW culture media made of 50% of Wnt3a conditioned media, 20% of R-Spondin conditioned media, 20% of Advanced DMEM/F12 (Invitrogen® 12634-010) with 1% Pen strep® (ThermoFisher® 15140148), 10mM HEPES, 2mM L-glutamine and B27 (Invitrogen® 17504044), 10% of Noggin conditioned media and 100ng/ml of EGF(R&D systems 236-EG-200). The conditioned media for Wnt3a, R-Spondin and Noggin were made as described previously (Matano et al., 2015; Sato et al., 2011; Sato et al., 2009). NSW media was made with 50% of Wnt3a conditioned media, 20% of R-Spondin conditioned media, 20% of Advanced DMEM/F12 (Invitrogen® 12634-010) with 1% Pen strep® (ThermoFisher® 15140148), 10mM HEPES, 2mM L-glutamine and B27 (Invitrogen® 17504044), 10% of Noggin conditioned media. NS media was made with 50% of DMEM with 10% FBS, 20%

of R-Spondin conditioned media, 20% of Advanced DMEM/F12 (Invitrogen® 12634-010) with 1% Pen strep® (ThermoFisher® 15140148), 10mM HEPES, 2mM L-glutamine and B27 (Invitrogen® 17504044), 10% of Noggin conditioned media. N media was made with 50% of DMEM with 10% FBS, 20% of Advanced DMEM/F12 with 1% Pen strep® (ThermoFisher® 15140148), 10mM HEPES and 2mM L-glutamine, 20% of Advanced DMEM/F12 (Invitrogen® 12634-010) with 1% Pen strep® (ThermoFisher® 15140148), 10mM HEPES, 2mM L-glutamine and B27 (Invitrogen® 17504044), 10% of Noggin conditioned media. Base media was made with 50% of DMEM with 10% FBS, 30% of Advanced DMEM/F12 with 1% Pen strep® (ThermoFisher® 15140148), 10mM HEPE and 2mM L-glutamin, 20% of Advanced DMEM/F12 (Invitrogen® 12634-010) with 1% Pen strep® (ThermoFisher® 15140148), 10mM HEPES, 2mM L-glutamine and B27(Invitrogen® 17504044).

3.4.4 Subcloning of lentivirus plasmid and packaging of lentivirus

Puromycin resistance gene in Puro.Cre empty vector (Addgene #17408) was replaced by hygromycin resistance gene PCR amplified from pBABE-hygro-hTERT (Addgene #1773) using primer listed below (Hyg F and R) by Gibson Assembly® cloning kit (NEB® #E5510S) generating Lenti-cre vector. Subsequently, Cre in the Lenti-cre vector was deleted by Gibson Assembly® cloning kit generating Lenti-empty vector using primers listed below (Cre deletion F and R).

Hyg F: TAACGCGCTAGCAAAGATGAAAAAGCCTGAACTCAC

Hyg R: GTAGAATGCGGCCGCCTATTCCTTTGCCCTCGG

Cre deletion F : CCGTAACCTGGATAGTGAAAC

Cre deletion R : CCTTCCTCTTCTTCTTGGG

Lentivirus was produced in Lenti-X™ 293T cell line transfected with Packaging vectors and Lenti-cre or Lenti-empty mixed with Xfect™ polymer. 72hr after the transfection, the media is collected and concentrated using Lenti-X™ concentrator.

3.4.5 Transduction of organoids with lentivirus

Organoids were collected from Matrigel® (Corning® #356231) using Cell Recovery solution (Corning® #354253). Organoids were broken into small piece of cells by repeated pipetting. The small pieces of cells were digested by 2U/ml of Dispase I for 20 minute at 37'C. Matrigel® is spread on the 12 well surface and the plate is incubated at 37°C to polymerize for 10 minutes. The digested organoids are mixed with virus and 8ug/ml Polybrene® (Sigma-Aldrich® #107689) in ENSW organoid culture media and plated on the solidified Matrigel®. After 24 hour, the media is removed and Matrigel® is spread on the organoids.

3.4.6 DNA/RNA isolation

Organoids were collected from Matrigel® (Corning® #356231) using Cell Recovery solution The collected organoids were broken into small piece of cells by repeated pipetting and incubated in 15ml ice cold media for 30min letting live cells precipitate. Live cells in bottom 3ml were recovered and mixed again with 12ml of media for second precipitation. After second precipitation, bottom 2ml of the media was collected and centrifuged at 1,000g for 1minute to make a pellet. From the pellet, DNA/RNA was extract using Allprep kit mini or micro (Qaigen)

3.4.7 Recombination specific PCR and genotyping

Mouse genotypes were determined by standard PCR of tail DNA. BRAF genotype and recombination is determined by a primer set of BRAF Fwd (5′-TGA GTA TTT TTG TGG CAA CTG C-3′) and BRAF Rev (5′-CTC TGC TGG GAA AGC GGC-3′). 185base pair, 308 base pair and 335 base pair fragments are generated from wild type allele, non-recombined mutant allele and recombined mutant allele respectively (Dankort et al., 2007). KRAS genotype is determined by PCR with KRAS mt Fwd (5′-CCA TGG CTT GAG TAA GTC TGC-3′) and KRAS mt Rev(5′-CGC AGA CTG TAG AGC AGC G-3′). Recombination of KRAS mutant allele is determined by a PCR with KRAS 1(5′-GTC TTT CCC CAG CAC AG TGC-3′) and KRAS 2(5′-AGC TAG CCA CCA TGG CTT GAG TAA GTC TGC A-3′). Recombined mutant allele generates 650base pair long fragments and wild type allele generates 622 base pair fragments with this PCR.

3.4.8 Organoid growth assay by CellTiter-Glo 3D

The organoids were collected using Cell Recovery solution (Corning #354253). The same volume of CellTiter-Glo3D® (Promega #G9681) was added to organoids suspension and mixed by vortexing at high speed for 5min. Then, the mixture was incubated for 25min at room temperature. The mixture was distributed in three wells of dark 96 well plates and its luminescence was measured by plate reader (POLARstar® Omega by BMG LABTECH)

3.4.9 Quantification of cell number for xenograft assay

The organoids were recovered from the Matrigel using Cell Recovery solution (Corning #354253). The organoids were disrupted and washed in the media 2 times to get rid of dead cells. Then, the fragmented organoids were serially diluted and each dilution was separated into two wells, one for CellTiter-Glo3D assay and the other for Quant-iT PicoGreen® ds DNA assay. The luminescence of CellTiter-Glo3D assay and fluorescence of Quant-iT PicoGreen® ds DNA assay were measured by plate reader (POLARstar® Omega by BMG LABTECH). A correlative standard curve between these two values in the serial dilution of the organoids was generated. Based on the size of mouse genome (2.8 x 10^9 base pairs), the amount of DNA per diploid genome is about 6 pg. Thus based on the amount of DNA, the number of cells were extrapolated for the standard curve. For organoids that were to be implanted, an aliquot of the organoids was fragmented as above and used to estimate the cell numbers using

the CellTiter-Glo3D assay and the standard curve above. Then proportions of intact organoid aliquots amounting to equal cell numbers of the different genetic backgrounds were used for implantation as described below.

3.4.10 Xenograft implantation

The organoids were recovered from the Matrigel using Cell Recovery sol (Corning #354253) without disrupting the structures. Then, using a portion of the organoids, CellTiter-Glo3D assay is performed. Using the formulation between CellTiter-Glo3D and cell number, cell number was estimated. Based on the estimation, 0.5 million cells were injected subcutaneously with 16G needle to minimize disruption of the organoid 3D structure in male NOD.Cg-Prkdc^{scid} Il2rg^{tm1Wjl}/SzJ (NSG) (JAX™) with Matrigel. Injection sites were examined every week for tumor growth. The volume of the tumors estimated by ellipsoid volume formula.

3.4.11 Flow cytometry

Organoids were collected from Matrigel using Cell Recovery solution (Corning #354253). Organoids were broken into small piece of cells. The small piece of cells were digested by 2U/ml of Dispase I (Sigma #D4818) for 20 minute at 37°C. Digested organoids were filtered through 70um cell strainer. The single cells were stained with CD44 antibody (ThermoFisher #A161693) and 200ng/ml of DAPI for live/dead cell staining. The cells were analyzed by flow cytometry

using a DakoCytomation MoFlo at flow cytometry core of Johns Hopkins School of Public Health.

3.4.12 Quantitative RT-PCR

RNA was converted to cDNA using qscript (Quanta #95048-025) following the standard protocol. Quantitative PCR reactions were run on the cDNA samples with triplicate technical replicates using Taqman probe assays, Mm99999915_g1 for GAPDH, Mm00448840_m1 for Sox9 and Mm01277161_m1 for Cd44. GAPDH was used as an endogenous control. It is selected based on stable gene expression pattern in gene expression array.

3.4.13 Gene expression microarray

For genome-wide gene expression analysis, we carried out gene expression array at the Sidney Kimmel Comprehensive Cancer Cencer (SKCCC) Microarray Core at the Johns Hopkins University. Breifly, around 400ng of total RNA was reverse-transcribed into cDNA by MMLV-RT using oligo dT primer. Then from the cDNA, labeled cRNA was generated through in vitro transcription by T7 RNA polymerase in presence of labeled by Cyainine-3 labeled CTP (Perkin Elmer). The labeled cRNA was purified using Rneasy mini kit (Qiagen). 825ng of each Cy3-labeled cRNA was hybridized to Agilent mouse GF 4x44K V2 microarray (G4846A) at 65°C for 17 hours. Then, the arrays were scanned by an Agilent G2565 scanner.

Expression data were analyzed in the R/Bioconductor environment using the limma package (PMID:25605792). Briefly, expression data was normalized by quantile normalization, and the probe level information was extrapolated to gene level information by estimating the medial of all probes corresponding to each gene. These gene level values were used in COGAPS analysis as described below.

3.4.14 Coordinated Gene Activity in Pattern Sets (CoGAPS) analysis

For genome-wide gene expression pattern analysis, we carried out CoGAPS analysis in collaboration with Elana Fertig as described previously (Fertig et al., 2010; Fertig et al., 2013; Fertig et al., 2012; Fertig et al., 2014; Speier and Ochs, 2012). With the list of genes in the patterns, we performed gene set enrichment using a permutation test in the CoGAPS gene set statistic (Fertig et al., 2010; Fertig et al., 2013; Fertig et al., 2012; Fertig et al., 2014; Speier and Ochs, 2012) to associate CoGAPS patterns with pathways. We further performed clustering analysis of genes determined to be uniquely associated with each pattern through a "PatternMarker" statistic. Specifically, we computed the Euclidean distance between the elements of the P matrix for a given pattern and the elements of the A matrix for a given gene. In order to account for the varying magnitude of expression across genes, the rows of both the A and P matrix are scaled to have a maximum of one. The genes were ranked within each meta-pathway by increasing distance with from its lp-norm. Unique sets of marker

genes were then generated by thresholding these rankings by the first gene to have a lower ranking, i.e. better fit to, a different meta-pathway.

3.4.15 Methyl-CpG binding domain sequencing (MBD-seq)

For genome-wide DNA methylation analysis, we carried out MBD-seq as described previously (Bock et al., 2010; Harris et al., 2010; Sinclair et al., 2015), but with significant modifications at the SKCCC Experimental and Computational Genomics Core at the Johns Hopkins University. Briefly, 100 ~ 200 ng of genomic DNA was sonicated to an average size of 200 ~ 400 bp and subsequently methylated DNA fragments were enriched using modified MBD polypeptides immobilized on protein A magnetic beads (NEB, EpiMark Methylated DNA Enrichment Kit) according to the manufacturer's protocol. Then, the enriched DNA fragments were eluted and prepared as barcoded next generation sequencing libraries using the ThruPlex DNA library preparation kit (Rubicon Genomics) according to the supplied protocols. The libraries were then sequenced by massively-parallel 50-bp single-end sequencing on an Illumina HiSeq 2500 in rapid run mode. Reads were aligned to the mm10 mouse reference genome using bowtie2 (Langmead and Salzberg, 2012) and duplicated reads were removed. For identifying differential methylated CpG island promoters, the data was normalized using TMM normalization (Trimmed Mean of M-values) (Robinson and Oshlack, 2010). After normalization, the sum of MBD-seq counts for each promoter region with CpG islands and without CpG island was

computed. Promoters with CpG islands are defined as any promoter TSS regions within 500bp from an annotated CpG island (downloaded from UCSC). Fisher test comparing the promoter regions in the test data set (BRAF^{CA}, BRAF$^{CA\text{-}IND}$ or KRAS^{CA}) with that in WT (Bock et al., 2010). Promoters that showed an 8-fold change in read counts and with a Benjamini & Hochberg corrected p-value < 0.05 were identified as significantly differential methylated promoters.

Table 3.1

	HALLMARK GENE SETS	NOM p-val	FDR q-val	FWER p-val
KRAS^{CA} vs WT	E2F_TARGETS	0	0	0
	G2M_CHECKPOINT	0	0	0
	MYC_TARGETS_V1	0	0	0
	MYC_TARGETS_V2	0	0	0
	MITOTIC_SPINDLE	0	0	0
	MTORC1_SIGNALING	0	0.00250339	0.018
	UNFOLDED_PROTEIN_RESPONSE	0.00261780	0.00800738	0.062
	SPERMATOGENESIS	0.00563380	0.02072442	0.174
	CHOLESTEROL_HOMEOSTASIS	0.03674540	0.04560930	0.39
	DNA_REPAIR	0.20118344	0.31184748	0.981
	MYOGENESIS	0.23529412	0.37969804	0.996
	TGF_BETA_SIGNALING	0.5048309	0.64634794	1
	ANGIOGENESIS	0.5347222	0.6647371	1
	WNT_BETA_CATENIN_SIGNALING	0.59951454	0.6888516	1
	NOTCH_SIGNALING	0.6683938	0.76876414	1
BRAF^{CA} vs WT	E2F_TARGETS	0	0	0
	G2M_CHECKPOINT	0	0	0
	MYC_TARGETS_V1	0	0	0
	MYC_TARGETS_V2	0	0	0
	UNFOLDED_PROTEIN_RESPONSE	0	0	0
	MITOTIC_SPINDLE	0	0	0
	MTORC1_SIGNALING	0	0.00105500	0.011
	WNT_BETA_CATENIN_SIGNALING	0.00806451	0.00573658	0.064
	DNA_REPAIR	0.00400801	0.01630587	0.196
	SPERMATOGENESIS	0.02036659	0.02939992	0.359
	CHOLESTEROL_HOMEOSTASIS	0.03326403	0.04109803	0.509
	NOTCH_SIGNALING	0.07307692	0.03790747	0.511

	ANGIOGENESIS	0.16458334	0.11320952	0.891
	GLYCOLYSIS	0.29299363	0.3629813	0.999
	TGF_BETA_SIGNALING	0.4217119	0.4582001	1
	MYOGENESIS	0.45841786	0.47525734	1
$BRAF^{CA\text{-}IND}$ vs WT	E2F_TARGETS	0	0	0
	G2M_CHECKPOINT	0	0	0
	MYC_TARGETS_V1	0	0	0
	MYC_TARGETS_V2	0	0	0
	MITOTIC_SPINDLE	0	8.75E-05	0.001
	UNFOLDED_PROTEIN_RESPONSE	0	4.06E-04	0.004
	DNA_REPAIR	0	3.48E-04	0.004
	WNT_BETA_CATENIN_SIGNALING	0.00411522	0.00112264	0.015
	SPERMATOGENESIS	0.01176470	0.02464920	0.292
	MTORC1_SIGNALING	0.00947867	0.02380177	0.308
	NOTCH_SIGNALING	0.15481171	0.08769937	0.798
	ANGIOGENESIS	0.4311377	0.50919443	1
	CHOLESTEROL_HOMEOSTASIS	0.86021507	0.96530354	1
	TGF_BETA_SIGNALING	0.92339545	0.9672655	1

Table 3.1 List of Hallmark gene sets that are highly enriched in KRAS^{CA,} BRAF^{CA} and BRAF$^{CA\text{-}IND}$ compared to WT

Figure 3.1

A

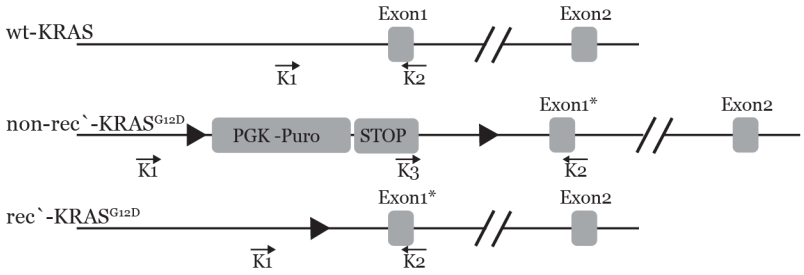

B

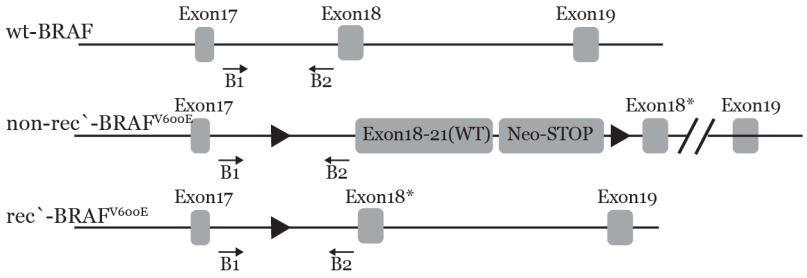

C

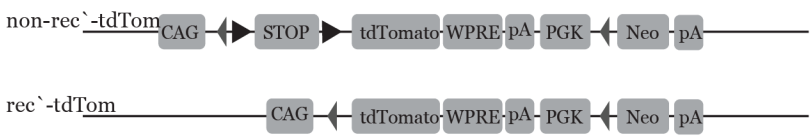

D

	BRAF	KRAS	Reporter
BRAF-Tom	BRAF^{V600E}/+	+/+	tdTom/+
KRAS-Tom	+/+	KRAS^{G12D}/+	tdTom/+
WT-Tom	+/+	+/+	tdTom/+

E

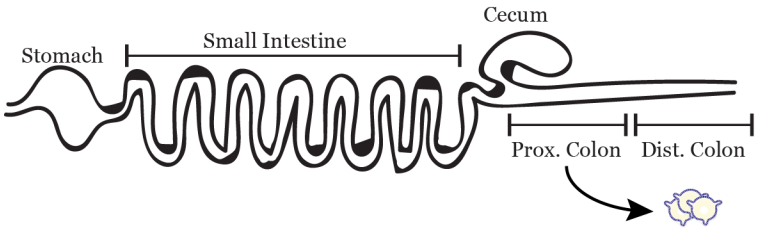

F

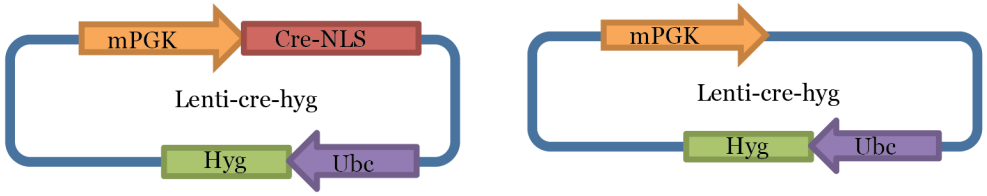

Figure 3.1 Modeling of right-sided CRCs with proximal colon organoids from genetically modified mouse

(A-C) Schematic diagram showing genetic composition of *KRAS*^{G12D} inducible mouse, *BRAF*^{V600E} inducible mouse and inducible tdTom mouse. Genetic structures after cre induction are also displayed. The "Exon1*" stands for *KRAS*^{G12D} allele. The "Exon18*" stands for *BRAF*^{V600E} allele. Arrows stands for PCR primers. (D) Summary of the mouse genotypes of BRAF$^{+/LSL}$, KRAS$^{+/LSL}$ and WT (E) Schematic diagram of anatomic location where the colon organoids were isolated. (D) Schematic diagram of the lentiviral constructs. Cre-NLS (nuclear localization signaling) is driven by mPGK (mouse phosphoglycerate kinase-1) and hygromycin resistance gene (Hyg) is driven by human ubiquitin C promoter (Ubc).

Figure 3.2

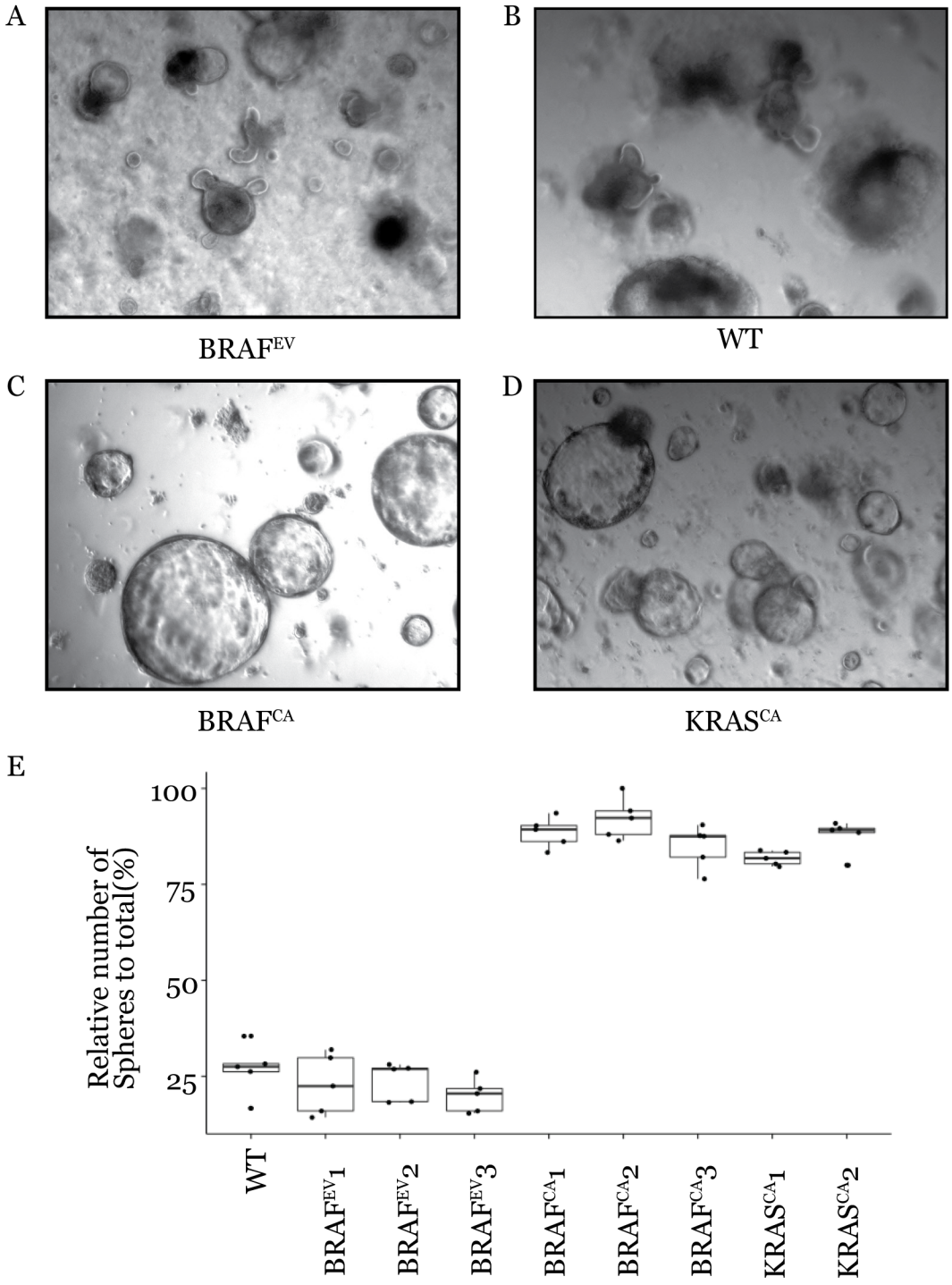
A
B
BRAFEV
WT
C
D
BRAFCA
KRASCA
E
Relative number of Spheres to total(%)
100
75
50
25
WT
BRAFEV1
BRAFEV2
BRAFEV3
BRAFCA1
BRAFCA2
BRAFCA3
KRASCA1
KRASCA2

Figure 3.2 *BRAF*^{V600E} and *KRAS*^{G12D} induce organoids to form spheroid

(A-D) Upon induction of *BRAF*^{V600E} and *KRAS*^{G12D}, organoids start to form spheres. WT and BRAF^{EV} didn't undergo morphological changes maintaining the conventional morphology of organoids with crypt-like buds growing outward. (E) Quantification of sphere formation in each organoids. All BRAF^{CA} and KRAS^{CA} organoids showed increased number of sphere formation compared to WT and three BRAF^{EV} controls.

Figure 3.3

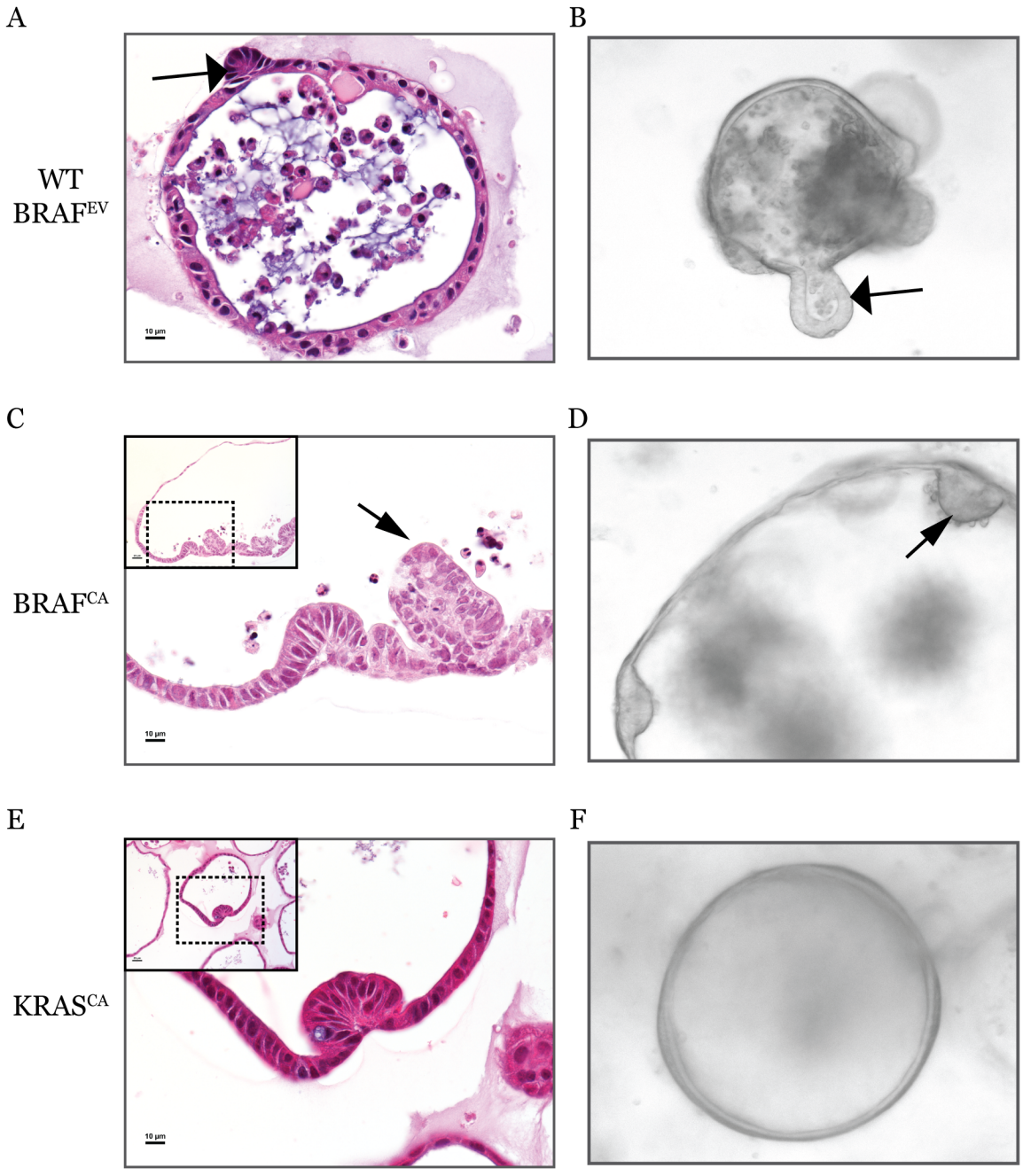

Figure 3.3 *BRAF*^{V600E} and to a lesser extent, *KRAS*^{G12D} induce organiods to manifest spheroid formation with inward polypoid growth

(A-B) H&E histology section and phase contrast image of wild-type organoids. The organoids consist of central cystic body of single layer of epithelial cells and outward crypt-like budding structure (wide triangle arrowhead). (C-D) H&E histology section and phase contrast image of BRAF^{CA}. The organoids showed inward budding structure (narrow triangle arrowhead) in the central cystic body and dysplastic changes such as high nuclear to cytosol ratio. (E-F) H&E histology section and phase contrast image of KRAS^{CA}. The organoids are forming spheroids consisting of single layer of epithelial cells. Occasionally, KRAS^{CA} organoids also have inward growth.

Figure 3.4

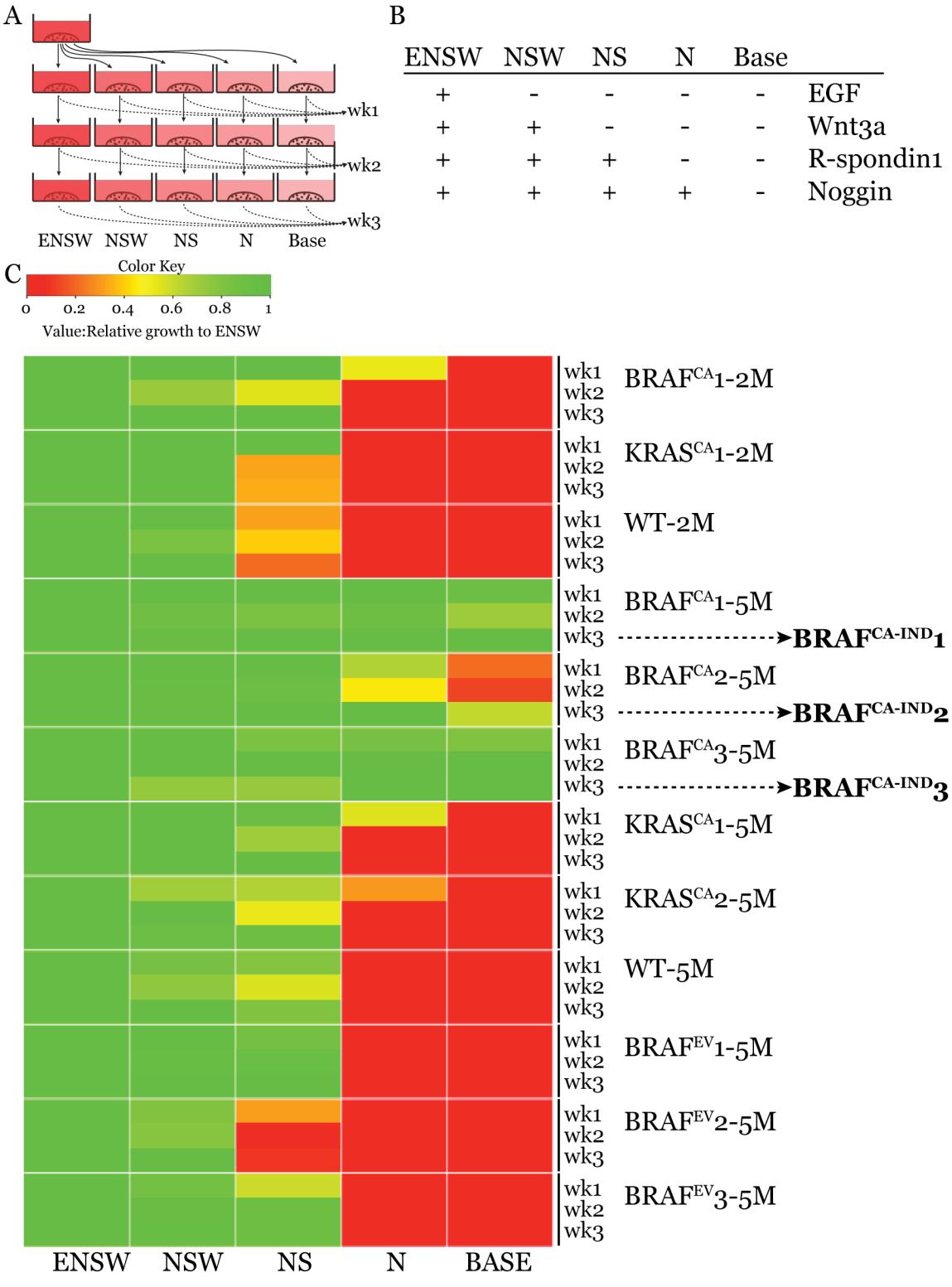
A
wk1
wk2
wk3
ENSW NSW NS N Base
B
ENSW NSW NS N Base
+ - - - - EGF
+ + - - - Wnt3a
+ + + - - R-spondin1
+ + + + - Noggin
C
Color Key
0 0.2 0.4 0.6 0.8 1
Value:Relative growth to ENSW
BRAFCA1-2M
KRASCA1-2M
WT-2M
BRAFCA1-5M
BRAFCA2-5M
BRAFCA3-5M
KRASCA1-5M
KRASCA2-5M
WT-5M
BRAFEV1-5M
BRAFEV2-5M
BRAFEV3-5M
BRAFCA-IND1
BRAFCA-IND2
BRAFCA-IND3
ENSW NSW NS N BASE

Figure 3.4 Only *BRAF*^{V600E} drives acquisition of stem cell niche factor independency

(A) Schematic diagram of niche factor dependency assay. Each organoid clone was grown in five different media conditions, full factor ENSW, partially deficient media NSW, NS and N and fully deficient media Base media for one week and their growth was quantified by CellTiter-Glo assay using half of the organoids in each well. The other half was plated for the subsequent culture and growth quantification for another two weeks. (B) Summary of media conditions. "+" means addition of the factor. "-" means deficiency of the factor. (C) Heatmap showing relative growth of each organoids in different media conditions in three weeks. Relative growth rates for each condition are calculated in comparison to ENSW media condition. The green color indicates equivalent growth as in ENSW. The red color indicates no growth. Only the three BRAF^{CA} replicates grown for 5 months (5M) were able to sustain growth in all media conditions including Base media. The continuing culture (dotted arrow) of the BRAF^{CA} replicates in Base media established independent organoids BRAF$^{CA\text{-}IND}$1-3. ("-2M" indicates organoids that had been cultured for 2 months after induction. "-5M" indicates organoids that had been cultured for 5 months after induction.)

Figure 3.5

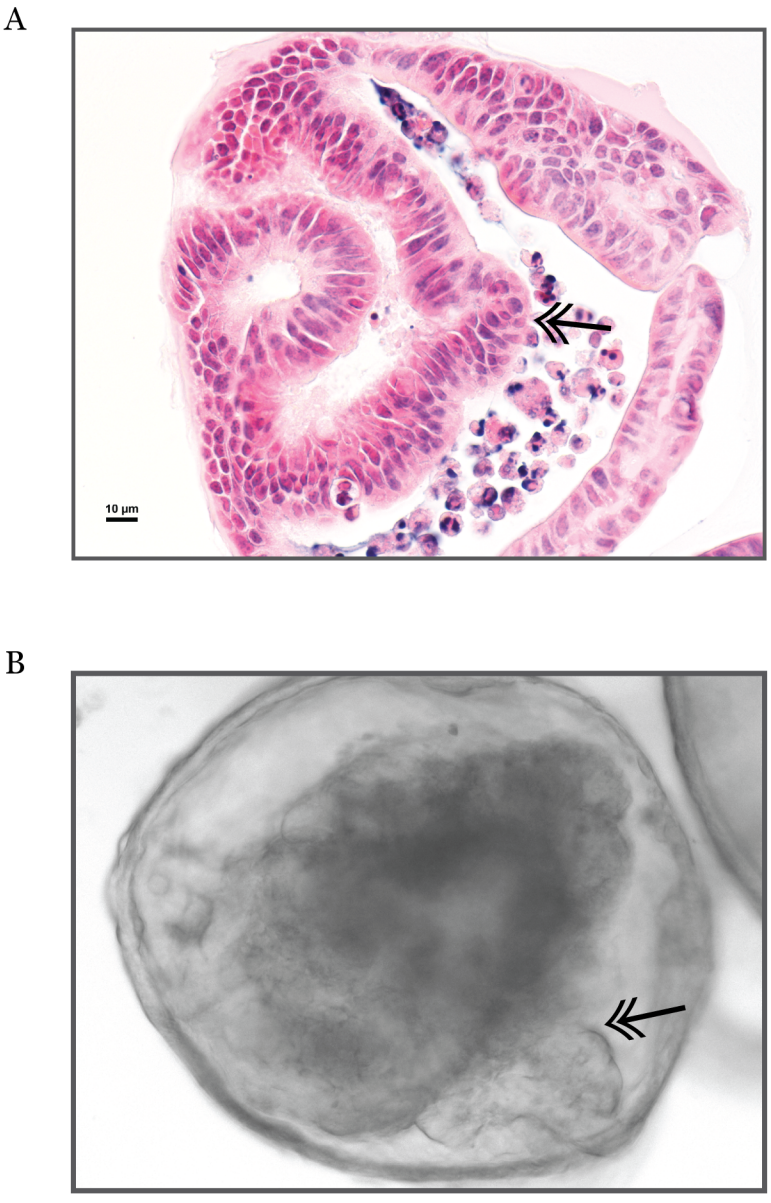

Figure 3.5 Niche factor independent BRAF^{CA} organoids (BRAF$^{CA\text{-}IND}$) manifest augmented polypoid growth and dysplasia

(A-B) H&E histology section and phase contrast image of BRAF$^{CA\text{-}IND}$. The organoids manifest inward multilayer growth (double simple arrowhead) and augmented dysplastic features.

Figure 3.6

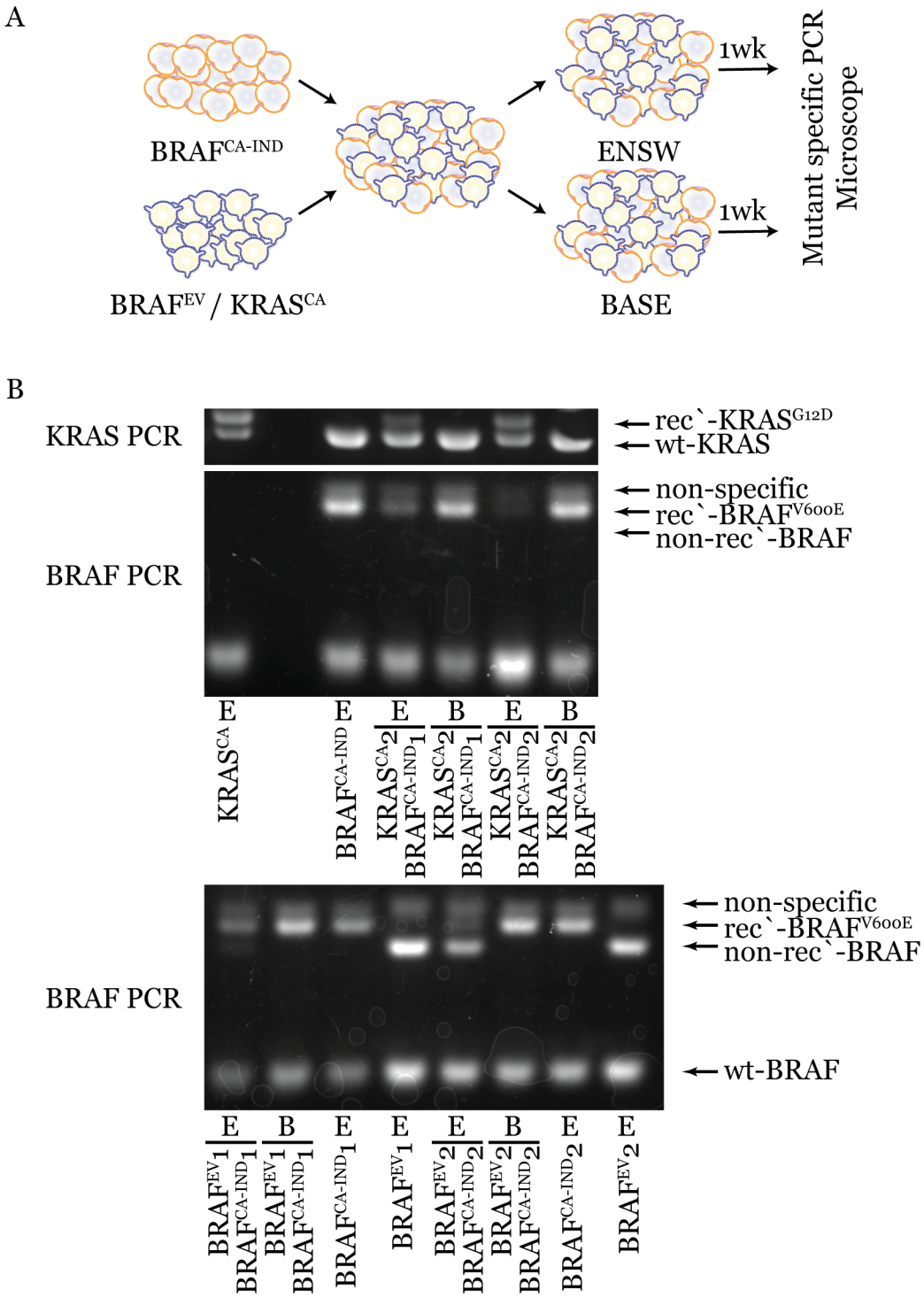
A
BRAF^CA-IND
BRAF^EV / KRAS^CA
1wk
ENSW
1wk
BASE
Mutant specific PCR
Microscope
B
KRAS PCR
rec`-KRAS^G12D
wt-KRAS
BRAF PCR
non-specific
rec`-BRAF^V600E
non-rec`-BRAF
E
KRAS^CA
E
BRAF^CA-IND
E
KRAS^CA2 BRAF^CA-IND1
B
KRAS^CA2 BRAF^CA-IND1
E
KRAS^CA2 BRAF^CA-IND2
B
KRAS^CA2 BRAF^CA-IND2
BRAF PCR
non-specific
rec`-BRAF^V600E
non-rec`-BRAF
wt-BRAF
E B E E E B E E
BRAF^EV1 BRAF^CA-IND1
BRAF^EV1 BRAF^CA-IND1
BRAF^CA-IND1
BRAF^EV1
BRAF^EV2 BRAF^CA-IND2
BRAF^EV2 BRAF^CA-IND2
BRAF^CA-IND2
BRAF^EV2

Figure 3.6 (continued)

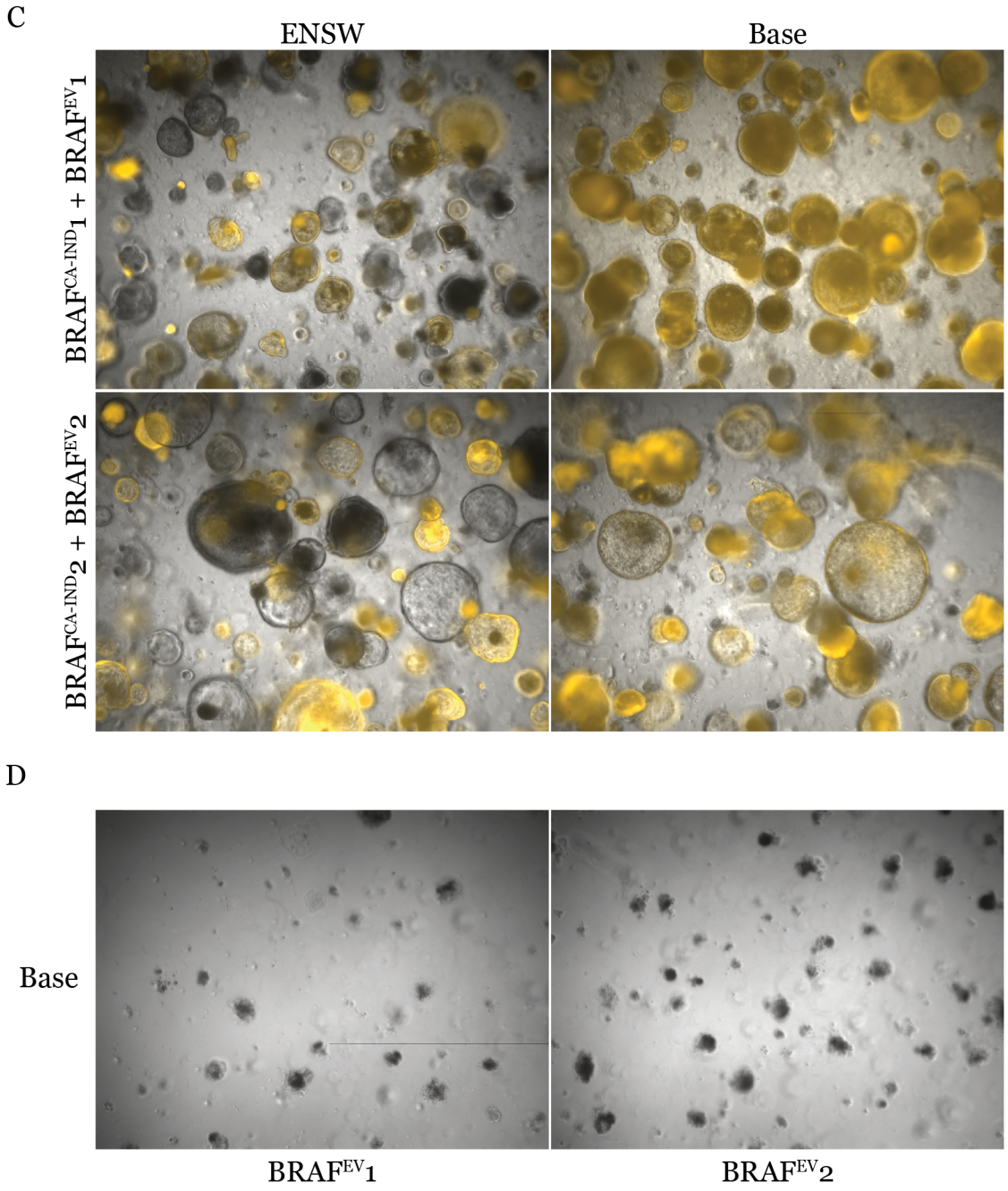

Figure 3.6 The niche factor independency of BRAF$^{CA\text{-}IND}$ organoids are not due to increased secretion of niche factors by the organoids

(A) Schematic diagram of co-culture experiment. BRAF$^{CA\text{-}IND}$ organoids were mixed with BRAF^{EV} or KRAS^{CA} and the mixed organoids were separated into two wells to grow in ENSW and Base for one week. After one week, the co-cultures were examined by mutant specific PCR and fluorescence microscope. (B) Mutant specific PCR to examine survival of each organoid types in the culture. The rec`-BRAF$^{V600E}$ band, the non-rec-BRAF band and the rec`-KRAS^{G12D} band indicate the presence of BRAF$^{CA\text{-}IND}$1-2, BRAF^{EV}1-2 and KRAS^{CA}2, respectively. Only the rec`-BRAF$^{V600E}$ originated from BRAF$^{CA\text{-}IND}$ was detected in both ENSW and Base media. The non-rec-BRAF from BRAF$^{EV}$ and rec`-KRAS^{G12D} from KRAS^{CA} were detected only in full factor ENSW media not in Base media. (C) Fluorescence microscope images of co-cultures of BRAF$^{CA\text{-}IND}$ with BRAF^{EV} in ENSW and Base media. BRAF$^{CA\text{-}IND}$ organoids are red-fluorescent due to expression of tdTomato and BRAF^{EV} are non-fluorescent. In ENSW media, both fluorescent BRAF$^{CA\text{-}IND}$ and non-fluorescent BRAF^{EV} survived. However, in Base media, only fluorescent BRAF$^{CA\text{-}IND}$ clones survived. (D) One week culture of BRAF^{EV} organoids in Base media showed complete disintegration of BRAF^{EV} organiods in absence of the niche factors.

Figure 3.7

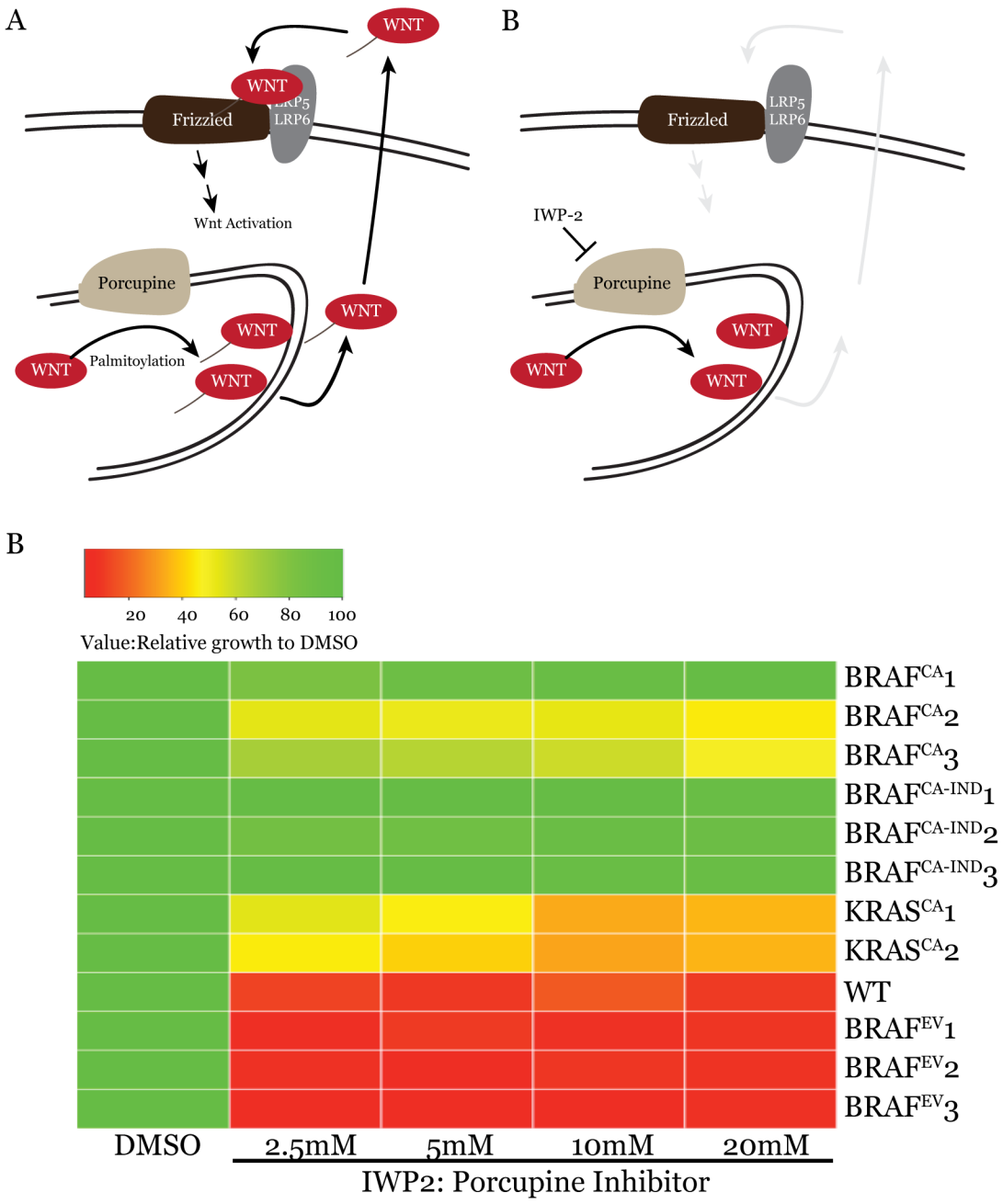
A
WNT
WNT
Frizzled
LRP5
LRP6
Wnt Activation
Porcupine
WNT
WNT
WNT
Palmitoylation
WNT
B
Frizzled
LRP5
LRP6
IWP-2
Porcupine
WNT
WNT
WNT
B
20
40
60
80
100
Value:Relative growth to DMSO
BRAF^{CA}1
BRAF^{CA}2
BRAF^{CA}3
BRAF$^{CA\text{-}IND}$1
BRAF$^{CA\text{-}IND}$2
BRAF$^{CA\text{-}IND}$3
KRAS^{CA}1
KRAS^{CA}2
WT
BRAF^{EV}1
BRAF^{EV}2
BRAF^{EV}3
DMSO
2.5mM
5mM
10mM
20mM
IWP2: Porcupine Inhibitor

Figure 3.7 BRAF$^{CA\text{-}IND}$ organiods are resistant to Porcupine inhibitor IWP2

(A) Schematic diagram of post-translational processing of Wnt ligands. Wnt proteins are palmitoylated by Porcupine and transported to the cis-Golgi network to be secreted outside. IWP2 inhibits palmitoylation of Wnt by Porcupine and therefore blocks secretion of Wnt. (B) Heatmap showing growth of each organoid in response to IWP-2, a Porcupine inhibitor in NS media. Relative growth rates of oragnoid at each IWP-2 concentration are calculated in comparison to the growth in DMSO treatment and are displayed as green for no growth inhibition and red for complete growth inhibition. The growth of WT and BRAF^{EV} was completely inhibited at as low as 2.5mM dose. However, the growth of KRAS^{CA} replicates was not completely inhibited although their growth was compromised. One of BRAF^{CA} replicates, BRAF^{CA}1 was completely resistant to IWP2 and the other two, BRAF^{CA}2-3 showed partial resistance to IWP2. All three BRAF$^{CA\text{-}IND}$ replicates showed complete resistance to IWP2.

Figure 3.8

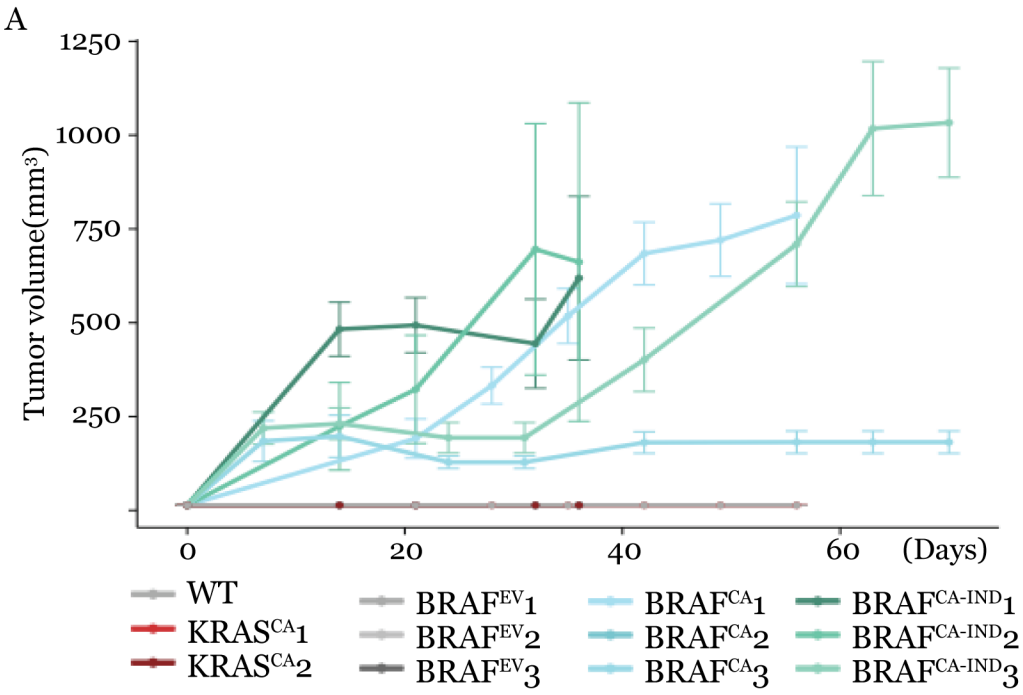

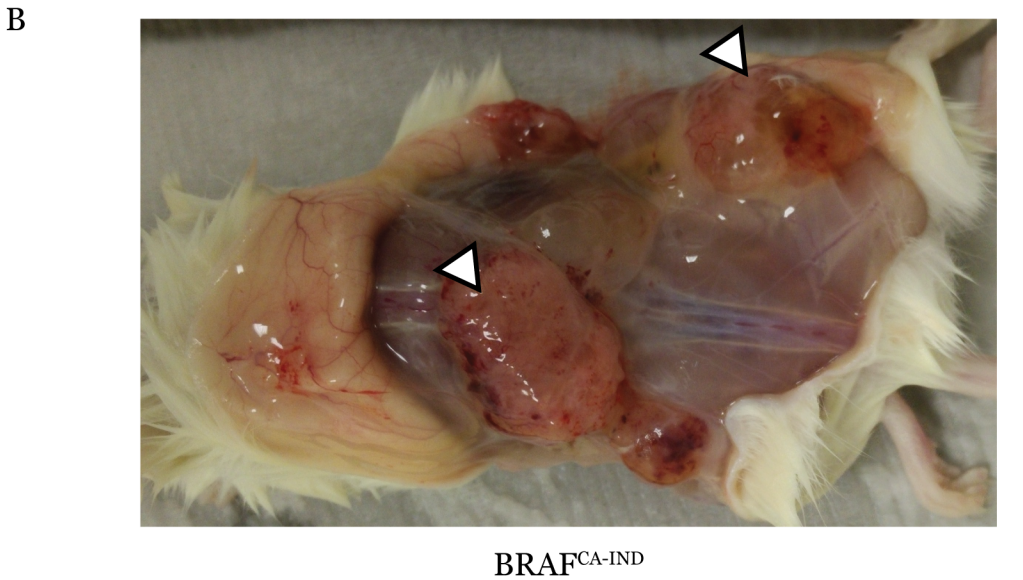

BRAF$^{CA\text{-}IND}$

Figure 3.8 (continued)

C

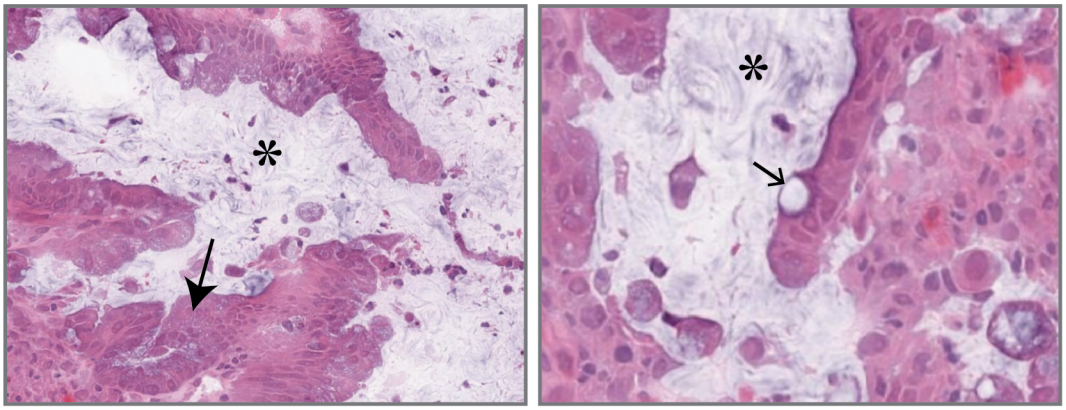

Human mucinous COAD : TCGA-AA-3877

D

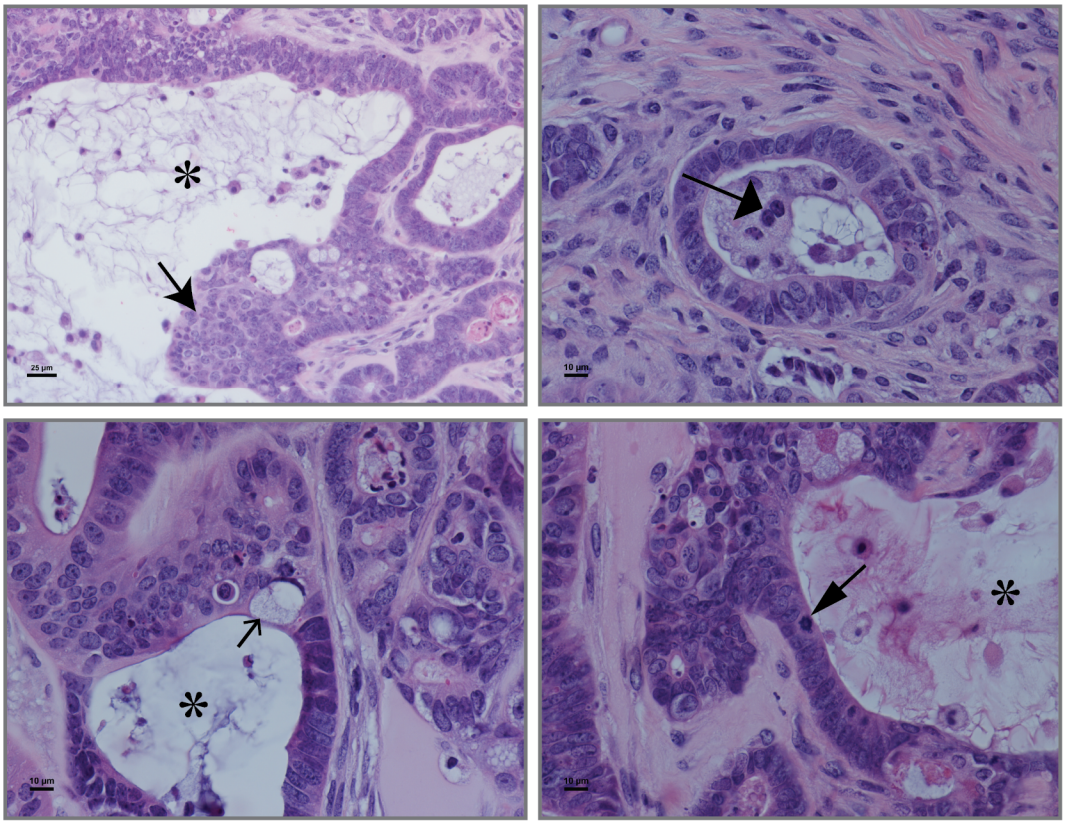

BRAF^{CA-XT}

Figure 3.8 A single step transformation by *BRAF*^{V600E} induces right-sided CRC phenotype

(A) Growth curve of xenograft tumors. None of WT and KRAS^{CA} forms tumors. All the implantations using BRAF$^{CA\text{-}IND}$ form tumors. Two replicates of BRAF^{CA} also form tumors as well. (B) Gross morphology of BRAF^{CA_IND} tumor. The tumors .(white triangle) were gelatinous with copious amount of mucin. (C) Histology of human mucinouse adenocarcinoma from TCGA database (TCGA-AA-3877). The tumor largely consists of mucin (*) filled cysts lined by piled up (barbed arrowhead) dysplastic cells. Occasionally, cells with a large vacuole (signet ring cell) present (simple arrow). (D) Histology of xenograft tumors (BRAF$^{CA\text{-}XT}$). The tumors consist of mucin (*) filled cysts lined by piled up dysplastic epithelial cells (barbed arrowhead) displaying high nuclear to cytoplasm ratio (double simple arrowhead), bizarre looking mitotic figures (narrow triangle arrowhead) and multinucleation (wide triangle arrowhead). Occasionally, signet ring cells (simple arrowhead) are observed.

Figure 3.9

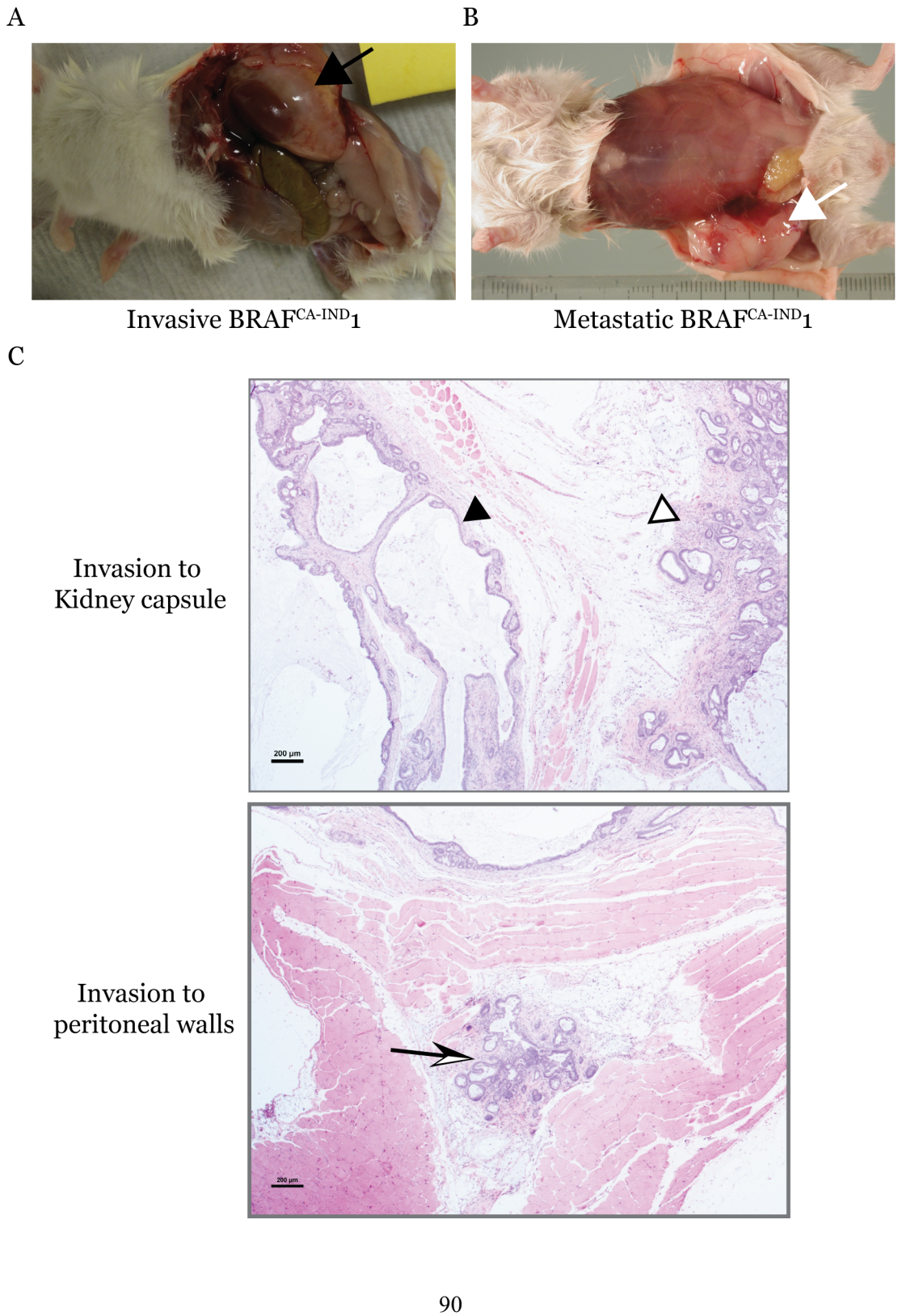
A
B
Invasive BRAF$^{CA\text{-}IND}$1
Metastatic BRAF$^{CA\text{-}IND}$1
C
Invasion to Kidney capsule
Invasion to peritoneal walls
200 µm
200 µm

Figure 3.9 The transformed *BRAF*^{V600E} organoids are invasive and metastatic

(A) Gross morphology of invading tumor (black triangle) (BRAF$^{CA\text{-}IND}$1). The organoids invaded to the peritoneum and grew as a tumor in the kidney capsule. (B) Gross morphology of metastatic tumor (white arrow) (BRAF$^{CA\text{-}IND}$1). The organoids were digested into single cells and one million cells were injected into tail vein of NSG mice. The cells injected into blood stream survived and formed xenograft tumors. (C) Histology of invading tumors. Tumors implanted in subcutaneous space (white triangle) invaded through peritoneal muscle layer and grew as a tumor in kidney capsule (black triangle). Occasionally, the tumor cells were observed in space between muscle layers (black and white barbed arrowhead) showing evidence of invasiveness.

Figure 3.10

A

	Mucinous adenocarcinoma	Adenocarcinoma
BRAF mutant	12	9
Others	20	176

* Fisher's test
p=1.676e-6 OR=11.49726

B

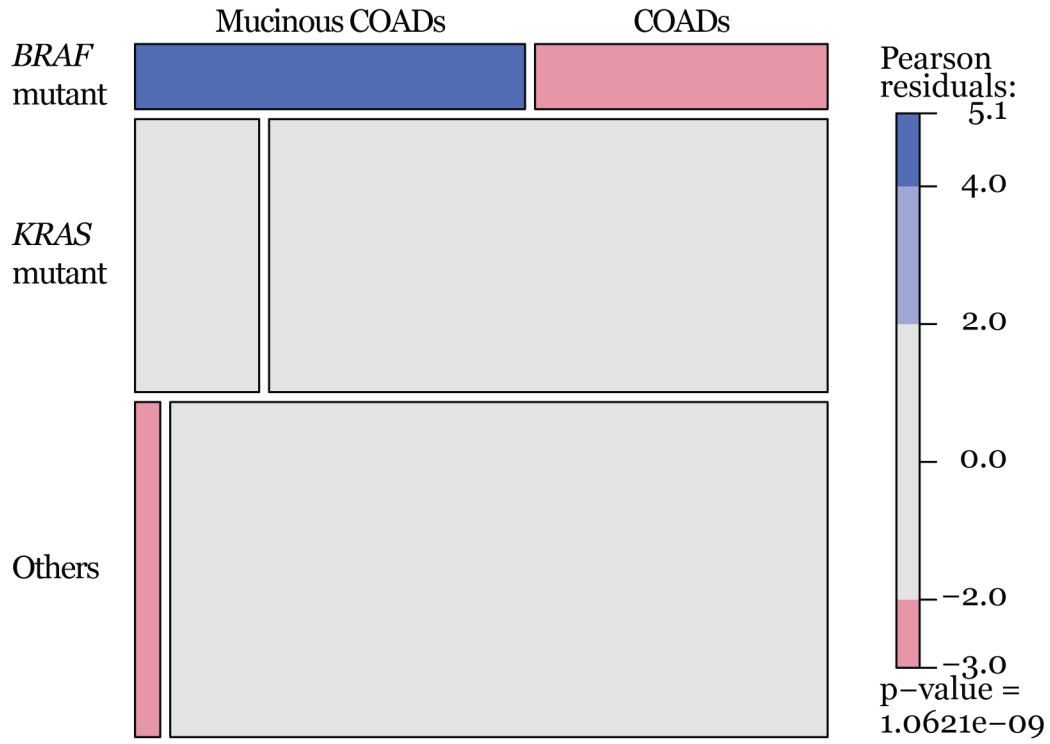

Figure 3.10 *BRAF* mutation is highly associated with mucinous adenocarcinoma histopathology type

(A) Contingency table between *BRAF* mutation status and tumor histopathology type (mucinous vs non-mucinous adenocarcinoma) (B) Contingency analysis between *BRAF* mutation status and tumor histopathology type (mucinous vs non-mucinous adenocarcinoma). *BRAF* mutation is highly associated with mucinous CRC.

Figure 3.11

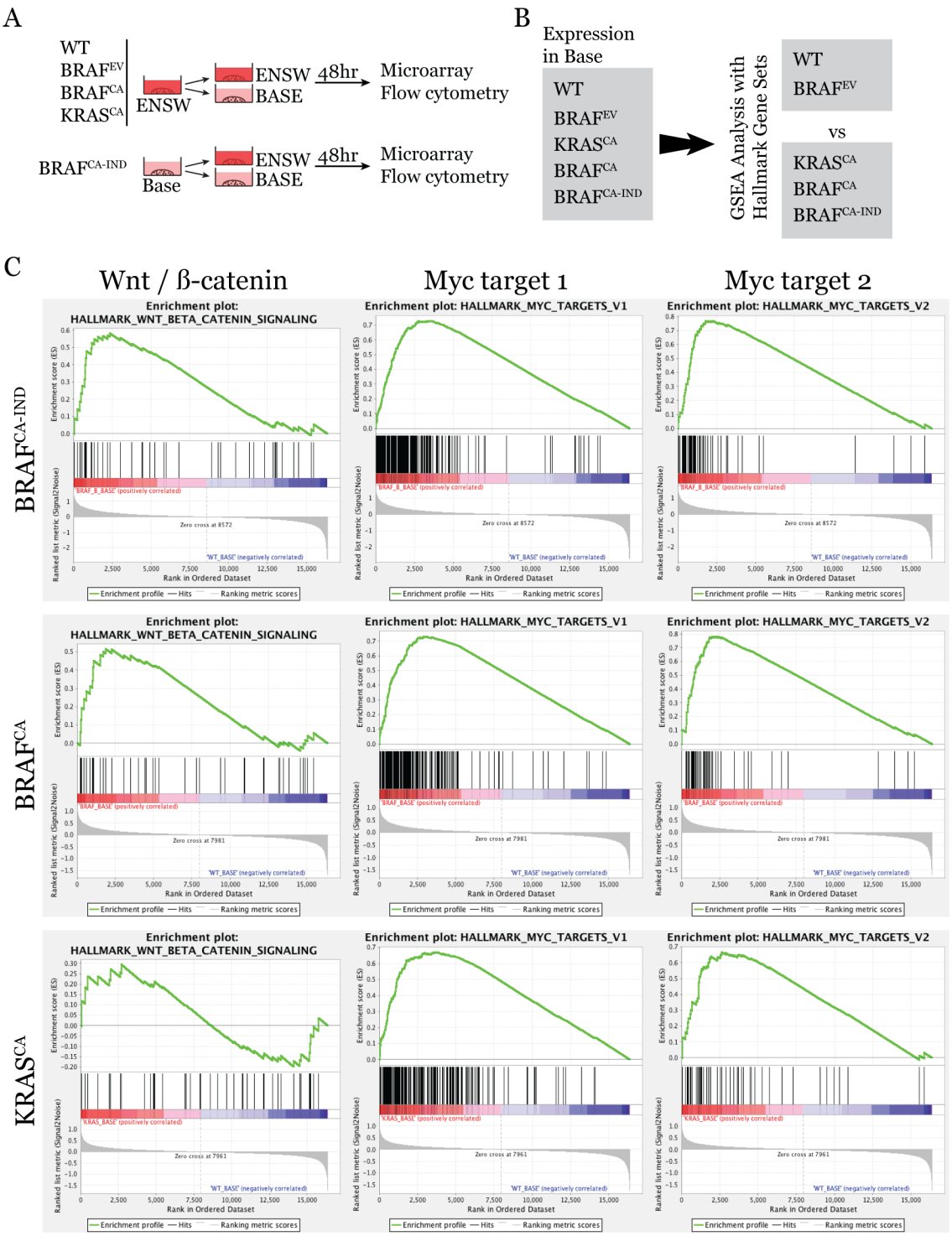
A
WT
BRAFEV
BRACA
KRASCA
ENSW
ENSW
BASE
48hr
Microarray
Flow cytometry
BRAFCA-IND
Base
ENSW
BASE
48hr
Microarray
Flow cytometry
B
Expression in Base
WT
BRAFEV
KRASCA
BRACA
BRAFCA-IND
GSEA Analysis with Hallmark Gene Sets
WT
BRAFEV
vs
KRASCA
BRACA
BRAFCA-IND
C
Wnt / ß-catenin
Myc target 1
Myc target 2
BRAFCA-IND
BRAFCA
KRASCA
Enrichment plot: HALLMARK_WNT_BETA_CATENIN_SIGNALING
Enrichment plot: HALLMARK_MYC_TARGETS_V1
Enrichment plot: HALLMARK_MYC_TARGETS_V2
Enrichment score (ES)
Ranked list metric (Signal2Noise)
Rank in Ordered Dataset
Enrichment profile
Hits
Ranking metric scores

Figure 3.11 Only *BRAF*^{V600E} induces Wnt / beta-catenin pathway in niche factor deficient media

(A) Schematic diagram of experiment design for gene expression microarray and flow cytometry analysis. WT, BRAF^{EV}, BRAF^{CA}, KRAS^{CA} and BRAF$^{CA\text{-}IND}$ were plated in two well separately and were grown in ENSW media and BASE media for 48hr. After 48hr, the organoids were harvested for gene expression microarray and flow cytometry. (B) Schematic diagram of GSEA analysis. The gene expression patterns of BRAF^{CA}, BRAF$^{CA\text{-}IND}$ and KRAS^{CA} are compared to those of WT and BRAF^{EV}. (C) Both *BRAF*^{V600E} and *KRAS*^{G12D} induce Myc targets. However, only *BRAF*^{V600E} but not *KRAS*^{G12D}, induces Wnt / beta-catenin pathway in niche factor deficient media.

Figure 3.12

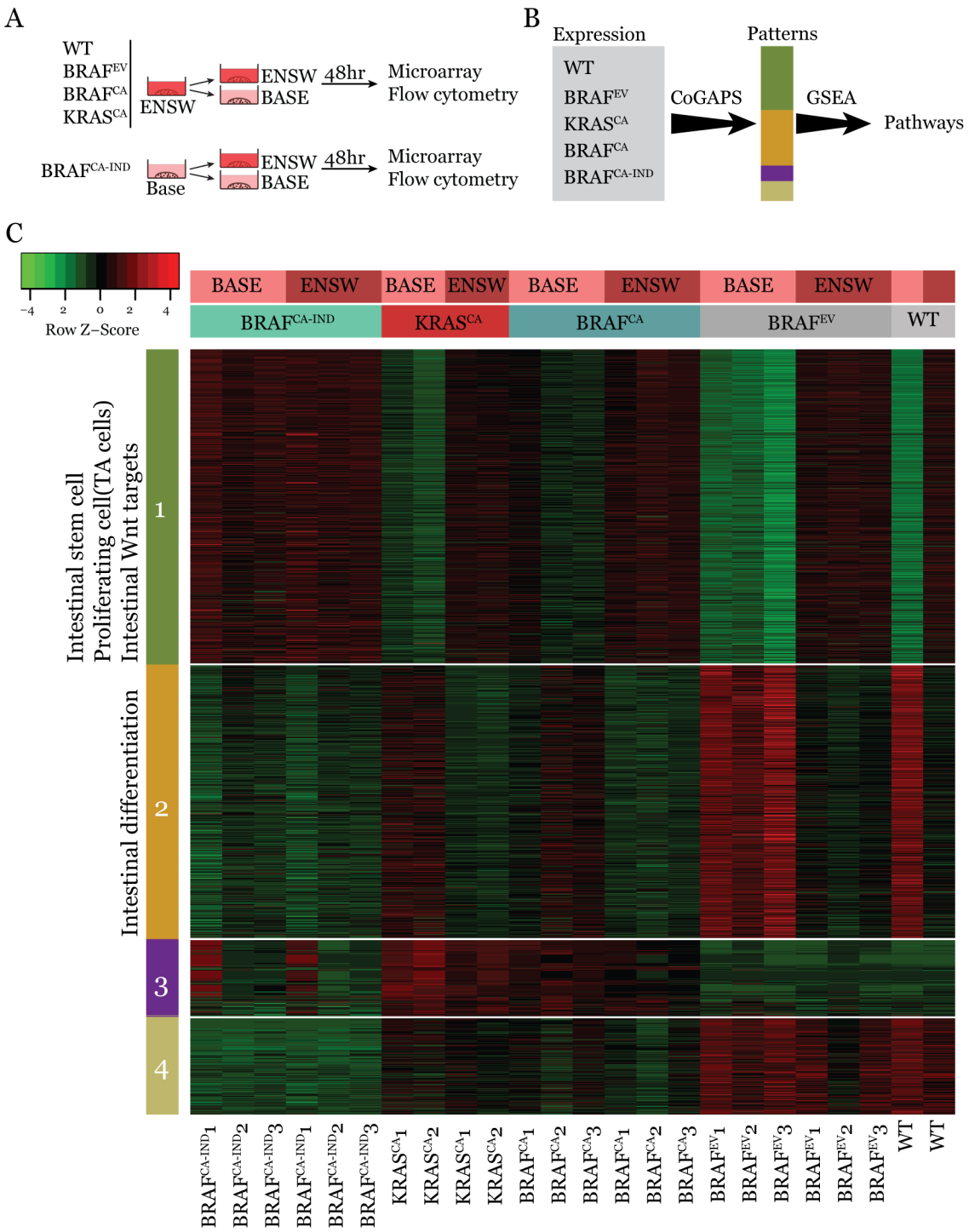
A
WT
BRAFEV
BRAFCA
KRASCA
ENSW
ENSW
BASE
48hr
Microarray
Flow cytometry
BRAFCA-IND
Base
ENSW
BASE
48hr
Microarray
Flow cytometry
B
Expression
WT
BRAFEV
KRASCA
BRAFCA
BRAFCA-IND
CoGAPS
Patterns
GSEA
Pathways
C
−4 2 0 2 4
Row Z−Score
BASE ENSW BASE ENSW BASE ENSW BASE ENSW
BRAFCA-IND KRASCA BRAFCA BRAFEV WT
Intestinal stem cell
Proliferating cell(TA cells)
Intestinal Wnt targets
1
Intestinal differentiation
2
3
4
BRAFCA-IND1
BRAFCA-IND2
BRAFCA-IND3
BRAFCA-IND1
BRAFCA-IND2
BRAFCA-IND3
KRASCA1
KRASCA2
KRASCA1
KRASCA2
BRAFCA1
BRAFCA2
BRAFCA3
BRAFCA1
BRAFCA2
BRAFCA3
BRAFEV1
BRAFEV2
BRAFEV3
BRAFEV1
BRAFEV2
BRAFEV3
WT
WT

Figure 3.12 The CoGAPs pattern analysis discovered four different patterns of gene expression in the different types of organoids

(A) Schematic diagram of experiment design for gene expression microarray and flow cytometry analysis. It is the same as in Figure 3.12. (B) Schematic diagram of CoGAPS analysis. CoGAPS algorithm is used to recognize agnostically patterns of gene expressions of the different organoids in ENSW and Base media. In each pattern, gene set enrichment analysis was done to discover specific pathways involved. (C) Heatmap of gene expression patterns. CoGAPS algorithm discovered four different patterns of gene expression. The pattern 1 genes are those up-regulated in ENSW media and dow-regulated in Base media in WT / BRAF^{EV}. However, their expression are sustained high in BRAF$^{CA\text{-}IND}$. Although their expression are not sustained in KRAS^{CA} and BRAF^{CA} in Base media as in WT / BRAF^{EV}, the extent of down-regulation is less than in WT / BRAF^{EV}. The pattern 2 has the opposite direction. The genes in the pattern 2 are down-regulated in ENSW and up-regulated in BASE in WT / BRAF^{EV}. However, their expression are sustained low in BRAF$^{CA\text{-}IND}$. Their expression in KRAS^{CA} and BRAF^{CA} are also up-regulated but to a lesser extent than in WT / BRAF^{EV}. The pattern 3 and 4 are genes that have genotype specific changes. Pattern 3 genes have high expression in WT / BRAF^{EV}. Pattern 4 genes have high expression in BRAF$^{CA\text{-}IND}$ and low expression in WT / BRAF^{EV}.

Figure 3.13

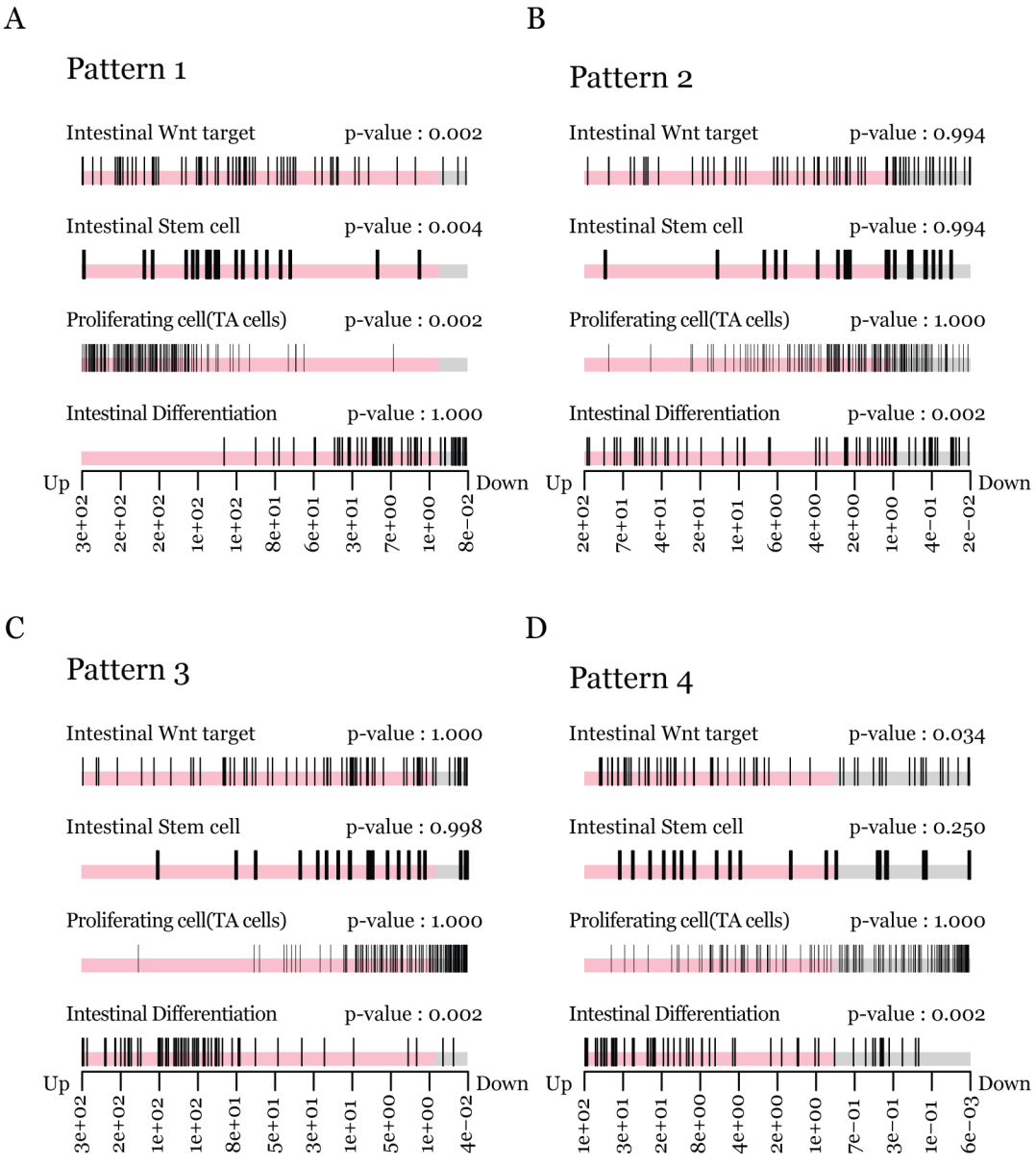
A
Pattern 1
Intestinal Wnt target
p-value : 0.002
Intestinal Stem cell
p-value : 0.004
Proliferating cell(TA cells)
p-value : 0.002
Intestinal Differentiation
p-value : 1.000
Up
Down
3e+02 2e+02 2e+02 1e+02 1e+02 8e+01 6e+01 3e+01 7e+00 1e+00 8e−02
B
Pattern 2
Intestinal Wnt target
p-value : 0.994
Intestinal Stem cell
p-value : 0.994
Proliferating cell(TA cells)
p-value : 1.000
Intestinal Differentiation
p-value : 0.002
Up
Down
2e+02 7e+01 4e+01 2e+01 1e+01 6e+00 4e+00 2e+00 1e+00 4e−01 2e−02
C
Pattern 3
Intestinal Wnt target
p-value : 1.000
Intestinal Stem cell
p-value : 0.998
Proliferating cell(TA cells)
p-value : 1.000
Intestinal Differentiation
p-value : 0.002
Up
Down
3e+02 2e+02 1e+02 1e+02 8e+01 5e+01 3e+01 1e+01 5e+00 1e+00 4e−02
D
Pattern 4
Intestinal Wnt target
p-value : 0.034
Intestinal Stem cell
p-value : 0.250
Proliferating cell(TA cells)
p-value : 1.000
Intestinal Differentiation
p-value : 0.002
Up
Down
1e+02 3e+01 2e+01 8e+00 4e+00 2e+00 1e+00 7e−01 3e−01 1e−01 6e−03

Figure 3.13 *BRAF*^{V600E} promotes sustained up-regulation of intestinal stem cell and proliferation genes and intestinal Wnt target genes even upon deprivation of all niche factors

(A) Pattern 1 is enriched for intestinal Wnt target genes and genes that are upregulated in intestinal stem cells and proliferating cells (TA cells). (B) Pattern 2 is enriched with genes upregulated in differentiated epithelial cells (C-D) Pattern 3 and 4 are enriched with differentiation genes.

Figure 3.14

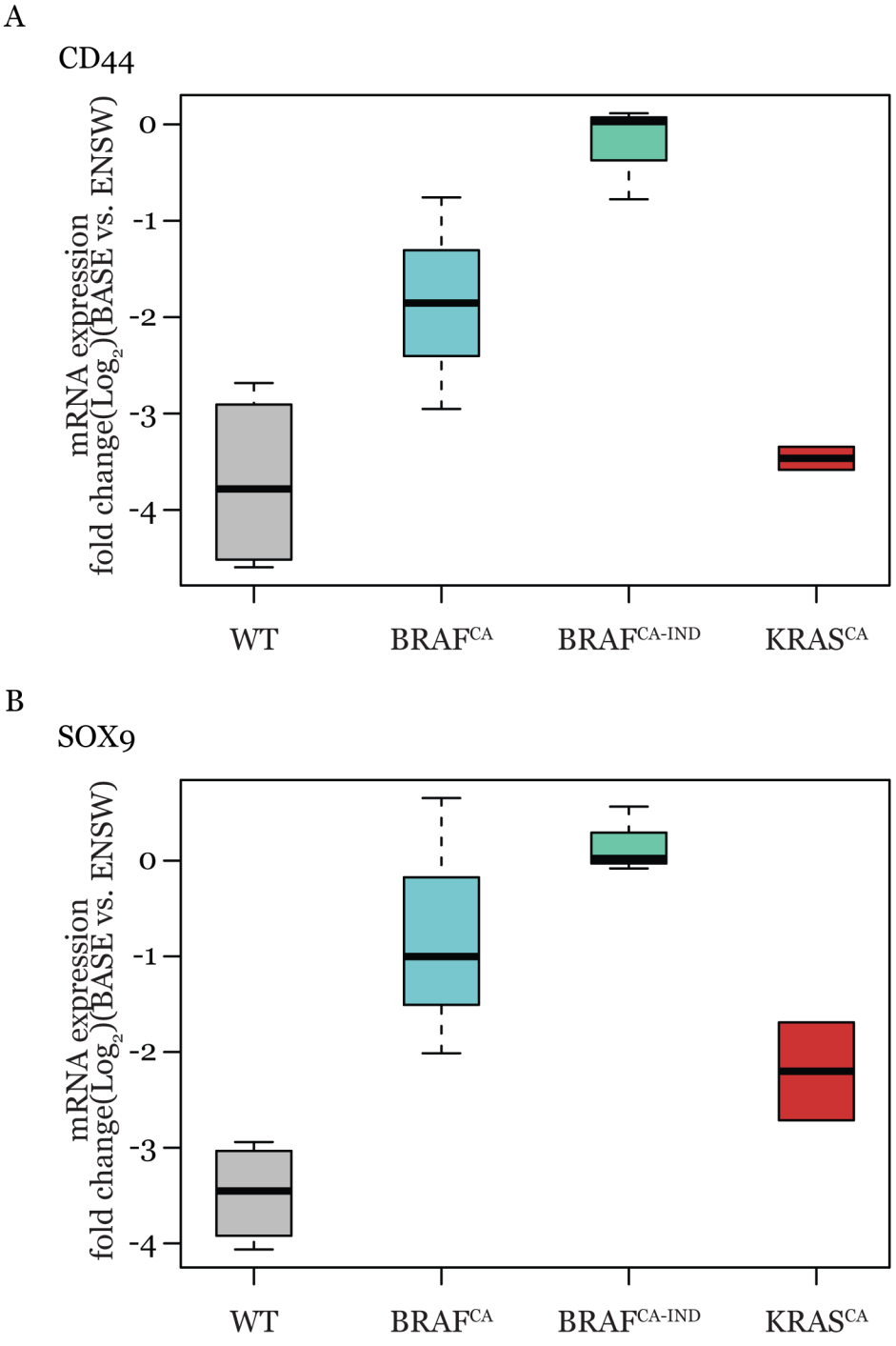
A
CD44
mRNA expression
fold change(Log2)(BASE vs. ENSW)
0
-1
-2
-3
-4
WT
BRAFCA
BRAFCA-IND
KRASCA
B
SOX9
mRNA expression
fold change(Log2)(BASE vs. ENSW)
0
-1
-2
-3
-4
WT
BRAFCA
BRAFCA-IND
KRASCA

Figure 3.14 Sustained up-regulation of intestinal stem cell markers, CD44 and Sox9 in BRAF$^{CA\text{-}IND}$ organoids

(A-B) Quantitative RT-PCR results of CD44 and Sox9. Ct values were normalized to GAPDH and fold changes in Base media culture compared to ENSW media were calculated. Grey color represents for WT / BRAF^{EV}, cadetblue for BRAF^{CA}, aquamarine for BRAF$^{CA\text{-}IND}$ and brown for KRAS^{CA}.

Figure 3.15

A ENSW media

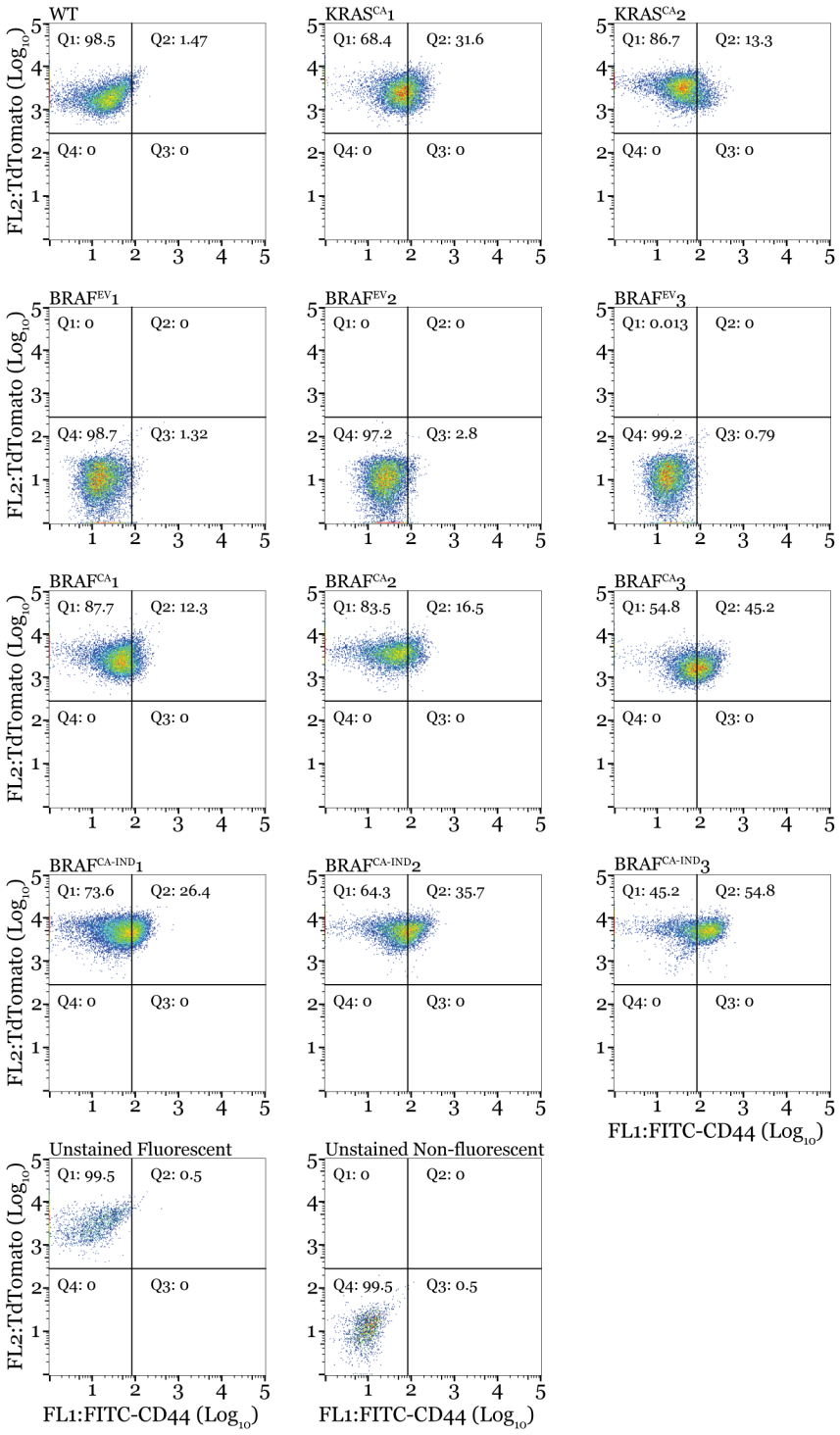

Figure 3.15 (continued)

B Base media

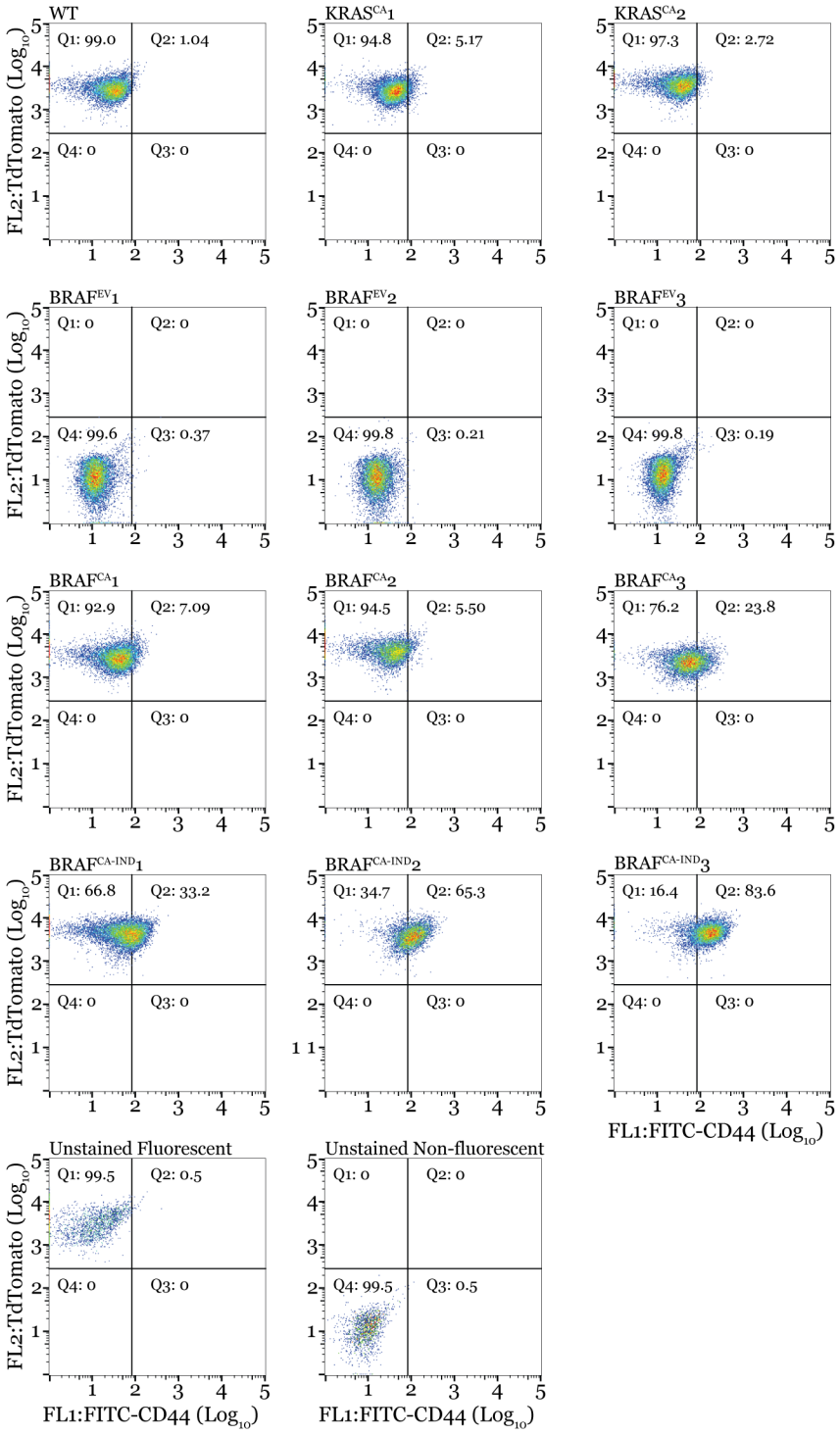

Figure 3.15 (continued)

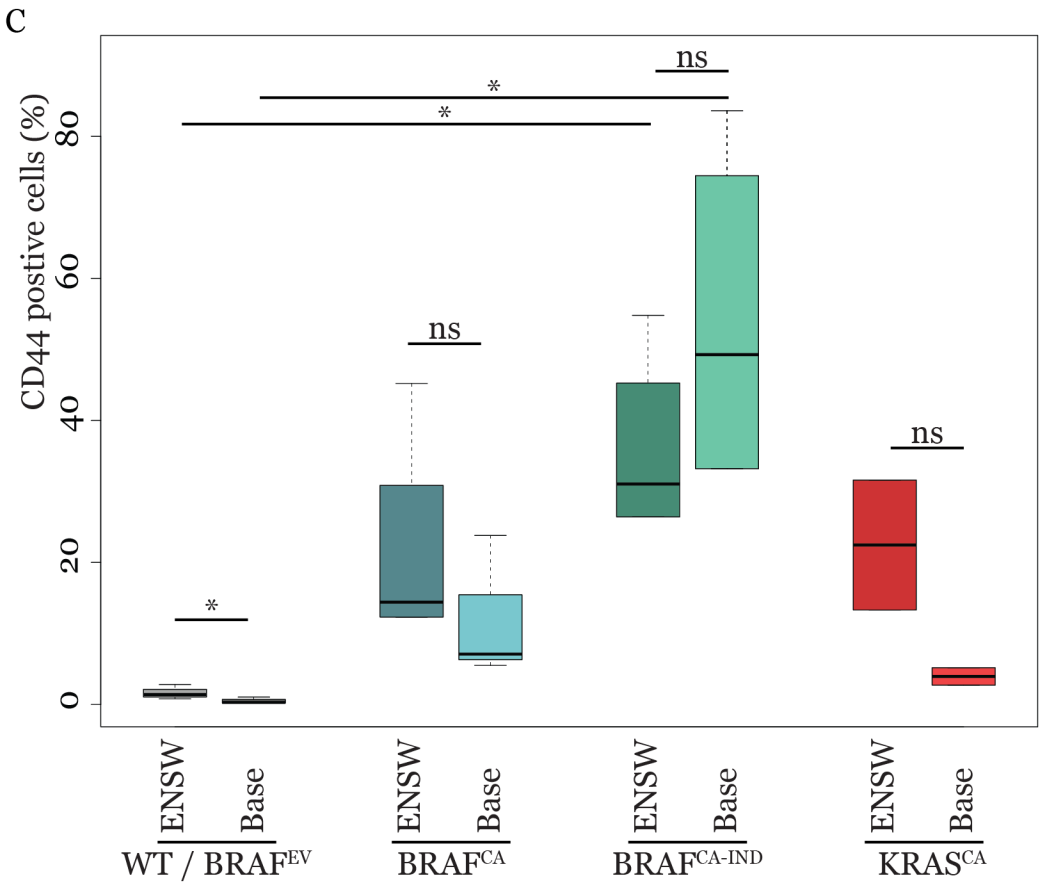

Figure 3.15 Sustained up-regulation of intestinal stem cells (CD44+) in BRAF$^{CA\text{-}IND}$ organoids

(A) Flow cytometry analysis for CD44 positive stem cells in organoids in ENSW and Base media. WT and BRAF^{EV} organoids consistently have the lowest number of CD44 positive stem cells in ENSW media. KRAS^{CA} and BRAF^{CA} have higher number than WT / BRAF^{EV} but less than BRAF$^{CA\text{-}IND}$. 48 hour deprivation of the niche factors reduces CD44 positive stem cells significantly in WT, BRAF^{EV}, KRAS^{CA} and BRAF^{CA}. However, the CD44 positive stem cells number is increased in all replicates of BRAF$^{CA\text{-}IND}$. (C) WT and BRAF^{EV} organoids consistently have the lowest number of CD44 positive stem cells in ENSW media. KRAS^{CA} and BRAF^{CA} have higher number than WT / BRAF^{EV} but less than BRAF$^{CA\text{-}IND}$. 48 hour deprivation of the niche factors reduces CD44 positive stem cells in WT, BRAF^{EV}, KRAS^{CA} and BRAF^{CA}. Only the reduction in WT / BRAF^{EV} is statistically significant. However, the CD44 positive stem cells number is increased in all replicates of BRAF$^{CA\text{-}IND}$. BRAF$^{CA\text{-}IND}$ replicates have higher number of stem cells compared to WT / BRAF^{EV} in both full media and deprivation media (Base) with a statistical significance.

Figure 3.16

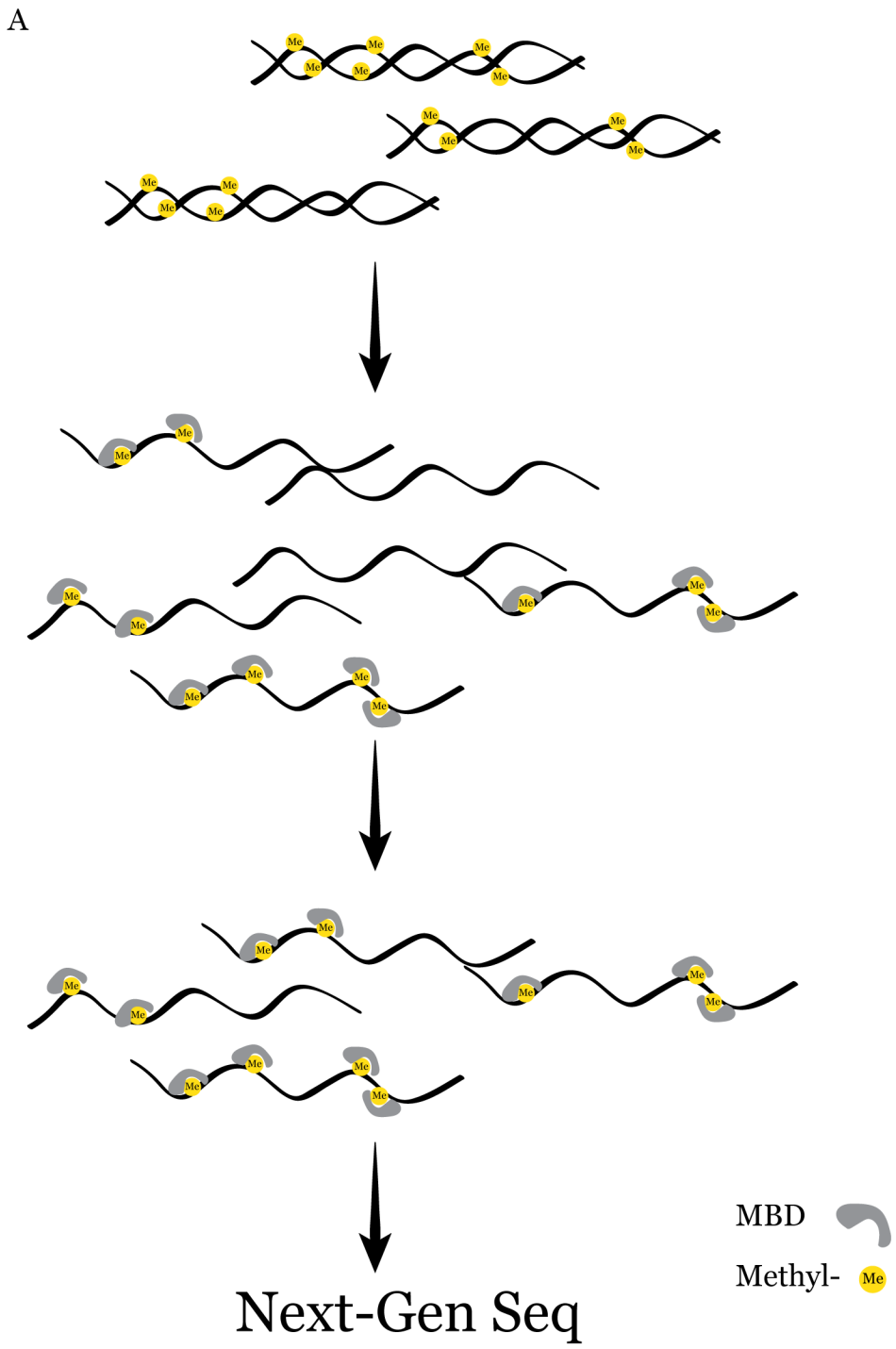

Figure 3.16 Schematic diagram Methyl CpG binding domain (MBD) DNA methylation sequencing

(A) Schematic diagram Methyl CpG binding domain (MBD) sequencing. The genomic DNA is sheared first and denatured. Then short single strands of DNA with CpG methylation are pulled down with Methyl CpG binding domain (MBD). The pull-down DNA strands are sequenced and aligned in the genome.

Figure 3. 17

A

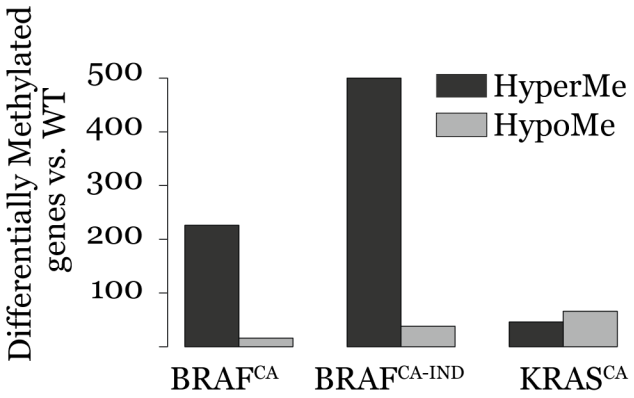

B

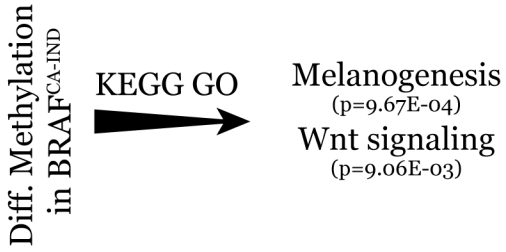

Figure 3.17 *BRAF*^{V600E} induces more differential DNA methylation than *KRAS*^{G12D} preferentially in Wnt pathway genes

(A) Graph showing differential DNA methylation in BRAF^{CA}, BRAF$^{CA\text{-}IND}$, KRAS^{CA} compared to WT. There is higher number of methylated genes in BRAF$^{CA\text{-}IND}$ compared to KRAS^{CA}. (B) KEGG gene ontology analysis revealed preferential methylation change in melanogenesis and Wnt signaling in BRAF$^{CA\text{-}IND}$.

Figure 3.18

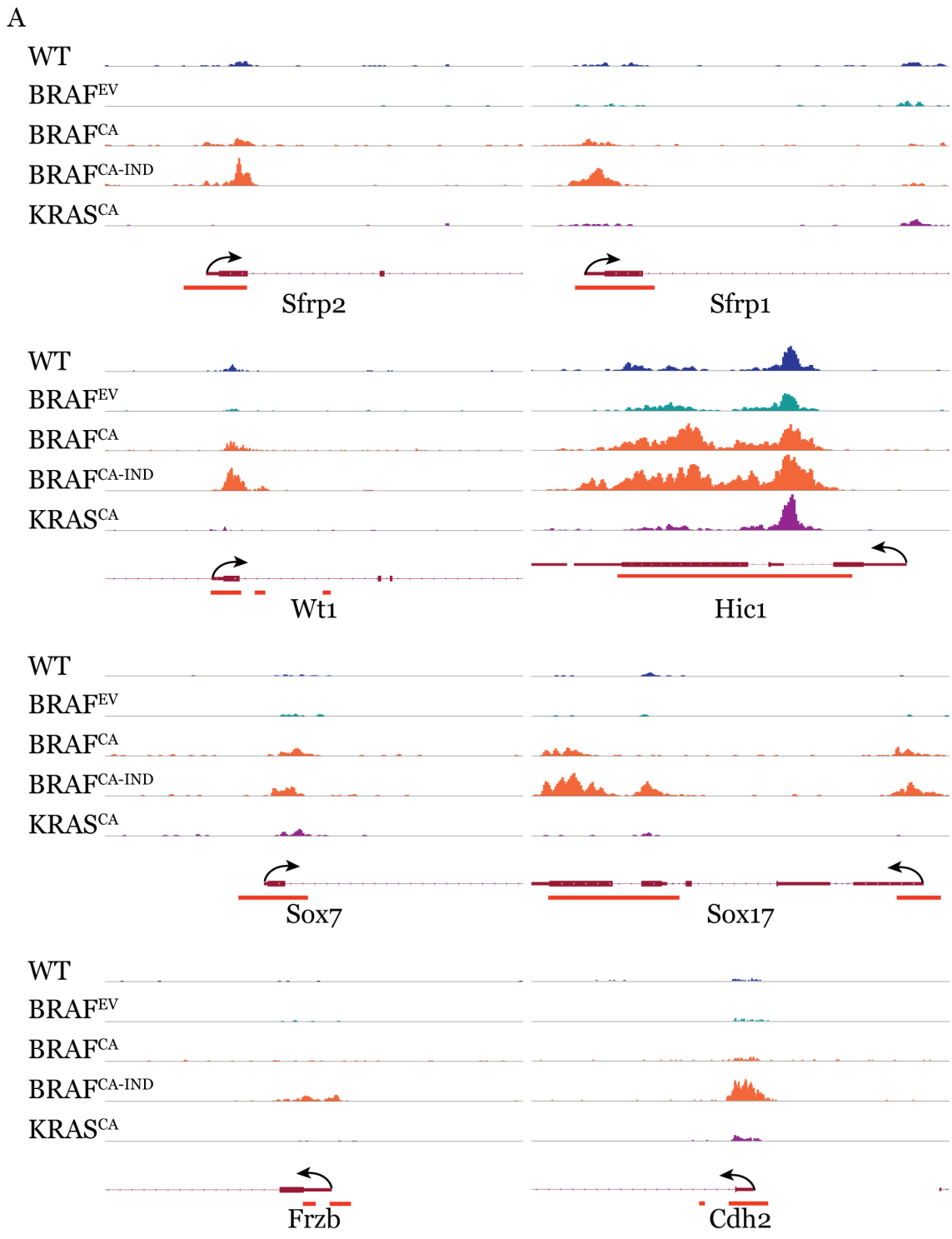
A
WT
BRAFEV
BRAFCA
BRAFCA-IND
KRASCA
Sfrp2
Sfrp1
Wt1
Hic1
Sox7
Sox17
Frzb
Cdh2

Figure 3.18 (Continued)

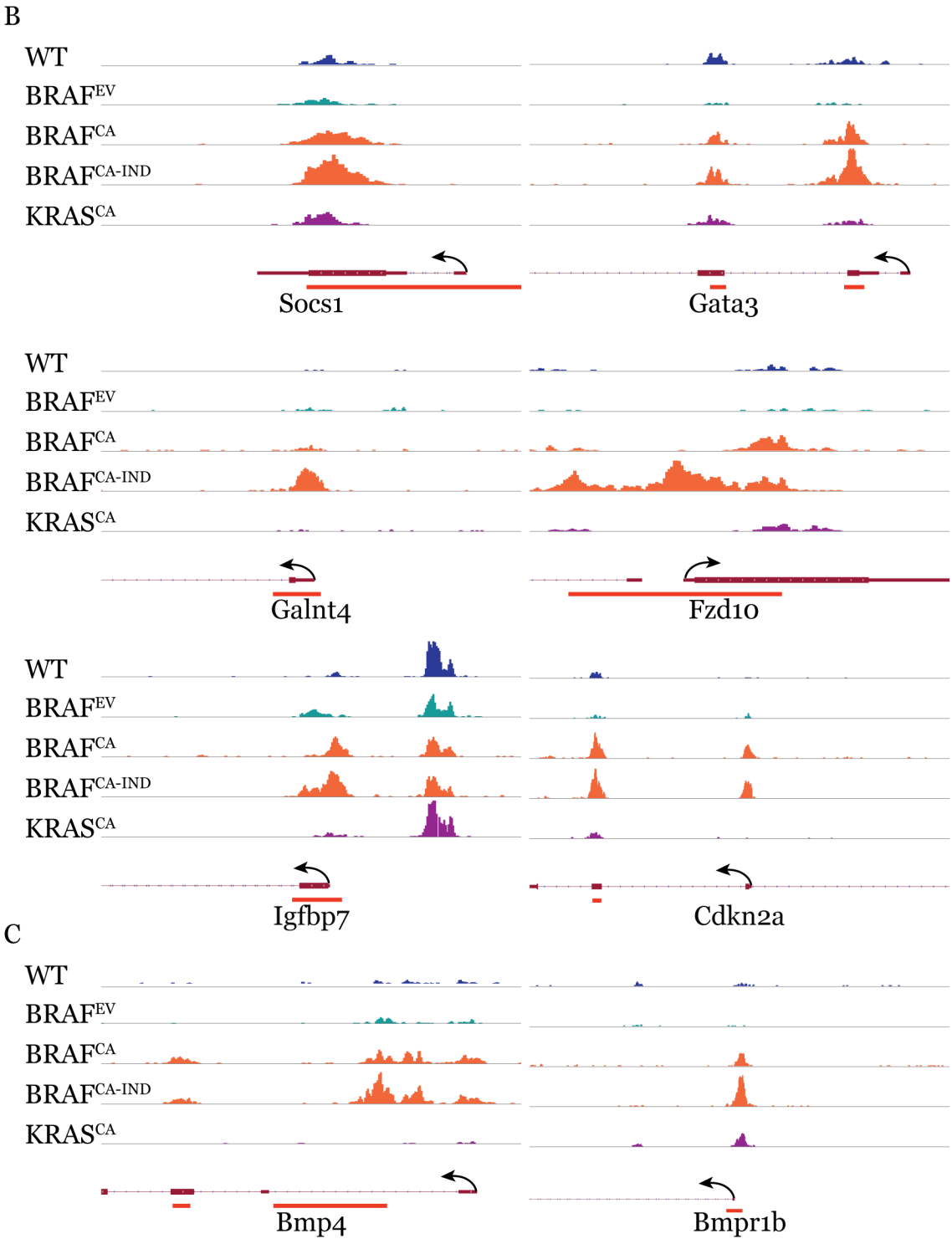

Figure 3.18 *BRAF*^{V600E} induces differential DNA methylation at the promoter CpG islands of Wnt negative regulators and CIMP marker genes

(A) Representative CpG island promoter regions of Wnt negative regulators. All of regions have an increase of DNA methylation at their promoter CpG island in BRAF$^{CA\text{-}IND}$ and partially in BRAF^{CA} implicating epigenetic silencing of Wnt negative regulators. (B) Representative CpG island promoter regions of CIMP genes. The regions have increased DNA methylation in BRAF$^{CA\text{-}IND}$ and partially in BRAF^{CA}. (C) Representative CpG island promoter regions of differentiation genes. Promoter CpG islands of those genes are methylated in BRAF$^{CA\text{-}IND}$ and partially in BRAF^{CA} implicating suppression of differentiation signaling in the organoids.

Figure 3.19

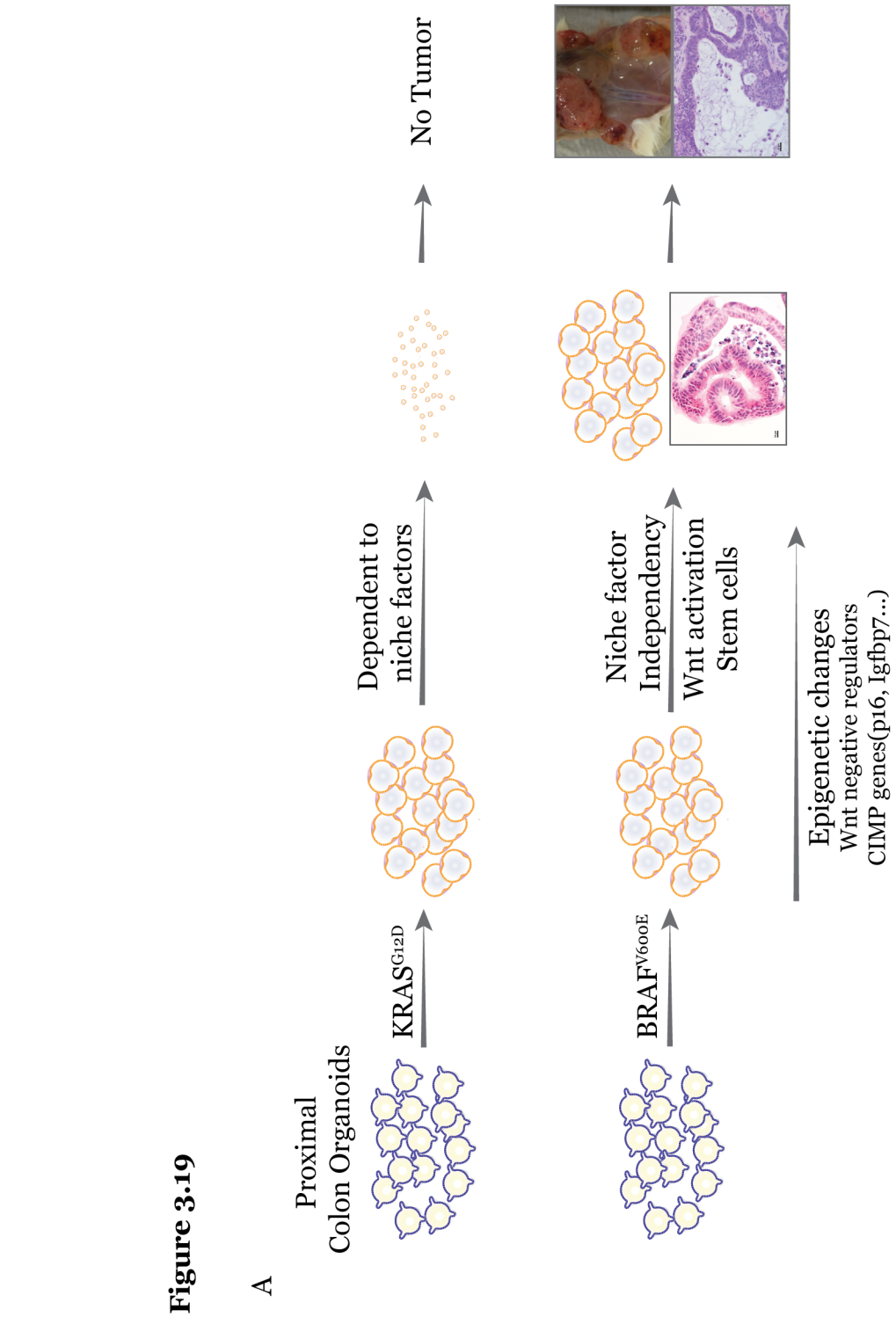
A
Proximal
Colon Organoids
KRAS^{G12D}
BRAF^{V600E}
Dependent to
niche factors
Niche factor
Independency
Wnt activation
Stem cells
Epigenetic changes
Wnt negative regulators
CIMP genes(p16, Igfbp7...)
No Tumor

Figure 3.19 A single-step induction of right-sided CRC phenotype by *BRAF*^{V600E} through acquired Wnt activation induced by accumulation of DNA methylation

(A) Upon induction of *BRAF*^{V600E}, the organoids accumulate DNA methylation on promoter CpG island of Wnt negative regulators and CIMP genes including cell cycle checkpoint genes. The accumulation of DNA methylation on those regions, in turn, induces niche factor independency through autonomous Wnt activation and sustained stemness. The niche factor independent organoids are fully transformed to form xenograft tumors which recapitulate human right-sided *BRAF* mutant tumors in terms of histopathology and DNA methylation patterns. However, induction of *KRAS*^{G12D} is not sufficient to make these changes and full transformation.

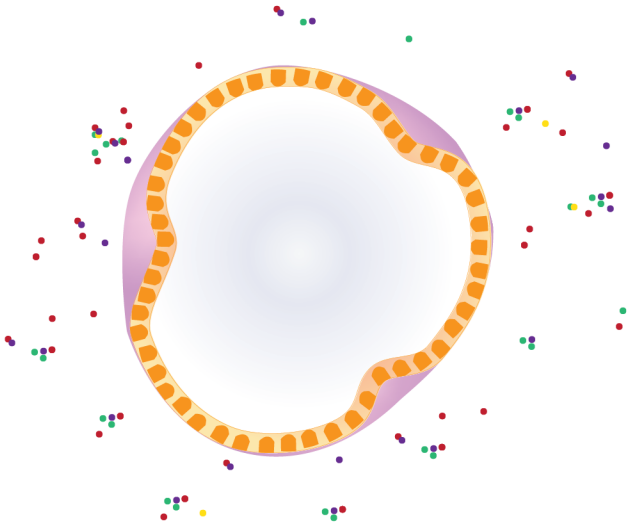

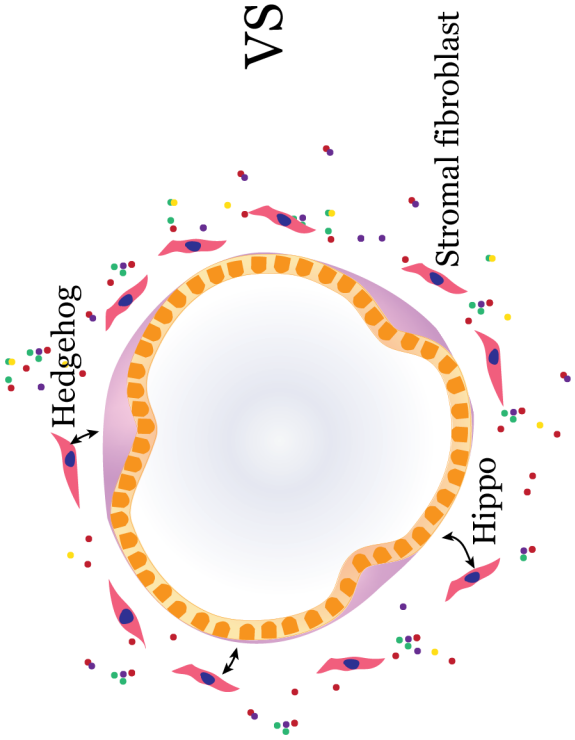

Figure 3.20

Figure 3.20 Interaction between organoids and stromal fibroblast can be modeled with the current *BRAF*^{V600E} mutant organoids

(A) Stromal fibroblast are reported to have a intensive interaction with epithelial cells through Hippo, Hedgehog and other signaling. The interaction can be modeled and studied by co-culturing our *BRAF*^{V600E} mutant organoids with intestinal stromal fibroblasts.

References

Arnold, C.N., Goel, A., Niedzwiecki, D., Dowell, J.M., Wasserman, L., Compton, C., Mayer, R.J., Bertagnolli, M.M., and Boland, C.R. (2004). APC promoter hypermethylation contributes to the loss of APC expression in colorectal cancers with allelic loss on 5q. Cancer Biol Ther *3*, 960-964.

Arnold, M., Sierra, M.S., Laversanne, M., Soerjomataram, I., Jemal, A., and Bray, F. (2016). Global patterns and trends in colorectal cancer incidence and mortality. Gut.

Basu, S., Haase, G., and Ben-Ze'ev, A. (2016). Wnt signaling in cancer stem cells and colon cancer metastasis. F1000Res *5*.

Baylin, S., and Bestor, T.H. (2002). Altered methylation patterns in cancer cell genomes: cause or consequence? Cancer Cell *1*, 299-305.

Baylin, S.B., and Jones, P.A. (2011). A decade of exploring the cancer epigenome - biological and translational implications. Nat Rev Cancer *11*, 726-734.

Baylin, S.B., and Ohm, J.E. (2006). Epigenetic gene silencing in cancer - a mechanism for early oncogenic pathway addiction? Nat Rev Cancer *6*, 107-116.

Bennecke, M., Kriegl, L., Bajbouj, M., Retzlaff, K., Robine, S., Jung, A., Arkan, M.C., Kirchner, T., and Greten, F.R. (2010). Ink4a/Arf and oncogene-induced senescence prevent tumor progression during alternative colorectal tumorigenesis. Cancer Cell *18*, 135-146.

Bettington, M., Walker, N., Clouston, A., Brown, I., Leggett, B., and Whitehall, V. (2013). The serrated pathway to colorectal carcinoma: current concepts and challenges. Histopathology *62*, 367-386.

Bhattacharjee, D., Shenoy, S., and Bairy, K.L. (2016). DNA Methylation and Chromatin Remodeling: The Blueprint of Cancer Epigenetics. Scientifica (Cairo) *2016*, 6072357.

Biegel, J.A., Busse, T.M., and Weissman, B.E. (2014). SWI/SNF chromatin remodeling complexes and cancer. Am J Med Genet C Semin Med Genet *166C*, 350-366.

Bock, C., Tomazou, E.M., Brinkman, A.B., Muller, F., Simmer, F., Gu, H., Jager, N., Gnirke, A., Stunnenberg, H.G., and Meissner, A. (2010). Quantitative comparison of genome-wide DNA methylation mapping technologies. Nat Biotechnol *28*, 1106-1114.

Burnett-Hartman, A.N., Newcomb, P.A., Potter, J.D., Passarelli, M.N., Phipps, A.I., Wurscher, M.A., Grady, W.M., Zhu, L.C., Upton, M.P., and Makar, K.W. (2013). Genomic aberrations occurring in subsets of serrated colorectal lesions but not conventional adenomas. Cancer Res *73*, 2863-2872.

Cancer Genome Atlas, N. (2012). Comprehensive molecular characterization of human colon and rectal cancer. Nature *487*, 330-337.

Carragher, L.A., Snell, K.R., Giblett, S.M., Aldridge, V.S., Patel, B., Cook, S.J., Winton, D.J., Marais, R., and Pritchard, C.A. (2010). V600EBraf induces gastrointestinal crypt senescence and promotes tumour progression through enhanced CpG methylation of p16INK4a. EMBO Mol Med *2*, 458-471.

Chen, B., Dodge, M.E., Tang, W., Lu, J., Ma, Z., Fan, C.W., Wei, S., Hao, W., Kilgore, J., Williams, N.S.*, et al.* (2009). Small molecule-mediated disruption of Wnt-dependent signaling in tissue regeneration and cancer. Nat Chem Biol *5*, 100-107.

Coyle, Y.M., Xie, X.J., Lewis, C.M., Bu, D., Milchgrub, S., and Euhus, D.M. (2007). Role of physical activity in modulating breast cancer risk as defined by APC and RASSF1A promoter hypermethylation in nonmalignant breast tissue. Cancer Epidemiol Biomarkers Prev *16*, 192-196.

Dankort, D., Filenova, E., Collado, M., Serrano, M., Jones, K., and McMahon, M. (2007). A new mouse model to explore the initiation, progression, and therapy of BRAFV600E-induced lung tumors. Genes Dev *21*, 379-384.

Date, S., and Sato, T. (2015). Mini-gut organoids: reconstitution of the stem cell niche. Annu Rev Cell Dev Biol *31*, 269-289.

de Lau, W., Barker, N., Low, T.Y., Koo, B.K., Li, V.S., Teunissen, H., Kujala, P., Haegebarth, A., Peters, P.J., van de Wetering, M., *et al.* (2011). Lgr5 homologues associate with Wnt receptors and mediate R-spondin signalling. Nature *476*, 293-297.

Dow, L.E., O'Rourke, K.P., Simon, J., Tschaharganeh, D.F., van Es, J.H., Clevers, H., and Lowe, S.W. (2015). Apc Restoration Promotes Cellular Differentiation and Reestablishes Crypt Homeostasis in Colorectal Cancer. Cell *161*, 1539-1552.

Drost, J., van Jaarsveld, R.H., Ponsioen, B., Zimberlin, C., van Boxtel, R., Buijs, A., Sachs, N., Overmeer, R.M., Offerhaus, G.J., Begthel, H., *et al.* (2015). Sequential cancer mutations in cultured human intestinal stem cells. Nature *521*, 43-47.

Du, L., Wang, H., He, L., Zhang, J., Ni, B., Wang, X., Jin, H., Cahuzac, N., Mehrpour, M., Lu, Y., *et al.* (2008). CD44 is of functional importance for colorectal cancer stem cells. Clin Cancer Res *14*, 6751-6760.

Ensari, A., Bosman, F.T., and Offerhaus, G.J. (2010). The serrated polyp: getting it right! J Clin Pathol *63*, 665-668.

Erdem, B., Kucukyildirim, S., Saglar, E., Polat, Z., and Mergen, H. (2014). Promoter hypermethylation of p16 and APC in gastrointestinal cancer patients. Turk J Gastroenterol *25*, 512-517.

Evans, G.S., Flint, N., and Potten, C.S. (1994). Primary cultures for studies of cell regulation and physiology in intestinal epithelium. Annu Rev Physiol *56*, 399-417.

Fang, M., Ou, J., Hutchinson, L., and Green, M.R. (2014). The BRAF oncoprotein functions through the transcriptional repressor MAFG to mediate the CpG Island Methylator phenotype. Mol Cell *55*, 904-915.

Fearon, E.R. (2011). Molecular genetics of colorectal cancer. Annu Rev Pathol *6*, 479-507.

Feng, Y., Sentani, K., Wiese, A., Sands, E., Green, M., Bommer, G.T., Cho, K.R., and Fearon, E.R. (2013). Sox9 induction, ectopic Paneth cells, and mitotic spindle axis defects in mouse colon adenomatous epithelium arising from conditional biallelic Apc inactivation. Am J Pathol *183*, 493-503.

Fertig, E.J., Ding, J., Favorov, A.V., Parmigiani, G., and Ochs, M.F. (2010). CoGAPS: an R/C++ package to identify patterns and biological process activity in transcriptomic data. Bioinformatics *26*, 2792-2793.

Fertig, E.J., Favorov, A.V., and Ochs, M.F. (2013). Identifying context-specific transcription factor targets from prior knowledge and gene expression data. IEEE Trans Nanobioscience *12*, 142-149.

Fertig, E.J., Ren, Q., Cheng, H., Hatakeyama, H., Dicker, A.P., Rodeck, U., Considine, M., Ochs, M.F., and Chung, C.H. (2012). Gene expression signatures modulated by epidermal growth factor receptor activation and their relationship to cetuximab resistance in head and neck squamous cell carcinoma. BMC Genomics *13*, 160.

Fertig, E.J., Stein-O'Brien, G., Jaffe, A., and Colantuoni, C. (2014). Pattern identification in time-course gene expression data with the CoGAPS matrix factorization. Methods Mol Biol *1101*, 87-112.

Foulke-Abel, J., In, J., Yin, J., Zachos, N.C., Kovbasnjuk, O., Estes, M.K., de Jonge, H., and Donowitz, M. (2016). Human Enteroids as a Model of Upper Small Intestinal Ion Transport Physiology and Pathophysiology. Gastroenterology *150*, 638-649 e638.

Fu, X., Li, J., Li, K., Tian, X., and Zhang, Y. (2009). Hypermethylation of APC promoter 1A is associated with moderate activation of Wnt signalling pathway in a subset of colorectal serrated adenomas. Histopathology *55*, 554-563.

Furlan, D., Sahnane, N., Bernasconi, B., Frattini, M., Tibiletti, M.G., Molinari, F., Marando, A., Zhang, L., Vanoli, A., Casnedi, S.*, et al.* (2014). APC alterations are frequently involved in the pathogenesis of acinar cell carcinoma of the pancreas, mainly through gene loss and promoter hypermethylation. Virchows Arch *464*, 553-564.

Gao, J., Aksoy, B.A., Dogrusoz, U., Dresdner, G., Gross, B., Sumer, S.O., Sun, Y., Jacobsen, A., Sinha, R., Larsson, E.*, et al.* (2013). Integrative analysis of complex cancer genomics and clinical profiles using the cBioPortal. Sci Signal *6*, pl1.

Geng, L., Zhu, M., Wang, Y., Cheng, Y., Liu, J., Shen, W., Li, Z., Zhang, J., Wang, C., Jin, G.*, et al.* (2016). Genetic variants in chromatin-remodeling pathway associated with lung cancer risk in a Chinese population. Gene *587*, 178-182.

Guerrero-Preston, R., Michailidi, C., Marchionni, L., Pickering, C.R., Frederick, M.J., Myers, J.N., Yegnasubramanian, S., Hadar, T., Noordhuis, M.G., Zizkova, V., *et al.* (2014). Key tumor suppressor genes inactivated by "greater promoter" methylation and somatic mutations in head and neck cancer. Epigenetics *9*, 1031-1046.

Guinney, J., Dienstmann, R., Wang, X., de Reynies, A., Schlicker, A., Soneson, C., Marisa, L., Roepman, P., Nyamundanda, G., Angelino, P., *et al.* (2015). The consensus molecular subtypes of colorectal cancer. Nat Med *21*, 1350-1356.

Haluskova, J., Lachvac, L., and Nagy, V. (2015). The investigation of GSTP1, APC and RASSF1 gene promoter hypermethylation in urine DNA of prostate-diseased patients. Bratisl Lek Listy *116*, 79-82.

Hanahan, D., and Weinberg, R.A. (2011). Hallmarks of cancer: the next generation. Cell *144*, 646-674.

Harris, R.A., Wang, T., Coarfa, C., Nagarajan, R.P., Hong, C., Downey, S.L., Johnson, B.E., Fouse, S.D., Delaney, A., Zhao, Y., *et al.* (2010). Comparison of sequencing-based methods to profile DNA methylation and identification of monoallelic epigenetic modifications. Nat Biotechnol *28*, 1097-1105.

Hatziapostolou, M., and Iliopoulos, D. (2011). Epigenetic aberrations during oncogenesis. Cell Mol Life Sci *68*, 1681-1702.

He, X., Yan, B., Liu, S., Jia, J., Lai, W., Xin, X., Tang, C.E., Luo, D., Tan, T., Jiang, Y., *et al.* (2016). Chromatin remodeling factor LSH drives cancer progression by suppressing the activity of fumarate hydratase. Cancer Res.

He, X.C., Zhang, J., Tong, W.G., Tawfik, O., Ross, J., Scoville, D.H., Tian, Q., Zeng, X., He, X., Wiedemann, L.M., *et al.* (2004). BMP signaling inhibits intestinal stem cell self-renewal through suppression of Wnt-beta-catenin signaling. Nat Genet *36*, 1117-1121.

Hiltunen, M.O., Alhonen, L., Koistinaho, J., Myohanen, S., Paakkonen, M., Marin, S., Kosma, V.M., and Janne, J. (1997). Hypermethylation of the APC (adenomatous polyposis coli) gene promoter region in human colorectal carcinoma. International journal of cancer Journal international du cancer *70*, 644-648.

Hinoue, T., Weisenberger, D.J., Lange, C.P., Shen, H., Byun, H.M., Van Den Berg, D., Malik, S., Pan, F., Noushmehr, H., van Dijk, C.M., *et al.* (2012). Genome-scale analysis of aberrant DNA methylation in colorectal cancer. Genome Res *22*, 271-282.

Hinoue, T., Weisenberger, D.J., Pan, F., Campan, M., Kim, M., Young, J., Whitehall, V.L., Leggett, B.A., and Laird, P.W. (2009). Analysis of the association between CIMP and BRAF in colorectal cancer by DNA methylation profiling. PloS one *4*, e8357.

Huang, H.T., Chen, S.M., Pan, L.B., Yao, J., and Ma, H.T. (2015). Loss of function of SWI/SNF chromatin remodeling genes leads to genome instability of human lung cancer. Oncol Rep *33*, 283-291.

Hughes, L.A., Khalid-de Bakker, C.A., Smits, K.M., van den Brandt, P.A., Jonkers, D., Ahuja, N., Herman, J.G., Weijenberg, M.P., and van Engeland, M. (2012). The CpG island methylator phenotype in colorectal cancer: progress and problems. Biochim Biophys Acta *1825*, 77-85.

Hughes, L.A., Melotte, V., de Schrijver, J., de Maat, M., Smit, V.T., Bovee, J.V., French, P.J., van den Brandt, P.A., Schouten, L.J., de Meyer, T., *et al.* (2013). The CpG island methylator phenotype: what's in a name? Cancer Res *73*, 5858-5868.

Inoue, A., Okamoto, K., Fujino, Y., Nakagawa, T., Muguruma, N., Sannomiya, K., Mitsui, Y., Takaoka, T., Kitamura, S., Miyamoto, H., *et al.* B-RAF mutation and accumulated gene methylation in aberrant crypt foci (ACF), sessile serrated adenoma/polyp (SSA/P) and cancer in SSA/P.

Inoue, A., Okamoto, K., Fujino, Y., Nakagawa, T., Muguruma, N., Sannomiya, K., Mitsui, Y., Takaoka, T., Kitamura, S., Miyamoto, H., *et al.* (2015). B-RAF mutation and accumulated gene methylation in aberrant crypt foci (ACF), sessile serrated adenoma/polyp (SSA/P) and cancer in SSA/P. British journal of cancer *112*, 403-412.

Jackson, E.L., Willis, N., Mercer, K., Bronson, R.T., Crowley, D., Montoya, R., Jacks, T., and Tuveson, D.A. (2001). Analysis of lung tumor initiation and progression using conditional expression of oncogenic K-ras. Genes Dev *15*, 3243-3248.

Jass, J.R. (2007). Classification of colorectal cancer based on correlation of clinical, morphological and molecular features. Histopathology *50*, 113-130.

Jin, Z., Tamura, G., Tsuchiya, T., Sakata, K., Kashiwaba, M., Osakabe, M., and Motoyama, T. (2001). Adenomatous polyposis coli (APC) gene promoter hypermethylation in primary breast cancers. British journal of cancer *85*, 69-73.

Jones, S., Chen, W.D., Parmigiani, G., Diehl, F., Beerenwinkel, N., Antal, T., Traulsen, A., Nowak, M.A., Siegel, C., Velculescu, V.E.*, et al.* (2008). Comparative lesion sequencing provides insights into tumor evolution. Proc Natl Acad Sci U S A *105*, 4283-4288.

Jorissen, R.N., Christie, M., Mouradov, D., Sakthianandeswaren, A., Li, S., Love, C., Xu, Z.Z., Molloy, P.L., Jones, I.T., McLaughlin, S.*, et al.* (2015). Wild-type APC predicts poor prognosis in microsatellite-stable proximal colon cancer. British journal of cancer *113*, 979-988.

Juhlin, C.C., Kiss, N.B., Villablanca, A., Haglund, F., Nordenstrom, J., Hoog, A., and Larsson, C. (2010). Frequent promoter hypermethylation of the APC and RASSF1A tumour suppressors in parathyroid tumours. PloS one *5*, e9472.

Kadoch, C., and Crabtree, G.R. (2015). Mammalian SWI/SNF chromatin remodeling complexes and cancer: Mechanistic insights gained from human genomics. Sci Adv *1*, e1500447.

Kambara, T., Simms, L.A., Whitehall, V.L.J., Spring, K.J., Wynter, C.V.A., Walsh, M.D., Barker, M.A., Arnold, S., McGivern, A., Matsubara, N.*, et al.* (2004). BRAF mutation is associated with DNA methylation in serrated polyps and cancers of the colorectum. Gut *53*, 1137-1144.

Kriegl, L., Neumann, J., Vieth, M., Greten, F.R., Reu, S., Jung, A., and Kirchner, T. (2011). Up and downregulation of p16(Ink4a) expression in BRAF-mutated polyps/adenomas indicates a senescence barrier in the serrated route to colon cancer. Mod Pathol *24*, 1015-1022.

Kuhnert, F., Davis, C.R., Wang, H.T., Chu, P., Lee, M., Yuan, J., Nusse, R., and Kuo, C.J. (2004). Essential requirement for Wnt signaling in proliferation of adult small intestine and colon revealed by adenoviral expression of Dickkopf-1. Proc Natl Acad Sci U S A *101*, 266-271.

Langmead, B., and Salzberg, S.L. (2012). Fast gapped-read alignment with Bowtie 2. Nat Methods *9*, 357-359.

Le, D.T., Uram, J.N., Wang, H., Bartlett, B.R., Kemberling, H., Eyring, A.D., Skora, A.D., Luber, B.S., Azad, N.S., Laheru, D., *et al.* (2015). PD-1 Blockade in Tumors with Mismatch-Repair Deficiency. N Engl J Med *372*, 2509-2520.

Lee, S., Cho, N.Y., Yoo, E.J., Kim, J.H., and Kang, G.H. (2008). CpG island methylator phenotype in colorectal cancers: comparison of the new and classic CpG island methylator phenotype marker panels. Arch Pathol Lab Med *132*, 1657-1665.

Levin, M.K., Wang, K., Yelensky, R., Cao, Y., Ramos, C., Hoke, N., Pippen, J., Jr., Blum, J.L., Brooks, B., Palmer, G., *et al.* (2015). Genomic alterations in DNA repair and chromatin remodeling genes in estrogen receptor-positive metastatic breast cancer patients with exceptional responses to capecitabine. Cancer Med *4*, 1289-1293.

Li, F.Y., and Lai, M.D. (2009). Colorectal cancer, one entity or three. J Zhejiang Univ Sci B *10*, 219-229.

Li, S.C., and Burgart, L. (2007). Histopathology of serrated adenoma, its variants, and differentiation from conventional adenomatous and hyperplastic polyps. Arch Pathol Lab Med *131*, 440-445.

Li, X., Nadauld, L., Ootani, A., Corney, D.C., Pai, R.K., Gevaert, O., Cantrell, M.A., Rack, P.G., Neal, J.T., Chan, C.W., *et al.* (2014). Oncogenic transformation of diverse gastrointestinal tissues in primary organoid culture. Nat Med *20*, 769-777.

Mahe, M.M., Sundaram, N., Watson, C.L., Shroyer, N.F., and Helmrath, M.A. (2015). Establishment of human epithelial enteroids and colonoids from whole tissue and biopsy. J Vis Exp.

Makinen, M.J. (2007). Colorectal serrated adenocarcinoma. Histopathology *50*, 131-150.

Malonia, S.K., Yadav, B., Sinha, S., Lazennec, G., and Chattopadhyay, S. (2014). Chromatin remodeling protein SMAR1 regulates NF-kappaB dependent Interleukin-8 transcription in breast cancer. Int J Biochem Cell Biol *55*, 220-226.

Matano, M., Date, S., Shimokawa, M., Takano, A., Fujii, M., Ohta, Y., Watanabe, T., Kanai, T., and Sato, T. (2015). Modeling colorectal cancer using CRISPR-Cas9-mediated engineering of human intestinal organoids. Nat Med *21*, 256-262.

Mayes, K., Qiu, Z., Alhazmi, A., and Landry, J.W. (2014). ATP-dependent chromatin remodeling complexes as novel targets for cancer therapy. Adv Cancer Res *121*, 183-233.

Merlos-Suarez, A., Barriga, F.M., Jung, P., Iglesias, M., Cespedes, M.V., Rossell, D., Sevillano, M., Hernando-Momblona, X., da Silva-Diz, V., Munoz, P.*, et al.* (2011). The intestinal stem cell signature identifies colorectal cancer stem cells and predicts disease relapse. Cell Stem Cell *8*, 511-524.

Michalopoulos, G., and Tzathas, C. (2013). Serrated polyps of right colon: guilty or innocent? Ann Gastroenterol *26*, 212-219.

Minoo, P., Moyer, M.P., and Jass, J.R. (2007). Role of BRAF-V600E in the serrated pathway of colorectal tumourigenesis. J Pathol *212*, 124-133.

Mohammadi, M., Bzorek, M., Bonde, J.H., Nielsen, H.J., and Holck, S. (2013). The stem cell marker CD133 is highly expressed in sessile serrated adenoma and its borderline variant compared with hyperplastic polyp. J Clin Pathol *66*, 403-408.

Morkel, M., Riemer, P., Blaker, H., and Sers, C. (2015). Similar but different: distinct roles for KRAS and BRAF oncogenes in colorectal cancer development and therapy resistance. Oncotarget *6*, 20785-20800.

Murakami, T., Mitomi, H., Saito, T., Takahashi, M., Sakamoto, N., Fukui, N., Yao, T., and Watanabe, S. (2015). Distinct WNT/beta-catenin signaling activation in the serrated neoplasia pathway and the adenoma-carcinoma sequence of the colorectum. Mod Pathol *28*, 146-158.

Nio, K., Yamashita, T., Okada, H., Kondo, M., Hayashi, T., Hara, Y., Nomura, Y., Zeng, S.S., Yoshida, M., Hayashi, T.*, et al.* (2015). Defeating EpCAM(+) liver cancer stem cells by targeting chromatin remodeling enzyme CHD4 in human hepatocellular carcinoma. J Hepatol *63*, 1164-1172.

Nosho, K., Irahara, N., Shima, K., Kure, S., Kirkner, G.J., Schernhammer, E.S., Hazra, A., Hunter, D.J., Quackenbush, J., Spiegelman, D., *et al.* (2008). Comprehensive biostatistical analysis of CpG island methylator phenotype in colorectal cancer using a large population-based sample. PloS one *3*, e3698.

O'Brien, M.J., Yang, S., Mack, C., Xu, H., Huang, C.S., Mulcahy, E., Amorosino, M., and Farraye, F.A. (2006). Comparison of microsatellite instability, CpG island methylation phenotype, BRAF and KRAS status in serrated polyps and traditional adenomas indicates separate pathways to distinct colorectal carcinoma end points. The American journal of surgical pathology *30*, 1491-1501.

Ogino, S., Cantor, M., Kawasaki, T., Brahmandam, M., Kirkner, G.J., Weisenberger, D.J., Campan, M., Laird, P.W., Loda, M., and Fuchs, C.S. (2006). CpG island methylator phenotype (CIMP) of colorectal cancer is best characterised by quantitative DNA methylation analysis and prospective cohort studies. Gut *55*, 1000-1006.

Oike, T., Ogiwara, H., Nakano, T., Yokota, J., and Kohno, T. (2013). Inactivating mutations in SWI/SNF chromatin remodeling genes in human cancer. Jpn J Clin Oncol *43*, 849-855.

Onuma, K., Ochiai, M., Orihashi, K., Takahashi, M., Imai, T., Nakagama, H., and Hippo, Y. (2013). Genetic reconstitution of tumorigenesis in primary intestinal cells. Proc Natl Acad Sci U S A *110*, 11127-11132.

Ootani, A., Li, X., Sangiorgi, E., Ho, Q.T., Ueno, H., Toda, S., Sugihara, H., Fujimoto, K., Weissman, I.L., Capecchi, M.R., *et al.* (2009). Sustained in vitro intestinal epithelial culture within a Wnt-dependent stem cell niche. Nat Med *15*, 701-706.

Ordonez-Moran, P., Dafflon, C., Imajo, M., Nishida, E., and Huelsken, J. (2015). HOXA5 Counteracts Stem Cell Traits by Inhibiting Wnt Signaling in Colorectal Cancer. Cancer Cell *28*, 815-829.

Pai, R.K., Jayachandran, P., Koong, A.C., Chang, D.T., Kwok, S., Ma, L., Arber, D.A., Balise, R.R., Tubbs, R.R., and Shadrach, B. (2012). BRAF-mutated, microsatellite-stable adenocarcinoma of the proximal colon: an aggressive adenocarcinoma with poor survival, mucinous differentiation, and adverse morphologic features. The American journal of surgical pathology *36*, 744-752.

Pfister, N.T., Fomin, V., Regunath, K., Zhou, J.Y., Zhou, W., Silwal-Pandit, L., Freed-Pastor, W.A., Laptenko, O., Neo, S.P., Bargonetti, J.*, et al.* (2015). Mutant p53 cooperates with the SWI/SNF chromatin remodeling complex to regulate VEGFR2 in breast cancer cells. Genes Dev *29*, 1298-1315.

Phipps, A.I., Limburg, P.J., Baron, J.A., Burnett-Hartman, A.N., Weisenberger, D.J., Laird, P.W., Sinicrope, F.A., Rosty, C., Buchanan, D.D., Potter, J.D.*, et al.* (2015). Association between molecular subtypes of colorectal cancer and patient survival. Gastroenterology *148*, 77-87 e72.

Pronobis, M.I., Rusan, N.M., and Peifer, M. (2015). A novel GSK3-regulated APC:Axin interaction regulates Wnt signaling by driving a catalytic cycle of efficient betacatenin destruction. Elife *4*, e08022.

Rad, R., Cadinanos, J., Rad, L., Varela, I., Strong, A., Kriegl, L., Constantino-Casas, F., Eser, S., Hieber, M., Seidler, B.*, et al.* (2013). A genetic progression model of Braf(V600E)-induced intestinal tumorigenesis reveals targets for therapeutic intervention. Cancer Cell *24*, 15-29.

Robinson, M.D., and Oshlack, A. (2010). A scaling normalization method for differential expression analysis of RNA-seq data. Genome Biol *11*, R25.

Sakai, E., Fukuyo, M., Ohata, K., Matsusaka, K., Doi, N., Mano, Y., Takane, K., Abe, H., Yagi, K., Matsuhashi, N.*, et al.* (2016). Genetic and epigenetic aberrations occurring in colorectal tumors associated with serrated pathway. International journal of cancer Journal international du cancer *138*, 1634-1644.

Sato, T., Stange, D.E., Ferrante, M., Vries, R.G., Van Es, J.H., Van den Brink, S., Van Houdt, W.J., Pronk, A., Van Gorp, J., Siersema, P.D.*, et al.* (2011). Long-term expansion of epithelial organoids from human colon, adenoma, adenocarcinoma, and Barrett's epithelium. Gastroenterology *141*, 1762-1772.

Sato, T., Vries, R.G., Snippert, H.J., van de Wetering, M., Barker, N., Stange, D.E., van Es, J.H., Abo, A., Kujala, P., Peters, P.J.*, et al.* (2009). Single Lgr5 stem cells build crypt-villus structures in vitro without a mesenchymal niche. Nature *459*, 262-265.

Saxena, K., Blutt, S.E., Ettayebi, K., Zeng, X.L., Broughman, J.R., Crawford, S.E., Karandikar, U.C., Sastri, N.P., Conner, M.E., Opekun, A.R.*, et al.* (2016). Human

Intestinal Enteroids: a New Model To Study Human Rotavirus Infection, Host Restriction, and Pathophysiology. J Virol *90*, 43-56.

Segditsas, S., Sieber, O.M., Rowan, A., Setien, F., Neale, K., Phillips, R.K., Ward, R., Esteller, M., and Tomlinson, I.P. (2008). Promoter hypermethylation leads to decreased APC mRNA expression in familial polyposis and sporadic colorectal tumours, but does not substitute for truncating mutations. Exp Mol Pathol *85*, 201-206.

Serra, R.W., Fang, M., Park, S.M., Hutchinson, L., and Green, M.R. (2014). A KRAS-directed transcriptional silencing pathway that mediates the CpG island methylator phenotype. Elife *3*, e02313.

Shin, K., Lee, J., Guo, N., Kim, J., Lim, A., Qu, L., Mysorekar, I.U., and Beachy, P.A. (2011). Hedgehog/Wnt feedback supports regenerative proliferation of epithelial stem cells in bladder. Nature *472*, 110-114.

Sievers, S., Fritzsch, C., Lehnhardt, M., Zahn, S., Kutzner, N., Kuhnen, C., and Muller, O. (2006). Hypermethylation of the APC promoter but lack of APC mutations in myxoid/round-cell liposarcoma. International journal of cancer Journal international du cancer *119*, 2347-2352.

Silva, A.L., Dawson, S.N., Arends, M.J., Guttula, K., Hall, N., Cameron, E.A., Huang, T.H., Brenton, J.D., Tavare, S., Bienz, M., *et al.* (2014). Boosting Wnt activity during colorectal cancer progression through selective hypermethylation of Wnt signaling antagonists. BMC Cancer *14*, 891.

Sinclair, S.H., Yegnasubramanian, S., and Dumler, J.S. (2015). Global DNA methylation changes and differential gene expression in Anaplasma phagocytophilum-infected human neutrophils. Clin Epigenetics *7*, 77.

Snover, D.C. (2011). Update on the serrated pathway to colorectal carcinoma. Hum Pathol *42*, 1-10.

Song, G.A., Deng, G., Bell, I., Kakar, S., Sleisenger, M.H., and Kim, Y.S. (2005). Mucinous carcinomas of the colorectum have distinct molecular genetic characteristics. International journal of oncology *26*, 745-750.

Soshnikova, N.V., Simonov, Y.P., Brechalov, A.V., Portseva, T.N., Pankratova, E.V., and Georgieva, S.G. (2016). The level of the Phf10 protein, a PBAF chromatin-remodeling complex subunit, correlates with the Mts1/S100A4 expression in human cancer cell lines. Dokl Biochem Biophys *467*, 162-164.

Speier, W., and Ochs, M.F. (2012). Updating annotations with the distributed annotation system and the automated sequence annotation pipeline. Bioinformatics *28*, 2858-2859.

Spring, K.J., Zhao, Z.Z., Karamatic, R., Walsh, M.D., Whitehall, V.L., Pike, T., Simms, L.A., Young, J., James, M., Montgomery, G.W.*, et al.* (2006). High prevalence of sessile serrated adenomas with BRAF mutations: a prospective study of patients undergoing colonoscopy. Gastroenterology *131*, 1400-1407.

Stansfield, J.C., Rusay, M., Shan, R., Kelton, C., Gaykalova, D.A., Fertig, E.J., Califano, J.A., and Ochs, M.F. (2016). Toward Signaling-Driven Biomarkers Immune to Normal Tissue Contamination. Cancer Inform *15*, 15-21.

Strum, W.B. (2016). Colorectal Adenomas. N Engl J Med *374*, 1065-1075.

Sugai, T., Habano, W., Jiao, Y.F., Tsukahara, M., Takeda, Y., Otsuka, K., and Nakamura, S. (2006). Analysis of molecular alterations in left- and right-sided colorectal carcinomas reveals distinct pathways of carcinogenesis: proposal for new molecular profile of colorectal carcinomas. J Mol Diagn *8*, 193-201.

Suva, M.L., Riggi, N., and Bernstein, B.E. (2013). Epigenetic reprogramming in cancer. Science *339*, 1567-1570.

Suzuki, H., Watkins, D.N., Jair, K.W., Schuebel, K.E., Markowitz, S.D., Chen, W.D., Pretlow, T.P., Yang, B., Akiyama, Y., Van Engeland, M.*, et al.* (2004). Epigenetic inactivation of SFRP genes allows constitutive WNT signaling in colorectal cancer. Nat Genet *36*, 417-422.

Tanaka, H., Deng, G., Matsuzaki, K., Kakar, S., Kim, G.E., Miura, S., Sleisenger, M.H., and Kim, Y.S. (2006). BRAF mutation, CpG island methylator phenotype and microsatellite instability occur more frequently and concordantly in mucinous than non-mucinous colorectal cancer. International journal of cancer Journal international du cancer *118*, 2765-2771.

Toyota, M., Ahuja, N., Ohe-Toyota, M., Herman, J.G., Baylin, S.B., and Issa, J.P. (1999). CpG island methylator phenotype in colorectal cancer. Proc Natl Acad Sci U S A *96*, 8681-8686.

Treanor, D., and Quirke, P. (2007). Pathology of colorectal cancer. Clin Oncol (R Coll Radiol) *19*, 769-776.

Vaegler, M., Schenke-Layland, K., and Stenzl, A. (2012). Words of wisdom: Re: Hedgehog/Wnt feedback supports regenerative proliferation of epithelial stem cells in bladder. Eur Urol *61*, 1263-1264.

Vakiani, E., and Yantiss, R.K. (2009). Pathologic features and biologic importance of colorectal serrated polyps. Adv Anat Pathol *16*, 79-91.

Visvader, J.E., and Clevers, H. (2016). Tissue-specific designs of stem cell hierarchies. Nat Cell Biol *18*, 349-355.

Vogelstein, B., Papadopoulos, N., Velculescu, V.E., Zhou, S., Diaz, L.A., Jr., and Kinzler, K.W. (2013). Cancer genome landscapes. Science *339*, 1546-1558.

Wajapeyee, N., Serra, R.W., Zhu, X., Mahalingam, M., and Green, M.R. (2010). Role for IGFBP7 in senescence induction by BRAF. Cell *141*, 746-747.

Wang, J.S., Guo, M., Montgomery, E.A., Thompson, R.E., Cosby, H., Hicks, L., Wang, S., Herman, J.G., and Canto, M.I. (2009). DNA promoter hypermethylation of p16 and APC predicts neoplastic progression in Barrett's esophagus. Am J Gastroenterol *104*, 2153-2160.

Wang, Y., Kumar, S., Rachagani, S., Sajja, B.R., Xie, Y., Hang, Y., Jain, M., Li, J., Boska, M.D., Batra, S.K., *et al.* (2016). Polyplex-mediated inhibition of chemokine receptor CXCR4 and chromatin-remodeling enzyme NCOA3 impedes pancreatic cancer progression and metastasis. Biomaterials *101*, 108-120.

Weisenberger, D.J., Siegmund, K.D., Campan, M., Young, J., Long, T.I., Faasse, M.A., Kang, G.H., Widschwendter, M., Weener, D., Buchanan, D., *et al.* (2006). CpG island methylator phenotype underlies sporadic microsatellite instability and is tightly associated with BRAF mutation in colorectal cancer. Nat Genet *38*, 787-793.

Wu, Q., Madany, P., Dobson, J.R., Schnabl, J.M., Sharma, S., Smith, T.C., van Wijnen, A.J., Stein, J.L., Lian, J.B., Stein, G.S., *et al.* (2016a). The BRG1 chromatin remodeling enzyme links cancer cell metabolism and proliferation. Oncotarget.

Wu, Q., Sharma, S., Cui, H., LeBlanc, S.E., Zhang, H., Muthuswami, R., Nickerson, J.A., and Imbalzano, A.N. (2016b). Targeting the chromatin remodeling enzyme BRG1 increases the efficacy of chemotherapy drugs in breast cancer cells. Oncotarget.

Wu, S., Ge, Y., Huang, L., Liu, H., Xue, Y., and Zhao, Y. (2014). BRG1, the ATPase subunit of SWI/SNF chromatin remodeling complex, interacts with HDAC2 to modulate telomerase expression in human cancer cells. Cell Cycle *13*, 2869-2878.

Xu, Y., Zhang, H., Nguyen, V.T., Angelopoulos, N., Nunes, J., Reid, A., Buluwela, L., Magnani, L., Stebbing, J., and Giamas, G. (2015). LMTK3 Represses Tumor Suppressor-like Genes through Chromatin Remodeling in Breast Cancer. Cell Rep *12*, 837-849.

Yamamoto, E., Suzuki, H., Yamano, H.O., Maruyama, R., Nojima, M., Kamimae, S., Sawada, T., Ashida, M., Yoshikawa, K., Kimura, T., *et al.* (2012). Molecular dissection of premalignant colorectal lesions reveals early onset of the CpG island methylator phenotype. Am J Pathol *181*, 1847-1861.

Yang, S., Farraye, F.A., Mack, C., Posnik, O., and O'Brien, M.J. (2004). BRAF and KRAS Mutations in hyperplastic polyps and serrated adenomas of the colorectum: relationship to histology and CpG island methylation status. The American journal of surgical pathology *28*, 1452-1459.

You, J.S., and Jones, P.A. (2012). Cancer genetics and epigenetics: two sides of the same coin? Cancer Cell *22*, 9-20.

Zachos, N.C., Kovbasnjuk, O., Foulke-Abel, J., In, J., Blutt, S.E., de Jonge, H.R., Estes, M.K., and Donowitz, M. (2016). Human Enteroids/Colonoids and Intestinal Organoids Functionally Recapitulate Normal Intestinal Physiology and Pathophysiology. J Biol Chem *291*, 3759-3766.

Zhang, C., Lu, J., and Zhang, P. (2016a). The Roles of Chromatin Remodeling Proteins in Cancer. Curr Protein Pept Sci *17*, 446-454.

Zhang, J.J., Ouyang, T., Wan, W.H., Xu, G.W., and Deng, G.R. (2007). [Detection and significance of APC gene promoter hypermethylation in serum of breast cancer patients]. Ai Zheng *26*, 44-47.

Zhang, Q., Yan, H.B., Wang, J., Cui, S.J., Wang, X.Q., Jiang, Y.H., Feng, L., Yang, P.Y., and Liu, F. (2016b). Chromatin remodeling gene AT-rich interactive domain-containing protein 1A suppresses gastric cancer cell proliferation by targeting PIK3CA and PDK1. Oncotarget.

Zhang, Y.Y., Chen, S.Q., Zhu, M., Li, J.T., Ma, G.J., Zhang, X.M., and Zhou, J.N. (2008). [Promoter hypermethylation and loss of heterozygosity of the APC gene in patients with familial adenomatous polyposis]. Zhonghua Yi Xue Yi Chuan Xue Za Zhi *25*, 378-381.

Zollner, S.K., Rossig, C., and Toretsky, J.A. (2015). Synovial sarcoma is a gateway to the role of chromatin remodeling in cancer. Cancer Metastasis Rev *34*, 417-428.

CURRICULUM VITAE

Byunghak Kang

The Johns Hopkins University, School of Medicine
Department of Cancer Biology
Bunting Blaustein Cancer Research Bldg. (CRB1) Suite 541
1650 Orleans Street
Baltimore, MD 21287
Email: dvm.kang@gmail.com / bkang7@jhmi.edu
Tel: 410-955-8506
Mobile: 443-326-7593

EDUCATION

Aug 2010 - present **The Johns Hopkins University**, School of Medicine, Baltimore, MD
PhD (expected in June 2016) in Pathobiology

Mar 2003 - Feb 2007 **Seoul National University (SNU)**, College of Veterinary Medicine, Seoul, South Korea
Doctor of Veterinary Medicine (*summa cum laude*)

Mar 2001 - Feb 2003 **SNU**, College of Natural Science, Seoul, South Korea
Pre-veterinary medicine course

RESEARCH EXPERIENCE

Aug 2010 - present **Graduate Student Researcher**
The Johns Hopkins University, School of Medicine, Baltimore, MD
- *Thesis Advisors*: Stephen B. Baylin, MD, and Hariharan Easwaran, PhD
- *Thesis*: Phenotypic and molecular profiling of Colorectal cancer tumorigenesi using colon organoid
- *Thesis committee*:
Dr. Benho Park, Associate Director, Breast and Ovarian Cancer Program
Dr. Srinivasan Yegnasubramanian, Director, Next Generation Sequencing Center
Dr. Nicholas Zachos, Director, Mouse Physiology Core

Sep 2009 - Jul 2010 **Research Assistant**
Chromatin Dynamics Research Center, College of Natural Sciences, SNU, Seoul, South Korea
- *Advisor*: Sung-hee Baek, PhD
- *Research Project*: Phenotyping of ROR-alpha mutant mouse with a focus on modulation of inflammatory signaling by ROR-alpha

May 2007 - Aug 2009 **Lecturer in Veterinary Pathology and Project Leader**
College of Veterinary Science, Asunción National University (UNA), Misiones Campus, Misiones, Paraguay
- *Funding*: Korea International Cooperation Agency (KOICA)
- *Research Project*: Epidemiologic study of Brucellosis and Tuberculosis in bovine population in San Juan Bautista using field diagnostic kits

Jul 2004 - Jan 2006 **Research Intern (during summer and winter breaks, four times in total)**
Veterinary Pathology Laboratory, College of Veterinary Medicine, SNU, Seoul, South Korea
- *Advisor*: Chanhee Chae, DVM, PhD
- *Research project*: A retrospective epidemiological study of swine hepatitis E virus in Korea between 1995 and 2004 (resulted in publication in *Vet. J.*)
- *Efficacy and safety test for a mycoplasma hyopneumoniae vaccine for pigs*: Participated in necropsies and gross and histologic evaluations of lesions
- *Diagnosis service*: Participated in daily necropsies and sign-outs (5-10 per day)

CLINICAL/PATHOLOGY EXPERIENCE

Aug-Sep 2015 **Translational Rotation at Phenotyping and Pathology Core (Director: Cory Brayton DVM, Diplomate ACLAM, ACVP)**
The Johns Hopkins University, School of Medicine, Baltimore, MD
-Implemented phenotyping projects: necropsy, trimming, data collection, and histological analysis
-Participated in group study sessions: Gross pathology and AFIP study set

May 2007- Aug 2009 **Attending Veterinarian**
College of Veterinary Science, UNA, Misiones campus, Misiones, Paraguay
- *Funding*: KIOCA
- Provided daily clinical services for mixed animals: Bovine (50%), Small animal (25%), Equine (10%), Ovine (10%), and others (5%)

Mar 2004- Sep 2006 **Founder and President**
Veterinary Volunteer Club, "Pallas," College of Veterinary Medicine, SNU, Seoul, South Korea
- *Advisor*: Hwayoung Yoon, DVM, PhD
- Organized regular clinical services for animal shelters every 2-3 months
- Planned and led two-week summer volunteering trip to Sri Lanka
- Provided Rabies vaccine and spay/neutering to stray dogs and cats

Feb 2006 **Winter Break Externship**
Hyunlee Large Animal Clinic, Kyunggi-do, South Korea
- Participated in daily clinical services for dairy and beef cows

Jul 2002- Feb 2003 **Extern (during summer and winter breaks)**
New York Animal Clinic, Seoul, South Korea
- Assisted clinical services for small animals

TEACHING & MENTORING EXPERIENCE

Jul 2014-
Mar 2016 **Supervisor** of laboratory students
The Johns Hopkins University, School of Medicine, Baltimore, MD
- Mentoring high school student (teaching basic laboratory skills and molecular biology techniques, including subcloning)
- Supervised first-year rotation graduate student through his rotation project (taught experimental techniques, such as 3D culture of crypt stem cells)

2014 &
2011 **Teaching Assistant** for graduate-level course, *Pathology for Graduate Students: Basic Mechanisms of Disease*
The Johns Hopkins University, School of Medicine, Baltimore, MD
- Developed and graded homework and examinations in 2011, prepared and gave lecture on anatomy and physiology of male reproductive organs in 2014

May 2007-
Aug 2009 **Lecturer in Veterinary Pathology**
College of Veterinary Science, UNA, Misiones campus, Misiones, Paraguay
- Co-taught veterinary pathology courses to second-year veterinary students: gave lectures and supervised necropsies and diagnostic tests
- Initiated and led outreach program for rural area of Paraguay with veterinary students during summer breaks (provided clinical services for mixed animals including vaccinations, deworming, diagnostic tests, and surgeries)

EXTRACURRICULAR ACTIVITIES

Sep 2011-
Aug 2012 **Manager of General Affairs**
Baltimore Life Scientist Association, Baltimore, MD
- Organized annual conference and monthly seminars

Mar 2004 -
Feb 2005 **Board Member of National Council of Veterinary Students**
- Attended monthly meetings of the council and discussed issues related to veterinary education and career development

Mar 2004 -
Feb 2005 **Vice President of Student Association of College of Veterinary Medicine**
College of Veterinary Medicine, SNU, Seoul, South Korea
- Organized quarterly board meetings and planned college's activities including spring and fall festivals and summer camps
- Led consulting project for veterinary curriculum reform (proposal was later accepted and implemented by College of Veterinary Medicine)

AWARDS AND FELLOWSHIPS

2016	**Graduate Student Association travel award**
2016	**Oustanding Abstract/Poster Award** Pathology Young Investigator Award
2015	**Best Poster Presentation Award** Johns Hopkins Pathobiology Program Annual Retreat
2015	**GI Core Grant for Pilot Studies** (US$25,000) Developed research strategies for the proposal
2015	**1st Place Winner**, Johns Hopkins Biotech and Healthcare Case Competition
2013	**Mokam Fellowship** (US$10,000), academic merit-based fellowship
2012	**Best Poster Presentation Award** Baltimore Life Scientist Association Annual Conference
Sep 2010 - Aug 2011	**Margaret Lee Fellowship** Financial support for tuition and stipends
2007	**Dean's Award at Graduation,** SNU Given to one student from each college based on academic achievements and extracurricular activities
Mar 2003 - Feb 2007	**Full Tuition Academic Scholarship** by College of Veterinary Medicine, SNU Given to student ranked number one in the class
	Partial Tuition Academic Scholarship by College of Veterinary Medicine, SNU Given to students in top 10% of class
Mar 2001 - Feb 2003	**Partial Tuition Academic Scholarship** by College of Natural Science, **SNU** Given to students in top 10% of class
1999	**Seoul High School Student Award** Given to students with outstanding academic potential in Seoul

CURRICULUM VITAE

PROFESSIONAL QUALIFICATIONS AND CERTIFICATIONS

2015 **Partial Completion of ECFVG(Educational Commission for Foreign Veterinary Graduate)**
Step 1: Registration and Proof of Graduation (*completed*)
Step 2: English Language Ability (*completed*)
Step 3: Basic and Clinical Science Examination (*completed*)
Step 4: Clinical Proficiency Examination (*completed 6 out of 7 sections*)

2012 **Completion of Mouse Pathobiology and Phenotyping Short Course**
Johns Hopkins University School of Medicine, Baltimore, MD, USA

2007 **Official Development Aid Training Certificate by KOICA**

2007 **Veterinary License in South Korea**

PUBLICATIONS

- **Kang B**, Maegawa S In J, Zachos NC, Huso DL, Issa JP Easwaran H, Baylin SB (*in preparation*). Oncogenic BRAF mutation V600E drives stem cell niche factors-independent growth and tumorigenic transformation in colon organoids.

- Sysa-Shah P, Tocchetti CG, Gupta M, Rainer PP, Shen X, **Kang B**, Belmonte F, Li J, Xu Y, Guo X, Bedja D, Gao WD, Paolocci N, Rath R, Sawyer DB, Naga Prasad SV, Gabrielson K(2016) Bidirectional cross-regulation between ErbB2 and β-adrenergic signaling pathways. *Cardiovasc Res*. 1;109(3):358-73.

- Le A, Stine ZE, Nguyen C, Afzal J, Sun P, Hamaker M, Siegel NM, Gouw AM, **Kang BH**, Yu SH, Cochran RL, Sailor KA, Song H, Dang CV (2014). Tumorigenicity of hypoxic respiring cancer cells revealed by a hypoxia-cell cycle dual reporter. *Proc Natl Acad Sci USA*. 111(34):12486-91.

- Sysa-Shah P, Xu Y, Guo X, Belmonte F, **Kang B**, Bedja D, Pin S, Tsuchiya N, Gabrielson K (2012). Cardiac-specific over-expression of epidermal growth factor receptor2 (ErbB2) induces pro-survival pathways and hypertrophic cardiomyopathy in mice. *PLoS One*. 7(8):e42805.

- Jung K, **Kang B**, Song DS, Chae C (2007). Prevalence and genotyping of hepatitis E virus in swine population in Korea between 1995 and 2004: A retrospective study. *Vet. J*. 173(3):683-687.

ABSTRACT & PRESENTATIONS

2016 Kang B, Easwaran H, Baylin S. Oncogenic BRAF mutation V600E drives stem cell niche factors-independent growth and tumorigenic transformation in colon organoids. Abstract/Poster presentation at American Association of Cancer Research Annual meeting, New Orleans LA.

2015 Kang B, Easwaran H, Baylin S. Oncogenic BRAF mutation V600E drives stem cell niche factors-independent growth and tumorigenic transformation in colon organoids. Abstract/Poster presentation at Johns Hopkins Pathobiology Program Annual Retreat, Baltimore MD.

2012 Kang B, Gabrielson K.Cross-talk between ErbB2 and β-adrenergic signaling pathways. Abstract/Poster presentation at Baltimore Life Scientist Association Annual Conference, Baltimore MD.

PROFESSIONAL MEMBERSHIPS

- ACVP (American College of Veterinary Pathology)

- STP (Society of Toxicologic Pathology)

- AVMA (American Veterinary Medical Association)

- KVMA (Korean Veterinary Medical Association)

- KSEA (Korean-American Scientists and Engineers Association)

- BLSA (Baltimore Life Scientist Association)

- KOV (Korean Overseas Volunteers)